DYNAMIC MODELLING AND SIMULATION OF CATALYTIC CARBON DIOXIDE METHANATION WITH GREEN HYDROGEN

Lappeenranta–Lahti University of Technology LUT

Master’s Programme in Chemical Engineering, master's thesis

2024

Phat Nguyen

Examiners: Docent. Arto Laari

Viet Hung Nguyen (M. Sc)

Supervisor: Viet Hung Nguyen (M. Sc)

ABSTRACT

Lappeenranta–Lahti University of Technology LUT

LUT School of Engineering Sciences

Chemical Engineering

Phat Nguyen

Dynamic modelling and simulation of catalytic carbon dioxide methanation with green hydrogen

Master's thesis

2024

85 pages, 49 figures, 10 tables and 3 appendices

Examiners: Docent Arto Laari and Viet Hung Nguyen (M. Sc)

Supervisor: Viet Hung Nguyen (M. Sc)

Keywords: Power-to-X, Power-to-Methane, catalytic CO_2 methanation, isothermal reactor, Aspen Plus, Aspen Plus Dynamics, dynamic modelling.

Power-to-gas is a method for chemically storing discontinuous green power. Renewable electricity is able to generate "green" hydrogen (H_2), which can be subsequently combined with carbon dioxide (CO_2) in catalytically cooled multi-tubular reactor(s) to synthesize methane (CH_4). However, the dynamic behavior of the process with variating inlet flow rates caused by the intermittency of renewable electricity is the biggest challenge of this technology. Therefore, the process' dynamic behavior should be investigated with variating inlet flow rates to design a control structure and to operate the process. In the first step, a steady-state model was built in Aspen Plus according to the capacity of a 35 MW electrolysis unit. After that, the model was exported to Aspen Plus Dynamics to study its dynamic behavior. Different H_2 feed flow rates were applied to investigate the composition of the product stream and the reactor. In addition, model's limitations were also determined by

testing different ramping rates and the minimum partial loading level of feed gases that can be achieved in the process model.

In the steady-state model, a methanation reactor was designed and simulated in Aspen Plus and Aspen Plus Dynamics using characteristics of the Koschany et al. kinetic model at 230 ℃ and 10 bar. Heat transfer coefficients were also calculated and applied to achieve a realistic model. As a consequence of the reactor type, the high stoichiometric ratio, and the fast and exothermic reaction, a hot spot of 768 ℃ appeared at the feed zone of the reactor. In the context of the absence of a recycle stream, the hot spot was 782℃, which is higher than with recycle. The composition of the product stream was 28.33% of H_2 mol-% and 70.79% of CH_4 mol-%. With the control system set up in Aspen Plus Dynamics, the controllers showed a quick response with different H_2 feed flow rate variations. Different H_2 loads were tested: +10%, −10%, and –30% of the maximum flow rate in steady-state simulation. When the feed flow changed from the maximum load, the peak temperature reached 752 ℃, 738 ℃, and 722 ℃ in cases +10%, −10%, and –30% of the full load respectively. In all tests, the product composition had no significant fluctuations, and H_2 and CH_4 molar fractions were stable and the same as at full-load. The model's limitations were determined; the maximum achieved ramping rate was ±50% change in 5 minutes, and the minimum H_2 feed flow rate was 138 kmol/h corresponding to ~ 44.8% of the full load. Notably, in all tests, the quality of the product stream always remained in the favorable range regarding the CO_2 concentration.

ACKNOWLEDGEMENTS

This master's thesis was carried out at Lappeenranta-Lahti University of Technology LUT from April 2024 to October 2024. The works were carried out on the Department of Process Engineering of LUT School of Engineering Science (LENS).

I would like to send my grateful thanks to my examiners Docent Arto Laari and my supervisor M. Sc Viet Hung Nguyen for their continuous support and guidance during this thesis project. Their insightful feedback and valuable suggestions have been important in shaping this research. In addition, I would like to express my gratitude for financial support to the project "Hydrogen and Carbon Value Chain in Green Electrification" (HYGCEL) funded by Business Finland.

My sincere gratitude to my friends and coworkers who provided encouragement and support throughout trying times. Your trust in me kept me going.

Finally, I wish to acknowledge my profound gratitude to my family and my girlfriend for your unwavering love, patience, and understanding during this journey.

Helsinki, 01.10.2024

Phat Nguyen.

ABBREVIATIONS

AEL	Alkaline Electrolysis
BM	Biological Methanation
CAPEX	Capital expenditure
FBRs	Fixed-bed reactors
GHSV	Gas Hourly Space Velocity
OP	Controller output
P2G	Power-to-Gas
P2H	Power-to-Hydrogen
P2X	Power-to-X
PEM	Proton Exchange Membrane Electrolysis
PV	Process Variable
Rec	Recycle ratio
RES	Renewable Energy Sources
RWGS	Reverse water-gas shift
SNG	Synthetic Natural Gas
SP	Set point of controller
SOEC	Solid Oxide Electrolysis
SMR	Steam methane reforming
STP	Standard Temperature and Pressure: 0°C, 101.325 Pa
TREMP	Topsøe Recycle Energy-efficient Methanation
WI	Wobble Index

SYMBOLS

A_{total}	Total heat transfer area of heat exchanger	m^2
A_{tube}	Tube's heat transfer area	m^2
Bi	Tube Biot number	_
C_p	Heat capacity of vapor fluid	J/(kg K)
D_l	Flash's diameter calculated by liquid velocity	m
D_p	Particle size (catalysts)	m
D_t	Tube's diameter	m
D_v	Flash's diameter calculated by vapor velocity	m
E	Activation energy	kJ/mol
$F_{v,G,in}$	Volumetric flow rate at STP	m^3/h
GHSV	Gas Hourly Space Velocity	h^{-1}
h_c	heat transfer coefficient between process fluid and catalyst	W/(m K)
h_w	heat transfer coefficient between process fluid and wall reactor	W/(m K)
K_i	surface adsorption constants in equilibrium	$bar^{-0.5}$
k_{er}	Effective radial thermal conductivity	W/(m K)
k_f	fluid thermal conductivity	W/(m K)
k_w	wall thermal conductivity	W/(m K)
k_r^0	effective catalyst thermal conductivity	W/(m K)
k_s	catalyst thermal conductivity	W/(m K)
L	Tube's length	m
M_{tubes}	Tube's mass	kg
N_{tubes}	Number of tubes in heat exchanger	_

Nu	Fluid-to-solid Nusselt number	–
Nu_m	Mechanical fluid Nusselt number	–
Nu_w	Wall Nusselt number	–
Nu_{w0}	Wall Nusselt number at zero flow	–
Nu_w^*	Wall film Nusselt number	–
$Pe_{h,r}$	Radial fluid phase Peclet number	–
P	Controller's gain parameter	%/%
Pr	Prandlt number	–
p	Pressure	bar
Re_0	Particle Reynold number	–
T	Temperature	℃
U	Overall heat transfer coefficient	W/(m^2 K)
U_t	Overall heat transfer coefficient between process fluid and wall reactor	W/(m^2 K)
u	Fluid's velocity	m/s
V_c	Catalyst loaded volume	m^3
V_g	Vapor volumetric flowrate	m^3/s
V_l	Liquid volumetric flowrate	m^3/s
V_{max}	Maximum vapor velocity	m/s
V_{shell}	Volume of shell in tube-shell heat exchanger	m^3
V_{tubes}	Volume of tubes in tube-shell heat exchanger	m^3
ρ_v	Density of vapor mixture	kg/m^3
μ	Fluid's viscosity	Pa s

ρ_m	Material's density	kg/m^3
ε	Catalyst bed voidage	_
Δw	Tube's wall thickness	m

Table of contents

Appendices

1 Introduction

Scientists are certain that human activities' emission is the primary reason for global warming; since the end of 19th century, the average global temperature has increased by 0.8℃ [1]. Global energy consumption is predicted to gain at an average annual rate of 0.7% through 2030, which is almost half the level of growth recorded over the previous decade [2]. Demand is predicted to rise by 2050, but CO_2 emissions are expected to fall behind by only 1.2% [2]. To keep on track with climate targets, actions must be taken to reverse the trend of change and restrict temperature rise to 1.5℃ over the pre-industrial period [2]. To minimize this alarming tendency, the European Union has established regulations for achieving carbon neutrality by 2050 through the "Clean Energy for all Europeans" legislation package [2]. Enhancing the contribution of renewable electricity to lessen the usage of fossil fuels is one of this package's main goals.

Carbon collecting, the creation of alternative energy sources to replace fossil fuels, and storage technologies are three of the many initiatives being aggressively explored to minimize CO_2 emissions [3]. For instance, developing energy plans that focus on the transition to renewable energy sources (RES) might successfully reduce reliance on fossil fuels and hence CO_2 emissions [4]. Studies on alternative energy sources have primarily concentrated on wind and solar energy, both of which offer limitless potential. In 2022, Finnish wind power production gained 41% of total final energy consumption during the year, reaching a record peak of 11.6 TWh in electricity consumption [5]. As can be seen from Figure 1, increasing in wind power usage, accounting for 14.1% of total electricity production, propelled it to the third position among electricity sources, surpassing wood-fueled electricity. By the end of 2023, 1601 wind turbine generators were established with the total capacity of 6946 MW [6]. Besides that, although Finland's solar power capacity increased by more than 60% in 2022, it still makes up a small amount of the country's overall electricity production [5,6,7]. However, due to the variability of RES generation influenced by weather patterns, there's a pressing need for a comprehensive, long-lasting energy storage solution to mitigate fluctuations in power generation and enhance grid stability [3,5].

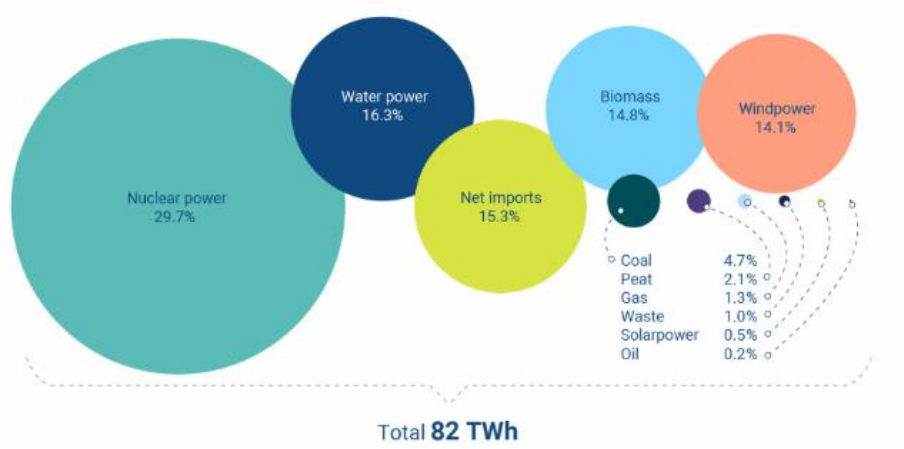

Figure 1. Finnish electricity production in 2022. [7]

As mentioned above, increasing the proportion of RES, such as wind and solar power, in contemporary energy systems has been proposed as a way to reduce CO_2 emissions [4]. However, due to the fluctuating availability of RES, energy storage is required when renewable power supply does not meet demand [3,5]. Among the potential energy storage technologies, Power-to-Gas (P2G) idea is potential concept [8]. It provides the option of transforming excess renewable power to energy in chemicals by producing energy carrier components such as CH_4, and H_2 [9].

Several studies emphasize the importance of P2G technology, as it plays a crucial role in shifting towards RES [10,11]. Nevertheless, additional studies and investigations are needed to grasp and address the technical and societal obstacles hindering the widespread embrace of P2G systems [12]. The main objective of this study is to assess the dynamic performance and operational limitations of catalytic CO_2 methanation under the variation of electrolytic H_2 feed rate. Based on data from the literature review, Aspen Plus was used to design a steady-state model of the methanation process with suitable:

- selected configuration at the plant level especially the number and type of reactor(s)
- operating, design parameters, and kinetic model.

Finally, the steady state model was exported to Aspen Plus Dynamics and a control structure was applied to the model to assess:

- the dynamic performance and operational limitations (minimum loading and maximum achievable ramping rate)
- the feasibility of accepting the generated gas into the network during the transition phase.

LITERATURE PART

2 Power-to-X Processes

Power-to-X (P2X) is a scheme that utilizes RES to manufacture a variety of products. The diversity and rising quantity of different products is signified by "X". These products encompass necessities like fuels, chemicals, heat as well as energy carriers for storage [13]. P2X technology offers several advantages as well as the replacement of nonrenewable energy. P2X improves energy security by balancing power supply and demand, and hence the power system. P2X also provides the ability to store energy in the final material [14]. The electricity produced by renewable energy can operate the water electrolysis process (Power-to-Hydrogen as known as P2H) which attracted many researchers during last decade [15]. Generally, H_2 -the main product- from water electrolysis is used as the energy carrier, additionally, oxygen (O_2) is also the product of water-split process [16]. Besides that, to continue advancing the P2X concept, the generated H_2 could undergo additional reactions with CO_2, ideally sourced from emissions of industrial manufacturing and power station (or eventually directly from the environment as the ultimate decarbonization goal) [16]. As illustrated in Figure *2*, to continue the P2X concept, the generated H_2 could be combined with CO_2, preferably obtained from production and power plant (and directly from the atmosphere as the final decarbonization aim). High-temperature co-electrolysis produces a combination of H_2 and CO; the product (or H_2 in the case of fundamental water electrolysis with CO_2 injection) is able to subsequently be fed into a methanation unit to produce CH_4. H_2 is also able to utilize to enhance biogas generated by anaerobic digestion of organic material. These are some possible routes of the P2G pathway that create synthetic natural gas (SNG). This thesis focuses on the P2G process, in which CH_4 is the final product.

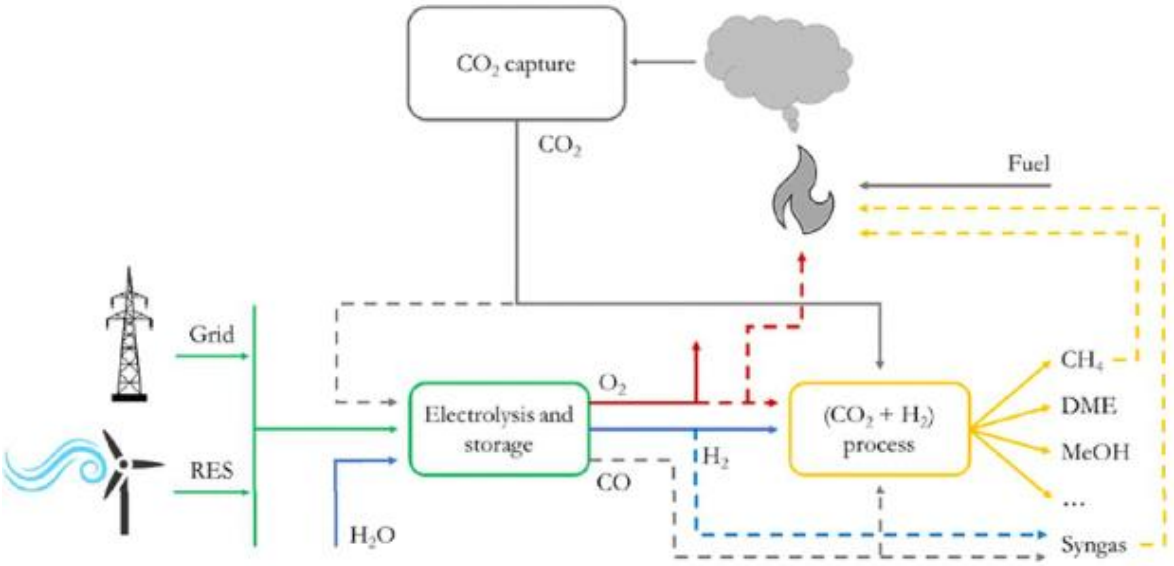

Figure 2. Diagram illustrating potential P2X pathways for RES and capturing carbon. [16]

2.1 Power-to-Gas

In general, P2G is described as the procedure of converting surplus electricity from RES to chemical energy stored in gaseous substances [17]. Within the P2X framework, carrier X utilized for storing electricity is represented by the chemical potential in a gaseous element. P2G is considered as an expansion of the P2H process, with the objective of obtaining an energy vector more compatible with current infrastructure and suitable for use in existing applications and appliances [16]. According to Buffo et al. (2019) [16], product of water electrolysis, H_2, plays a crucial character in the P2H-to-P2G cycle, in which both H_2 and its derivatives (SNG or CH_4) can be transformed to electricity. When the last sector of this electricity energy storage solution passed the P2G concept's borders, incorporating other products such as liquid fuels (alcohols, dimethyl ether, etc.) and sustainable chemicals could be the next pathways. In fact, CO_2 is not the only element, but also other chemicals could be part of various P2X systems which lead to green chemicals, such as nitrogen (N_2) in the power-to-ammonia notion.

There is also a high demand for pure H_2 with low CO_2 emissions, as more than 95% of H_2 is generated from nonrenewable fuels; and the global production capacity and CO_2 emissions are 115 Mt/a and 830 Mt/a respectively [15]. Substituting H_2 produced from fossil-based with “green” H_2 could quickly decrease Greenhouse Gas emissions because the process does not produce CO_2 or need additional synthesis step after electrolysis [15]. Water electrolysis,

which transforms electrical energy into chemical energy in H_2 gas, is a crucial link in the P2G chain. Later on, the generated H_2 can be refined to create other fuels or used in fuel cells or gas-fired power plants to generate electricity once more. Because it only produces water during combustion and has a very high heat value (LHV = 120 MJ/kg), H_2 is a fuel with a lot of promise [18]. It is the smallest, lightest element, and low density, which makes transportation and storage challenging. At criterion temperature and pressure, molecular H_2 has a density of only 0.084 kg/m^3, but in liquid phase (at boiling point −252℃), its density is 70.8 kg/m^3 [19]. Gaseous H_2 necessitates substantial storage volumes, and the process of liquefaction imposes an energy consumption equivalent to approximately 40–50% of its energy content [18]. H_2 is susceptible to leakage and diffusion through materials, which can also lead to material degradation because of its diminutive molecular size. Furthermore, when compared to other materials such as natural gases, hydrogen's low ignition energy and flammability pose challenges to transportation, storage, and safety [18].

Alkaline electrolysis cell (AEL), proton exchange membrane electrolysis cell (PEMC), and solid oxide electrolysis cell (SOEC) are the three primary types of water electrolysis [14,16,19,20]. Table 1 below shows the main operation conditions of these types of technologies.

Among the three electrolysis methodologies contemplated for P2G facilities, AEL stands out as the most established and comprehensively understood option. It has been commercially accessible for decades [20]. Conditions and requirements for AEL are provided in Table 1. According to Götz et al. (2015) [20], AEL electrolysers offer a versatile operational range, allowing them to function effectively from 20% to 100% of their design capacity. This flexibility operational condition helps AEL electrolysers well-suited for P2G systems, which rely on variable and intermittent RES. Additionally, this technology boasts comparatively low capital costs as an advantage in contrast to PEM or SOEC. With investment expenses ranging approximately between 800 and 1500 €/kW, maintenance expenses estimated at 2 – 3% of the annual expenditure costs, and high durability (55000 − 120000 hours); AEL electrolysers present an economically attractive option. However, the primary drawback of AEL technology lies in the corrosive nature of its utilized electrolytes, typically alkaline solutions such as 20–30% potassium hydroxide solution. This corrosiveness results in heightened maintenance requirements, leading to increased operational costs [20].

Table 1. Reactions and conditions of three types of electrolysis technologies. [14,19]

	AEL	*PEMC*	*SOEC*
Cathode's reaction	$2H_2O + 2e^- \rightarrow H_2 + 2OH^-$	$2H^+ + 2e^- \rightarrow H_2$	$H_2O + 2e^- \rightarrow H_2 + O^{2-}$
Anode's reaction	$2OH^- \rightarrow \frac{1}{2} O_2 + H_2O + 2e^-$	$H_2O \rightarrow \frac{1}{2} O_2 + 2H^+ + 2e^-$	$O^{2-} \rightarrow \frac{1}{2} O_2 + 2e^-$
Scale production	Commercial	Commercial	Laboratory
Dynamic flexibility	20 – 100%	0 – 100%	–100 – 100%
Product's stream	< 760 m^3h^{-1} ≈ 2.7 MW	≈ 450 m^3h^{-1} ≈ 1.6 MW	_
Electrolyte	Alkaline solution	Solid polymer membrane	yttria-stabilized zirconia
Charge provider	OH^-	H_3O^+/ H^+	O^{2-}
Cell temperature	40 – 90℃	20 – 100℃	800 – 1000℃
Typical pressure	1 – 30 bars	20 – 50 bars	_
Cell voltage	1.8 – 2.4 V	1.8 – 2.2 V	0.91 – 1.3V
Total power requirement	4.5 – 8.2 kWh/m^3 H_2	4.5 – 7.5 kWh/m^3 H_2	_
Cold start time	Minutes-hours	Seconds-minutes	_
Lifetime	Up to 30 years	5 years	_

According to Gahleitner (2012) [21], PEM technology offers several key advantages, including fast cold start, greater flexibility, enhanced compatibility with dynamic-intermittent systems, and H_2 high purity levels. However, PEM systems are currently more costly than AEL technology, primarily due to expenses associated with the membrane and the use of high-quality catalysts. Furthermore, PEM technology suffers from a limited lifespan, which represents another disadvantage.

In the case of SOEC technology, this electrolysis is essentially the inverted process taking place in a fuel cell. One notable advantage of SOEC technology lies in its potential for heat combination with exothermic processes, for example methanol production. Additionally, SOEC technology provides flexibility of operating across electrolysis and battery. As H_2 generated in this system can later be turned back into electricity utilizing a battery, this technology presents a chance to accumulate surplus electricity produced by RES like wind or solar power. However, a significant drawback hindering the large-scale deployment of SOEC technology is the rapid degradation of materials, leading to low stability. This degradation is primarily attributed to the high temperatures involved and the extended duration of operation [22].

2.2 Power-to-Methane

In fundamentals, a P2M plant is made up of an electrolyzer, a CO_2 capture unit in the event that CO_2 is unavailable as a purified material or in an appropriate gas combination, and methanation reactors [23,24]. RES is utilized to operate the electrolyzer which separates water into H_2 and O_2. The products of CH_4 and H_2O are formed by electrolytic H_2 and captured CO_2. Following that the rich CH_4 gas generated can be enhanced to SNG. SNG can be utilized in a similar way that ordinary natural gas is. Therefore, CH_4 becomes a fascinating fuel because natural gas facilities currently exist, and the infrastructure for exploiting SNG is established and available. SNG has several applications, including mobility fuel, industrial feedstock, heating, and power generation in combined cycle facilities [25]. CH_4 is the main product because it is easy to inject into natural gas network [26]. According to Wulf et al. (2020) [26], H_2 is utilized to generate CH_4 in 22% of the P2X projects in Europe; only P2H is ahead of P2M with a significant proportion of 69% of the projects. However, P2M is selected over H_2 due to its available infrastructure and higher safety levels [25,27]. H_2 has a

larger flammability zone and requires less ignition energy than CH_4. Furthermore, because of its tiny size, H_2 may quickly exit structures and be in contact with oxygen, increasing the danger of explosion [27]. The methanation process is in more detail in section 3 .

The commercial potential for renewables has recently risen. The Paris Agreement sets novel legislation, targets for emission, and proposed plan. For instance, every nation of the European Union has committed to a 42.5% renewable energy target for 2030. The new legislation and plans promote the utilization of P2G and SNG as RES. The potential for P2G and CH_4 fuel is predicted to increase as the transition to RES accelerates [28].

However, one of the biggest challenges of P2M is the difference in the cost of generated SNG and the cost of fossil-based gases [29]. McDonagh et al. (2018) [29] predicted SNG prices of a 10MWe P2G plant in 2030 and 2040 to be 105 €/MWh and 93 €/MWh, respectively; while the electricity price used for the plant is 35 €/MWh. They investigated several operational methods and concepts for energy supply and the influences of the costs of production in the P2G process. When evaluating expenditures, the efficiency gains for 2050 were also taken into account. Based on the results, SNG manufacturing using the P2G scheme would be feasible by 2030, and significantly greater by 2050. In addition, according to Frambri et al. (2022) [30], the cost of SNG for optimal P2G processes is between 70 – 132 €/MWh in 2030 and 37 – 99 €/MWh in 2050, the SNG prices were calculated by using electricity price in range 0 – 30 €/MWh. They also noted that interest in P2G concept and SNG use as a source of energy is likely to rise by 2050.

In Finland, the cost of SNG was 1.72 €/kg (131.3 €/MWh) in May of 2024, and biogas was 2.15 €/kg (159.26 €/MWh), including tax [31]. The costs were for road transportation.

3 Methanation

Methanation is the last step of the P2M process, in which electrolytic H_2 and captured CO_2 react under different conditions and convert to CH_4 products. Chemical and biological are two methodologies of CO_2 methanation process. The primary distinction between the two methanation methods lies in their catalysts. Metal catalysts are employed in catalytic methanation, in contrast to biocatalysts in biological methanation. These pathways are described in detail in this chapter.

3.1 Catalytic Methanation

Catalytic methanation has been known since 1902 when Sabatier and Senderens used metal catalysts (groups 8 – 10) to synthesis CH_4 from CO_2 and H_2 [32,33,34]. The reaction of CO_2 methanation process (Eq. 1) is the combination of CO methanation (Eq. 3) and reverse water-gas shift reaction (RWGS) (Eq. 2)[32,33,34]. While the (Eq. 4) is the reverse dry reforming reaction (RDR) [34].

$CO_2 + 4H_2$	$\rightleftarrows$	$CH_4 + 2H_2O$	$\Delta_r^o H = -165\ kJ\ mol^{-1}$	(Eq. 1)
$CO_2 + H_2$	$\rightleftarrows$	$CO + H_2O$	$\Delta_r^o H = 41\ \text{kJ mol}^{-1}$	(Eq. 2)
$CO + 3H_2$	$\rightleftarrows$	$CH_4 + H_2O$	$\Delta_r^o H = -206\ \text{kJ mol}^{-1}$	(Eq. 3)
$2CO + 2H_2$	$\rightleftarrows$	$CH_4 + CO_2$	$\Delta_r^o H = -247\ \text{kJ mol}^{-1}$	(Eq. 4)

As the simplest method, captured CO_2 is directly used to produce CH_4 (Eq. 1). In terms of economics, the value of CH_4 is not same as electrolytic H_2, but it might be made economically feasible in some circumstances given the costs associated with CO_2 (both direct and indirect) and the difficulties in implementing a hydrogen facility [34].

On the other hand, as a thermodynamic model, only RWGS (Eq. 2) is an endothermic reaction, and other reactions are exothermic. The total released enthalpy of reactions is – 165 $kJmol^{-1}$. Besides that, carbon (C) residue is formed in some side reactions (Eq. 5) to (Eq. 8) need to be avoided, to achieve higher selectivity of catalysts and prevent gradually deactivation [34, 35, 36].

$2CO$	$\rightleftarrows$	$C + CO_2$	$\Delta_r^o H = -172\ \text{kJ mol}^{-1}$	(Eq. 5)
CH_4	$\rightleftarrows$	$C + 2H_2$	$\Delta_r^o H = 75\ \text{kJ mol}^{-1}$	(Eq. 6)
$CO + H_2$	$\rightleftarrows$	$C + H_2O$	$\Delta_r^o H = -131\ \text{kJ mol}^{-1}$	(Eq. 7)
$CO_2 + 2H_2$	$\rightleftarrows$	$C + 2H_2O$	$\Delta_r^o H = -90\ \text{kJ mol}^{-1}$	(Eq. 8)

Temperature (*T*) and pressure (*p*) are parameters which directly affect these above reactions [32,34,36,37,38,39]. In accordance with Le Chatelier's principle, CH_4 yield will be affected by increasing pressure and decreasing temperature (due to exothermal character). As reported by Sahebdelfar & Ravanchi (2015) [37], the CO_2 conversion and CH_4 selectivity are analyzed by adjusting temperature, pressure, and stoichiometric ratio of H_2:CO_2.

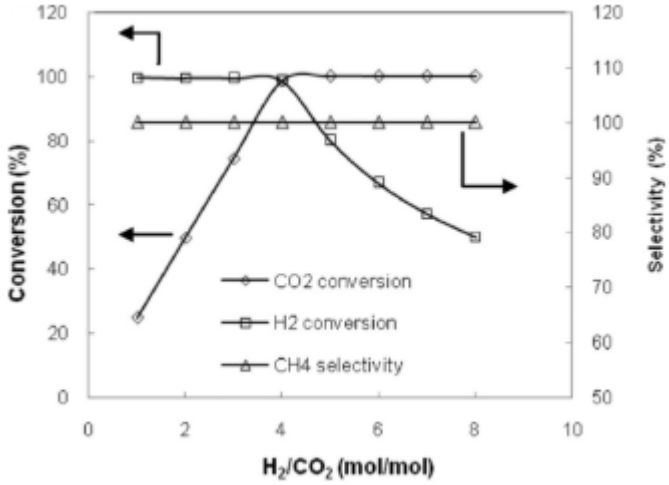

Figure 3. CO_2 conversion and CH_4 selectivity in equilibrium with different H_2/CO_2 molar ratio (T = 300°C and p = 25 bar). [37]

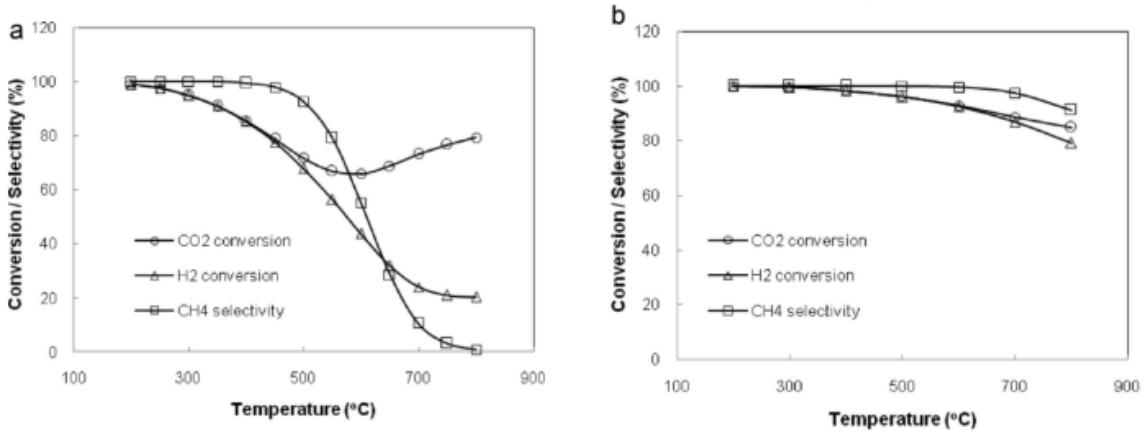

Figure 4. The influence of temperature on CO_2 conversion and CH_4 selectivity in equilibrium (with H_2/CO_2 ratio = 4 and (a) *p* = 1 bar; (b) *p* = 25 bar) [37]

Figure 3 illustrates effects of H_2:CO_2 molar ratio to equilibrium CO_2 conversion and CH_4 selectivity (*T* = 300°C and *p* = 25 bar). The equilibrium conversion rises with H_2/CO_2 below

the stoichiometric ratio before balancing. Throughout the composition range displayed, the CH_4 selectivity is almost unity, and maximal equilibrium methanation is identified at the stoichiometric feed ratio, thus, the ideal ratio for methanation process is $H_2/CO_2 = 4$.

In thermodynamic equilibrium, the lower temperature obtains higher CH_4 selectivity. In addition, as shown in Figure 4, at 1 bar pressure, the CO_2 conversion (T = 300℃ and T = 500℃) is around 98% and 78% respectively. On other hand, with p = 25 bar, the CO_2 conversion is only dropped by 5% (almost 100% and 95%) between T = 300℃ and T = 500℃. With higher pressure, the CO_2 conversion is greater if higher temperature applies at the same time. It is important to carefully consider the trade-off between both impacts, particularly when switching to a rate-based process. Both factors do, in fact, have an impact on the plant's capital expenditures (CAPEX) because higher pressure necessitates more expensive construction for resistant substances and increases operational expenses for compression, whereas the ability to work at higher temperatures and pressures promotes kinetics with small equipment volumes, which is further limited by the intense pressure in operation [34]. Pressure is a significant factor that promotes the hydrogenation process. Moreover, using a high pressure can raise the temperature at which C residue become a prevention, as some scientists have proposed [37]. Finding a balance between the expense of compression and the boost in CO_2 conversion is necessary, with a range of pressure of 8–16 bar being recommended as optimal [34].

As mentioned above, coke formation according to (Eq. 5) to (Eq. 8) occurs in some conditions. Gao et al. (2011) [38] investigated that a C residue was formed when H_2/CO_2 molar ratio was smaller than 4 no matter how much the pressure is increased. Furthermore, adding H_2O or CH_4 steam to feed stream were also considered by Gao et al. and Jürgensen et al. (2014) [38,39]. Although adding H_2O and CH_4 steam does not have significant effects to CO_2 conversion and CH_4 selectivity, the parameters that influence the CO_2 methanation process should be specified.

3.1.1 Reactor Technologies

The CO_2 methanation reactions are extremely exothermic, necessitating careful heat control to avoid hot spot expansion and subsequent catalysts destruction. Therefore, equilibrium limits at high temperatures can be controlled. Appropriate reactor selection and design are

often the keys successfully to achieving heat management [20,34,36]. There are some typical reactors utilized for CO_2 methanation such as fixed-bed reactors (including adiabatic and isothermal) (FBR) and fluidized-bed reactors. The operation conditions, technical parameters, advantages, and disadvantages of these reactors have been extensively investigated.

Adiabatic fixed-bed reactors are the most common method for scaling up operations [34]. To achieve the required standard, one or more reactors are employed in sequence. Reactor design should be handled with extra caution. They frequently operate at high pressure to enhance the reaction thermodynamically [20,32,34]. The primary disadvantages include the process's limited flexibility, relatively large pressure drops and potential for creating coke or carbon monoxide in the event of hotspots [32]. In addition, catalysts deactivation at high temperature is also needed to be considered, because the temperature at the first part of reactor usually reaches 500 – 650 ℃ [32]. Currently, some scheme of adiabatic methanations have developed to commercial scale for example Air Liquide (formerly Lurgi), Haldor Topsøe (TREMP - Topsøe Recycle Energy-efficient Methanation model) (Figure 5), Clariant and Foster Wheeler, Johnson Matthey (Davy Technologies), etc. [34,40]. TREMP process uses three adiabatic FBRs and concentrates on high temperature methanation (<700℃). This model has applied at GoBiGas plant in Gothenburg (Sweden) [32].

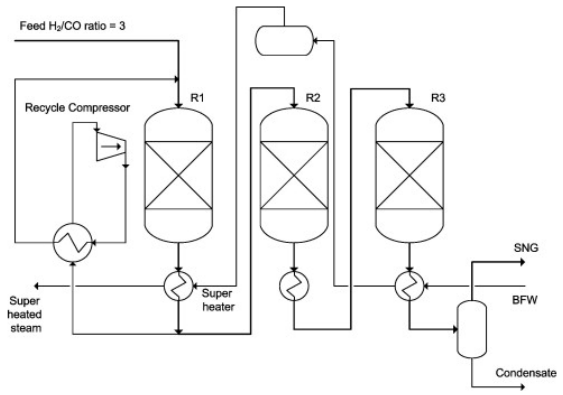

Figure 5. Haldor Topsøe's adiabatic fixed-bed reactors model with cooling and gas recycles system (TREMP model). [40]

In isothermal or cooled fixed-bed reactors, cooling mediums such as oil, steam or pressurized boiling water are utilized to decrease the high temperature (exothermic reactions) in reactors [41]. There are various types of cooled FBR, for instance, multi-tubular reactors or tube-cooled reactors [36]. Compared to adiabatic FBR, isothermal FBR has the potential to reduce complication of process. Nevertheless, temperature control and pressure drop still are drawbacks of isothermal FBR [36]. Additionally, isothermal reactors are more costly; however, this can be compensated for by the utilization of fewer reactors to accomplish the comparable CO_2 conversion and enhanced process temperature control [40]. Some companies such as Etogas and Linde have developed isothermal/cooled FRBs, but only Linde uses this technology for commercial purposes [36]. Figure 6 shows the process diagram of Linde SNG with the combination of two types of FBR. With this pathway, the CH_4 yield can be increased by using product of the isothermal reactor as the inlet of adiabatic one.

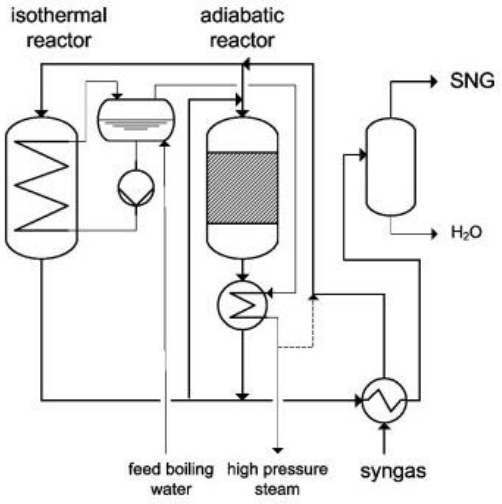

Figure 6. Process scheme of Linde with one isothermal and one adiabatic FBR. [40]

Fluidized-bed reactors offer better thermal management than FBR. Because of outstanding heat transfer, fluidized-bed reactors have almost isothermal temperature inside the reactor. Therefore, the reactor operation can be easily and simply managed [40]. In fluidized bed reactors, efficient solid mixing is accomplished, which significantly influences their performance. A remarkable characteristic of fluidized-bed reactors is their great feed flowrate flexibility that is important for P2M application to control feed load fluctuation. A challenge in this design is to ensure sufficient contact space between the fluidized bed and the heat exchanger to regulate the thermal produced during exothermic processes. In fact, lower bed diameter is necessary to guarantee bed fluidization because of the compression of

gas volume that occurs during methanation processes, which causes significant restrictions on internal heat exchanger. To mitigate the challenge, increasing fluidized bed size or reducing catalyst particle diameter could be applied [42]. Hervy et al. (2021) [42] investigated the thermodynamic, CO_2 conversion, and SNG quality of the fluidized-bed reactor and found that they are similar to or higher than in adiabatic FBR conventional process. Figure 7 illustrates the optimal model in Hervy et al. report. In which, a fluidized-bed reactor, a condensation stage, a recycle stream to reactor's inlet, and a low temperature polishing reactor were utilized.

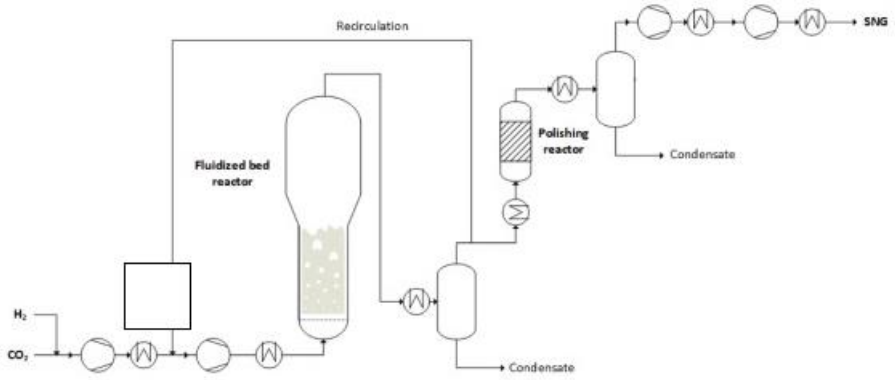

Figure 7. Process scheme of Hervy et al. report. [42]

Three-phase reactors were investigated as a potential concept for catalytic methanation [43, 44, 45]. A liquid, such as heat transfer oils like dibenzyl toluene, is generally injected into a slurry reactor, where small catalyst particles are suspended because of process fluid. The liquid's heat capacity enables accurate and efficient temperature management, fully eliminating heat reaction and allowing roughly isothermal operation of the reactor, which simplifies the process design. The issues associated with using slurry reactors arise from the evaporation and degradation of the suspension liquid as well as mass-transfer resistances in gas liquids [43].

A comparation of several methanation scheme was given by Rönsch et al. (2016) [32]. The primary difference among methanation units is the temperature pattern inside it. Typically, adiabatic, isothermal, and polytropic are three types of temperature patterns.

The temperature behavior of FBR without internal and external cooling is typically adiabatic, the appearance of hot spot as well as high reactor outlet stream temperatures. Gas recycle or injection steam are necessary because catalysts may be damaged at high temperature (550 –

700℃). The principal advantages are the ability to generate steam at high temperatures and the high reaction rate. But the procedure for design is quite intricate.

About isothermal reactors, fluidized bed and three-phase reactors have significant CO_2 conversion due to lower operation temperature. Besides that, catalysts are also less affected by thermal than in adiabatic reactors. However, low reaction rate and high catalyst consumption are drawbacks of these reactors. Hot spots usually appear near cooled FBR and micro-reactor's inlet. But temperature is lower than adiabatic reactors and the generated gas temperature is also moderated (around 300℃). These hot spots promote a higher reaction rate, and the lower product temperature allows a high conversion rate within thermodynamic boundary. However, polytropic reactors have the highest cost. Table 2 summaries the relevant information about reactors.

Table 2. Comparison among reactor technologies. [32]

Concept	*Adiabatic FBR*	*Cooled FBR*	*Micro-reactors*	*Fluidized-bed reactors*	*Three-phase reactors*
Types	Adiabatic	Polytropic	Polytropic	Isothermal	Isothermal
Reactor steps	2 – 7	1 – 2	1 – 2	1 – 2	1 – 2
Gas recirculation	Usually	Sometimes	No	Sometimes	No
Temperature range	250-700℃	250-500℃	250-500℃	300-400℃	300-350℃
State of catalyst	Packing	Packing	Coated	Fluidized	Fluidized or suspended
Particles size	Millimeters	Millimeters	<200 μm	100–500 μm	<100 μm
Mechanical stress of catalyst	Low	Low	Low	High	Moderate
Thermal stress of catalyst	High	Moderate	Moderate	Low	Low
Complexity of set up	High	Low	Low	Low	Low
Reactor costs	Medium	High	Very high	Low	Low-medium
Technology readiness level	9	7	4 – 5	7	4 – 5

Comparing the reactors performance, Gas Hourly Space Velocity (GHSV) can be utilized. However, to compare, the similar conversion rate should be similar in comparison [20]. In technical plants, the GHSV values for FBR are in range 2000 – 5000 h^{-1} and the higher GHSV can be reached in lab scale. The calculation of GHSV in catalytic methanation process is shown in (Eq. 9).

$$GHSV = \frac{F_{v,G,in}}{V_c} \quad \text{(Eq. 9)}$$

Where $F_{v,G,in}$ is the volumetric flow rate at STP of inlet gas with no appearance of inert gas and with ratio of H_2/CO_2. V_c is catalyst loaded volume.

3.1.2 Catalysts

In CO_2 methanation, an oxidized carbon (C^{4+}) reduces fully to CH_4 with C^{4-}, which means eight electrons involve in the reaction. Therefore, the reaction requires catalysts which are effective and efficient over the high kinetic obstacle [46]. As mentioned above, Nickel (Ni) was utilized as a catalyst in formation of CH_4 from CO_2 and H_2, reported by Sabatier and Senderens. Since 1902, many metals (in group 8 – 10) have been researched as catalysts in methanation process [32]. Mills and Steffgen (1974) [47] stated metals which are essential catalysts for methanation process including rhodium (Ru), Ni, iron (Fe), cobalt (Co), and molybdenum (Mo). Metals can be sorted based on their activities and CH_4 selectivity.

Metals' activity: Ru > Fe > Ni > Co > Mo [47]

CH_4 selectivity: Ni > Co > Fe > Ru [47]

The Ni/Al_2O_3 is the primary choice for catalytic methanation reactions [32]. Ni offers a high level of activity and selectivity for CH_4, and it is also cost-effective. One major drawback of Ni is its strong inclination to be oxidized in oxidizing environments, similar to non-noble metals Fe and Co. Furthermore, nickel carbonyl, a substance highly harmful to the human body, has the potential to be created. Although Fe is inexpensive, it exhibits poor CH_4 selectivity. Co exhibits decreased activity levels and comes with a higher price compared to Ni. While, Ru, which is a noble metal, possesses advantageous properties including high reactivity, CH_4 selectivity (in flexible temperatures), and strong resistance to oxidizing environments. Its primary disadvantage is the expensive cost which restricts its usage. [46]

Methanation catalyst activity is affected by the active metal, as well as supports, promoters, and preparation conditions, all of which are vital for achieving high catalyst activity and selectivity [46]. Metal oxide with large surface area, such as alumina (Al_2O_3), silica (SiO_2), or titania (TiO_2), are commonly applied for methanation catalysts. In which, Al_2O_3, particularly the γ-modification, is commonly utilized among them [46]. Alongside supported methanation catalysts, unsupported catalysts are also applied, for instance Raney-Nickel, which also requires high surface contacts to achieve adequate methanation activity [48]. Recently, several publications have presented results on different types of catalyst supports such as zeolites, foams, and biochar [32]. Typically, the active metal is placed onto a surface to increase the catalyst's area. A catalyst's high surface area is achieved by placing small active metal particles on large surface areas supports [32].

Garbarino et al. (2015) [49] studied CO_2 methanation by using commercial catalyst 3%wt Ru/Al_2O_3 from Acta S.p.A. The experiment was examined at GHSV = 15000 h^{-1} and T = 300°C; achieved 96% CH_4 selectivity without CO formation. Additionally, it was demonstrated that the catalyst remained highly active even after being started and stopped multiple times, indicating its potential for use in a discontinuous process. A comparation between Ni (4–20% wt) or Ru (1–5% wt) with alumina support was investigated by Quindimil et al. [50]. In the results, Ru catalysts demonstrated greater stability and activity; at 375°C, 4% wt Ru/Al_2O_3 led to 85% CO_2 conversion and the CH_4 selectivity that was consistently more than 98%.

The primary issue in any application using heterogeneous catalysis is the deactivation of catalysts. There are two types of deactivations: chemical and physical. Fouling, sintering, and attrition are physical phenomena deactivation [51]. Because attrition is caused by the catalyst particles rubbing against and with the reactor walls, it is a deactivation process that becomes significant when discussing fluidized bed reactors [51]. Sintering and fouling are the primary phenomena involved in CO_2 methanation. In general, catalysts are not able to tolerate temperatures higher than 550–700°C, and above that point, thermal sintering and the reduction in active surface area occur [51]. In contrast, lower than 230°C operating temperature combined with high CO partial pressure and Ni-catalyst results in the creation of extremely hazardous nickel tetra-carbonyl ($Ni(CO)_4$) and chemical sintering [52]. Nevertheless, by following manufacturer instructions and utilizing appropriate reactor strategy, these problems may be mostly prevented [33]. Volatile molecules may form,

leading to the reduction in the active phase and the potential release of hazardous substances from the reactor. During poisoning, contaminants can inhibit catalyst's active sites, which cause deactivation [32]. NiS is formed when inorganic sulfur compounds, such as H_2S, cause the active sites of catalysts are blocked. The H_2S level should be kept in range 10 – 100 ppb to prevent catalyst deactivation, which is less than the 500ppm tolerance limit for using biogas for heat and electricity cogeneration [32].

3.2 Biological Methanation

Biological Methanation (BM), which utilizes methanogenic microorganisms as biocatalysts, is another method for P2G [20]. Typically, BM's reaction is anaerobic and operates in an aqueous solution under atmosphere condition and temperature range from 20 (mesophilic) to 70℃ (thermophilic) [20].

As mentioned above, catalytic methanation has been established and applied to commercial scale since 2013, whereas BM has just been reached commercial scale from 2023 [53]. When compared to catalytic methanation, the BM operates under low temperature and exhibits a low volumetric mass transfer coefficient, therefore the reaction rate is also decreased [20]. In addition, inlet gas contains impurities, decreases the efficiency and quality of the final CH_4 product [54]; however, this is also an advantage of BM, the process can be operated under high tolerance of impurities such as sulfur or oxygen from CO_2 inlet stream [20]. Benefits result from the synergistic interaction of BM with the biogas system. The conversion of CO_2 to CH_4 in biogas results in a large increased calorific value following CO_2 reduction by H_2 injection in the process. As a result, BM may make converting biogas to high quality products less expensive [55].

In BM process, there are two technical methods that can be utilized (Figure 8). The first pathway is in-situ process, in which H_2 is injected into an anaerobic reactor and produced CO_2 can be covert to CH_4. On the other hand, injection simultaneously CO_2 and H_2 with H_2/CO_2 ratio 4:1 into digester is considered as ex-situ process [56]. Continuous stirred-tank reactors (CSTR), FBR, tricked-bed reactors, or membrane reactors can be utilized in BM [57]. These reactor types have the same limitation, which is low gas-liquid mass transfer of H_2 [57]. If the biological capacity for H_2 conversion reaches its limit, the concentration of dissolved H_2 may exceed endogenous levels. Consequently, increased concentrations of

dissolved H_2 can contribute to the formation of vapor fatty acids, inducing acidification within the reactor broth. This acidification has the potential to substantially diminish overall microbial activity and finally lead to process failure. [58]

In conclusion, as discussed in this section, the comparation between catalytic methanation and BM are listed in Table 3.

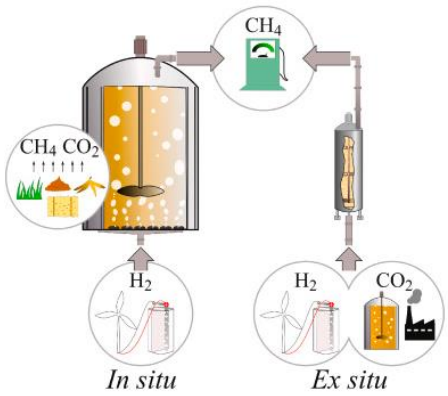

Figure 8. P2M process with in-situ and ex-situ concept. [57]

Table 3. Comparation of different methanation processes. [32,34,57]

	BM (ex-situ)	*Isothermal catalytic methanation*	*Adiabatic Methanation*
Production scale	Commercial	Average plants	Commercial (>100MW)
Advantages	High tolerance of impurities, Low temperature operation	Waste heat can be recycled, Simple setup	High valuable steam can be generated
Disadvantages	Large reactor volumes are needed, Mass transfer in gas-liquid phase of H_2	Mass transfer resistances	Complex setup, High costs

4 Modelling of Catalytic Methanation

The reactor is an essential factor in all chemical transformations. The modeling and simulation are crucial for a commercial scale-up and are frequently the creative aspect of the entire process [32]. A description of the fundamental kinetic reactions for CO_2 methanation is provided in this section. There are many research and results about kinetic reactions in CO_2 methanation. Nevertheless, kinetic reactions in CO methanation (including RWGS reaction) are preferred despite approaching new rate equations for CO_2 methanation [59].

P2G projects are attracting attention over the world [60], and in this section, some essential concepts are described. Both catalytic and biological methanation are considered, but in this chapter the catalytic methanation will be focused.

4.1 Reaction kinetics

Langmuir-Hinshelwood-Hougen-Watson (LHHW) rate equations type or power-law are applied to develop reaction kinetics [59]. These equations were developed based on different catalysts, reactors, or operating conditions. Table 4 lists the information of main kinetic models, in which operating conditions, reactor parameters, and catalysts are given in detail.

Table 4. Kinetic model for CO2 Methanation using Ni-based and Ru-based catalysts. [61,59,62,63]

Model	Catalysts	Temperature	Pressure	Reactor
Xu & Froment	15% Ni/$MgAl_2O_4$, D_p = 018 – 0.25mm	300 – 400 ℃	3 – 10 bar	FBR
Kopyscinski	50% Ni/Al_2O_3, D_p < 45 µm	280 – 360 ℃	2 bar	Channel flow reactor
Koschany et al.	Ni/$Al(O)_x$, D_p = 0.15 – 0.2mm	180 – 340 ℃	1 – 15 bar	FBR
Falbo et al. modification	0.5 wt.% Ru/γ-Al_2O_3, D_p = 3.2mm	204 – 371 ℃	1.01 bar	FBR

4.1.1 Xu & Froment model

The rate-based model for the steam methane reforming (SMR) process was presented by Xu and Froment (1989) [61], and it was developed using a 15.2% Ni/$MgAl_2O_4$ catalyst. LHHW equations were put out for RWGS (Eq. 11) and CO and CO_2 hydrogenation ((Eq. 10) and (Eq. 12)). In the kinetic experiments, 0.4 g of catalyst was ground into particles with sizes ranging from 0.18 to 0.25 mm and added to 8 mL of α-Al_2O_3. The diameter of the reactor in operation is 1.07 cm. In a fixed-bed reactor, the kinetic data for the methanation process was evaluated for temperature ranges and pressure ranges of 300 – 400℃ and 3 – 10 bar, respectively. The main barrier to this kinetic model's applicability to CO_2 methanation is that, because these data were obtained for the SMR, which is typically carried out at temperatures of 482℃ or above, the rate is restricted at low temperatures (< 371℃).

- CO methanation

$$r_1 = k_1 \frac{p_{H2}^{-2.5}\left(p_{H2O}\cdot p_{CH4} - \frac{p_{H2}^3 \cdot p_{CO}}{K_1}\right)}{DEN^2} \qquad E_{A1} = 240.1 \text{ kJ mol}^{-1} \qquad \text{(Eq. 10)}$$

- RWGS

$$r_2 = k_2 \frac{p_{H2}^{-1}\left(p_{CO}\cdot p_{H2O} - \frac{p_{H2}\cdot p_{CO2}}{K_2}\right)}{DEN^2} \qquad E_{A2} = 66.1 \text{ kJ mol}^{-1} \qquad \text{(Eq. 11)}$$

- CO_2 methanation

$$r_3 = k_3 \frac{p_{H2}^{-3.5}\left(p_{H2O}^2\cdot p_{CH4} - \frac{p_{H2}^4 \cdot p_{CO2}}{K_1 . K_2}\right)}{DEN^2} \qquad E_{A3} = 243.9 \text{ kJ mol}^{-1} \qquad \text{(Eq. 12)}$$

$$DEN = 1 + K_{CO}.p_{CO} + K_{H2}.p_{H2} + K_{CH4}.p_{CH4} + \frac{K_{H2O}.p_{H2O}}{p_{H2}} \qquad \text{(Eq. 13)}$$

The equations' rate constants k_1, k_2, k_3 are expressed in terms of temperature and reported in (Eq. 14) to (Eq. 16).

$$k_1 = 9.49 \times 10^{16} \exp\left(-\frac{28879}{RT}\right) \qquad \text{(Eq. 14)}$$

$$k_2 = 4.39 \times 10^{4} \exp\left(-\frac{8074.3}{RT}\right) \qquad \text{(Eq. 15)}$$

$$k_3 = 2.29 \times 10^{16} \exp\left(-\frac{29336}{RT}\right) \qquad \text{(Eq. 16)}$$

K_{CO} , K_{CH4}, K_{H2} , K_{H2O} are the surface adsorption constants in equilibrium (Eq. 17) to (Eq. 20).

$$K_{CO} = 8.11 \times 10^{-5} \times \exp\left(\frac{70230}{RT}\right) \quad \text{(Eq. 17)}$$

$$K_{CH4} = 1.995 \times 10^{-3} \times \exp\left(\frac{36650}{RT}\right) \quad \text{(Eq. 18)}$$

$$K_{H2} = 7.05 \times 10^{-9} \times \exp\left(\frac{82550}{RT}\right) \quad \text{(Eq. 19)}$$

$$K_{H2O} = 1.68 \times 10^{4} \times \exp\left(-\frac{85770}{RT}\right) \quad \text{(Eq. 20)}$$

K_1 , K_2, K_3 are the equilibrium constant of methanation reactions (Eq. 21) to (Eq. 23).

$$K_1 = 10266.76 \times \exp\left(\frac{26830}{T} + 30.11\right) \quad \text{(Eq. 21)}$$

$$K_2 = \exp\left(\frac{4400}{T} - 4.063\right) \quad \text{(Eq. 22)}$$

$$K_3 = K_1 K_2 \quad \text{(Eq. 23)}$$

4.1.2 Kopyscinski model

Kopyscinski model [59] has been developed and applied to CO_2 methanation. The reactor is constructed up of a channel flow reactor with a metal plate attached at the bottom that has been coated with catalyst. A commercial catalyst with a 50% Ni/Al2O3 content was utilized to coat the plate. For the experimental studies, a total of 57 – 246 mg of catalyst and diameter smaller than 45 μm were utilized. All kinetic tests were completed at different temperatures in range 280 to 360 ℃ and pressures of 2 bar. CO methanation's rate and water gas shift rate is illustrated in (Eq. 24) and (Eq. 25).

- CO methanation

$$r_1 = k_1 \frac{K_C \cdot p_{CO}^{0.5} \cdot p_{H2}^{0.5}}{(1 + K_C \cdot p_{CO} + K_{OH} \cdot p_{H2O} \cdot p_{H2}^{-0.5})^2} \qquad E_{A1} = 74.1 \text{ kJ mol}^{-1} \quad \text{(Eq. 24)}$$

- Water-gas shift

$$r_2 = k_2 \frac{K_a \cdot p_{CO} \cdot p_{H2O} - \frac{p_{CO2} \cdot p_{H2}}{K_{eq}}}{p_{H2}^{0.5} \cdot (1 + K_C \cdot p_{CO} + K_{OH} \cdot p_{H2O} \cdot p_{H2}^{-0.5})^2} \qquad E_{A2} = 161.6 \text{kJ mol}^{-1} \quad \text{(Eq. 25)}$$

The rate constants k_1, k_2 are defined in terms of temperature as (Eq. 26) and (Eq. 27).

$$k_1 = 3.34 \times 10^6 \exp\left(-\frac{74000}{RT}\right) \quad \text{(Eq. 26)}$$

$$k_2 = 3.0421 \times 10^4 \exp\left(-\frac{161740}{RT}\right) \quad \text{(Eq. 27)}$$

K_{OH} , K_c are the surface adsorption constants in equilibrium (Eq. 28) and (Eq. 29).

$$K_{OH} = 3.97 \times 10^{-7} \exp\left(\frac{72650}{RT}\right) \quad \text{(Eq. 28)}$$

$$K_c = 8.1 \times 10^{-6} \exp\left(\frac{61200}{RT}\right) \quad \text{(Eq. 29)}$$

K_a is a combination of the adsorption constants of CO, H_2, CO_2 and H_2O or OH, while K_{eq} is the equilibrium constant of water-gas shift reaction (Eq. 30) and (Eq. 31).

$$K_a = 9.3 \times 10^{-2} \exp\left(\frac{6500}{RT}\right) \quad \text{(Eq. 30)}$$

$$K_{eq} = \exp\left(\frac{4400}{RT} - 4.063\right) \quad \text{(Eq. 31)}$$

4.1.3 Koschany et al. model

Koschany et al. (2016) [62] introduced the reaction rate equations for CO_2 methanation utilizing the co-precipitated $Ni/Al(O)_x$ catalyst. Kinetic results were completed by using particles of 0.15 – 0.20 mm dissolved 1:9 with carborundum (SiC). The reactor utilized has an inner diameter of 4 mm. 258 results were emplyed to estimate the parameters for the formation of CH_4 rate in temperature between 180 – 340℃ and the 1 – 15 bar pressure range. Several kinetic methods were created. Power-law rate equations with inhibitors, such as water, and the LHHW model (Eq. 32) have been proven to be valid throughout several different situations, from low conversion to thermodynamic equilibrium. The kinetic parameters are shown in Table 5.

$$r = k\,\frac{p_{CO2}^{0.5}.p_{H2}^{0.5} - \frac{p_{CH4}.p_{H2O}^2}{p_{CO2}^{0.5}.p_{H2}^{3.5}.K_{eq}})}{(1 + K_{OH}.\frac{p_{H2O}}{p_{H2}^{0.5}} + K_{H2}.p_{H2}^{0.5} + K_{mix}.p_{CO2}^{0.5})^2} \qquad E_A = 77.5\text{kJ mol}^{-1} \quad \text{(Eq. 32)}$$

The equilibrium constant (K_{eq}) is calculated by (Eq. 33). [62]

$$K_{eq} = 137 \exp\left(\frac{158700}{RT}\right) T^{-3.998} \quad \text{(Eq. 33)}$$

Table 5. Predicted parameters used in Koschany et al. model with the reference temperature T_{ref} = 282℃. [62]

k_0	K_{OH}	ΔH_{OH}	K_{H2}	ΔH_{H2}	K_{mix}	ΔH_{mix}
3.46×10^{-4}	64.1	22.4	0.115	-6.2	0.1	-10

Note: ΔH_i are the adsorption constant, unit kJ mol^{-1}, K_i are the surface adsorption constants in equilibrium, unit $bar^{-0.5}$.

4.1.4 Falbo et al. modification to Lunde & Kester model

In 1973, Lunde & Kester introduced a kinetic model (Eq. 34) for CO_2 methanation using 0.5 wt.% Ru/γ-Al_2O_3 catalyst [64]. The experiment was taken place with atmosphere pressure and temperature between 204 – 371℃. The catalyst particles were utilized with size 6.4mm×6.4mm cylindrical pellets. Falbo et al. (2017) [63] (Eq. 35) developed this model based on previous study. In this development, an extra parameter (α) was evaluated in kinetic terms to account for the decrease in active site caused by water adsorption [63]. The kinetic model is based only on CO_2 methanation, because CH_4 selectivity is nearly optimal in all experimental settings under given catalyst.

- Lunde & Kester Ru-based kinetic model

$$r_{CO2} = k\,(p_{CO2}^{n}.p_{H2}^{4n} - \frac{p_{CH4}^{n}.p_{H2O}^{2n}}{(K_{eq}(T))^{n}}) \qquad E_A = 68.1 \text{ kJ mol}^{-1} \qquad \text{(Eq. 34)}$$

- Falbo et al. modified model

$$r_{CO2} = \frac{k}{1+\alpha.p_{H2O}}(p_{CO2}^{n}.p_{H2}^{4n} - \frac{p_{CH4}^{n}.p_{H2O}^{2n}}{(K_{eq}(T))^{n}}) \qquad E_A = 75.3\text{kJ mol}^{-1} \qquad \text{(Eq. 35)}$$

The kinetic model parameters of two kinetic equations are listed in Table 6.

Table 6. Kinetic parameters of two models with the mean percentage error (MPE) [63,64]

	E_A (kJ mol^{-1})	n (_)	α (1/ata)	MPE (%) (*)
Lunde & Kester	68.1	0.14	_	5.11
Falbo et al.	75.3	0.152	0.91	2.76

(*) The mean percentage error (MPE) is the calculated average of percentage errors between a model's forecasts and the actual values of the quantity being forecasted.

4.2 Process modelling

Research of SNG-producing plants that rely on simulations inherently involves methanation modeling (Figure 2). The main goals of these studies include comparing concepts, integrating process and heat, estimating performance, and gathering data for technological as well as economic evaluation. In addition, the operation conditions are also important parameters to evaluate the whole methanation process. The investigation of dynamic behavior is critical for estimating the necessary time for the design to approach steady-state conditions and monitoring the temperature profile across the methanation equipment [65]. Hot spot needs to be prevented since excessively high temperatures could potentially damage the catalyst, resulting in catalyst deactivation [65]. Essentially, modeling and simulation activities focus on four goals: process design, process evaluation, process optimization, and process adaptability [32].

Process design is an important aspect of computer-aided tasks in chemical engineering. Key design characteristics for methanation reactors include reactor size and the place of gas injectors or cooling systems. Because of the exothermic behavior of methanation processes, the temperature of the reactor is of particular relevance. Reactor design (diameter, length, cooling, and insulation), process structure (residence time, feed gas content), and catalysts can define reactor temperature. [32]

Process evaluation relates to the performance and economic aspects of methanation process. Simulation-based process settings involving temperature, product composition, and heat of reactions are frequently used to evaluate the effectiveness of methanation process (for example, efficiency, steam output, CO_2 conversion, CH_4 selectivity, and yield). For financial assessments, these data are supplemented with design requirements including reactor size as well as additional financial factors (material costs) [32]. For instance, Konttila [66] minimized the cost of P2M process with dynamic modelling in order to determine the reliability of transient P2M.

Process optimization (simulate-based) is based on modification of parameters using steady-state simulation models. Feed gas and fluid's parameters such as content, temperature, flow rate, pressure are modified [3,37,38,39].

Process adaptation: Existing process developments rely mainly on CO methanation proposals from the 1970s and 1980s. It's especially accurate for the recent CO_2 methanation processes used in P2G facilities. Modeling and simulation are used to investigate how reactor design and operation concepts could be applied to current CO_2 methanation operations. [67,68,69]

4.2.1 Dynamic modelling

Discontinuous hydrogen generation via the P2G process results in intermittent operation. Therefore, simulation models are utilized to evaluate and predict the behaviors of relevant reactors caused by variations in feed flow or reactor start-up over the time [65,70,71,72]. Mathematically, dynamic behaviors can be stated by using differential equations. As discussed in previous section, P2X technologies offer great promise for long-term energy storage and potential development for chemical synthesis. Nevertheless, these processes are fundamentally dynamic due to fluctuations in RES input, and therefore H_2 generation. As a result, developing a well-performing dynamic design for the P2M plant is essential before designing the pilot plant and, eventually, a commercial facility [65].

The usual issues generated by intermittent methanation processing in fixed-bed reactors include moving hot spots and wrong-way behavior. Moving hot spots occurs in case of increasing in the feed loads or feed compositions that leads to the shift of the reaction zone to downstream. In this phenomenon, the reactor is possibly extinguished by high-temperature and reaction zone explosion. Whereas wrong-way phenomenon happens when a lower temperature is applied to the reactor’s feed stream, reducing reaction rates and increasing reactant concentrations. These higher concentration reactants move downstream faster, resulting in increasing reaction rates and elevated temperatures at the reactor’s downstream. These are reactions caused by changes in input factors including loading flow, temperature, and pressure. These occurrences have several disadvantages, including damaged catalysts, faster deactivation due to sintering, poisoning, or carbon deposition, initiation of exothermic processes, and decreased CH_4 selectivity. All phenomena above may lead to crucial economic consequences, and the reactor's safe operation may be affected in many circumstances [73].

Volatile temperatures in the reactor over transient operation are harmful to the quality of CH_4. For example, dynamic catalytic methanation process was simulated and evaluated by Colelli et al. (2024) [70] using Aspen Plus Dynamics. In the report, adiabatic and cooled configurations were utilized to study dynamic behaviors. The control systems of feed stream, and cooled configuration are shown in Figure *9*. The dynamic models are developed based on steady-state models. In cooled configuration, two cooled reactors were employed (p = 34 bar at bubble point, T = 242 ℃) to produce CH_4 from pure H_2 and CO_2 with the H_2/CO_2 ratio of 4.3. In the result, CO_2 molar fraction, H_2 volumetric fraction, Wobbe Index (WI), and CO_2 conversion were recorded during load changes (±5%, −30%). The WI accurately represents the heating value of SNG entering from the gas pipe at the point wherein the burner is installed [74], the lower and upper WI of CH_4 in Finland is 47 and 54 MJ/m^3, respectively [75].

To maintain the small over-stoichiometric number, the H_2 flowrate was controlled by "FC_H2" controller with the adjustable set point value, and the CO_2 flowrate controller ("FC_CO2", slave) values are provided by block R following values H_2 flowrate. Figure 9 shows the control structure which was used in Colelli et al. report, and this feed streams control scheme was utilized for cooled configuration. Only cooled configuration is considered in this thesis.

In case of cooled configuration, pressure controller was utilized in both reactors, and flashes for safety (Figure 10). In addition, level control was also used for flash drums and all required valves as the last control components were calibrated and their control response was determined.

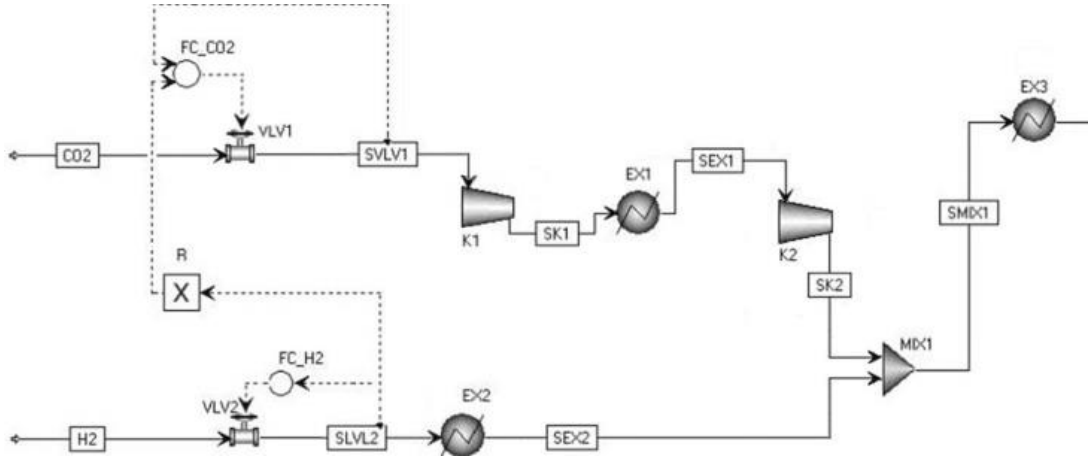

Figure 9. Control structure of feed streams to the process with H_2 flowrate is 750 Nm^3/h and CO_2 flowrate is 175 Nm^3/h. [70]

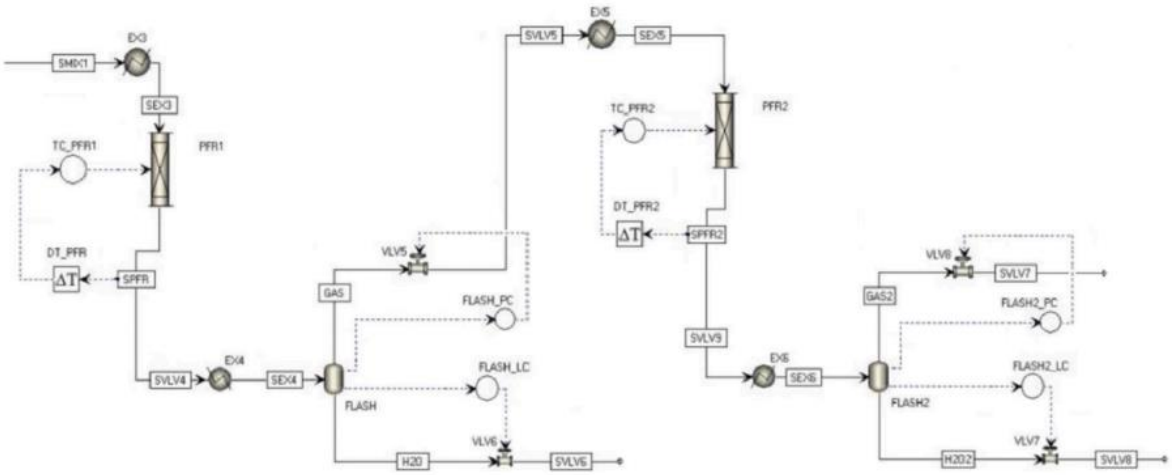

Figure 10. Control structure of CO_2 methanation in cooled configuration by using pressure, temperature controllers for reactor, drum; and valves for pressure control. [70]

In this simulation, Colelli et al. [74] varied the inlet H_2 load (±5% and –30%) after 15 minutes from the beginning. The results of cooled configuration are shown in Figure 11. The trend of CO_2 conversion was almost the same as adiabatic configuration results. When the H_2 load decreases by 5% and 30%, the CO_2 conversion in reactor 1 was higher than in steady state due to higher residence time, besides that, the coolant flow rates also decreased. On the other hand, when increasing H_2 load by 5%, the coolant flow rate inside reactors gained and the CO_2 conversion in reactor 1 went down, but in total after changing H_2 loads, the CO_2 conversions in whole process are always higher than 99.5%.

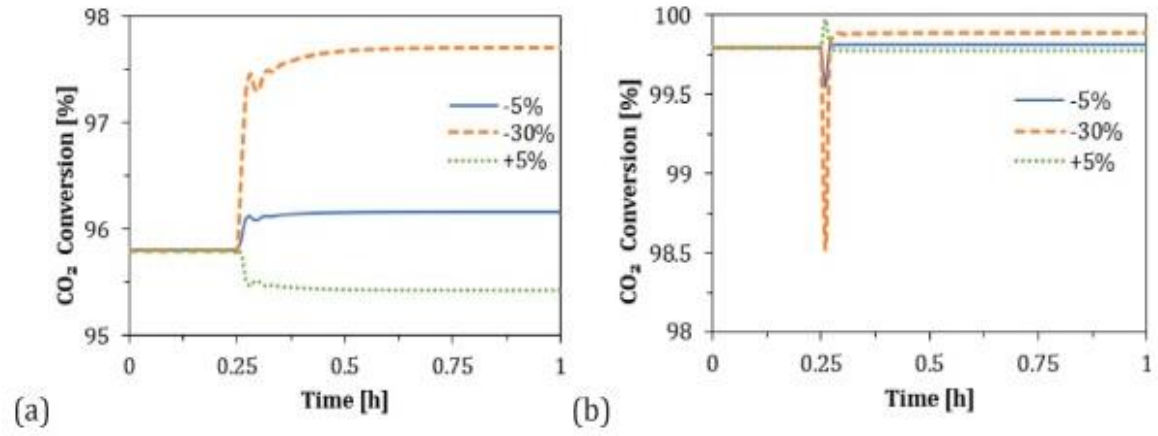

Figure 11. CO_2 conversion results for reactors 1 and 2 in the cooled scheme, respectively. [70]

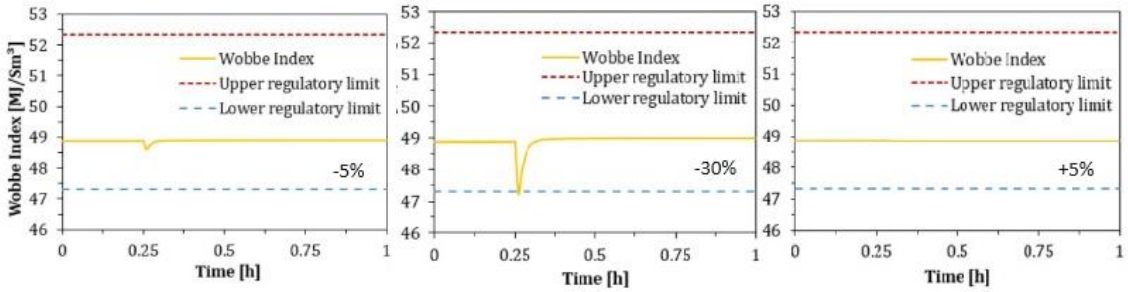

Figure 12. The WI results during H_2 load changes in cooled scheme. [70]

As can be seen from Figure 12, the WI in cooled configuration generally is in CH_4 grid requirements, in case of –30% H_2 feed load, the WI had small excess the limitation. In this experiment, the comparison between two schemes was also discussed. For slight decreasing in H_2 load (–5%), it is obvious that both designs meet the requirements of the regulation (Figure 13). However, the cooled design showed relatively milder fluctuations in response to the disturbance than the adiabatic design. Additionally, in cooled reactors, the H_2 concentration in product stream slightly reduces (Figure 13b). In contrast, adiabatic reactors can generate the product with a greater WI and a smaller mol-% of CO_2 (Figure 13a and c).

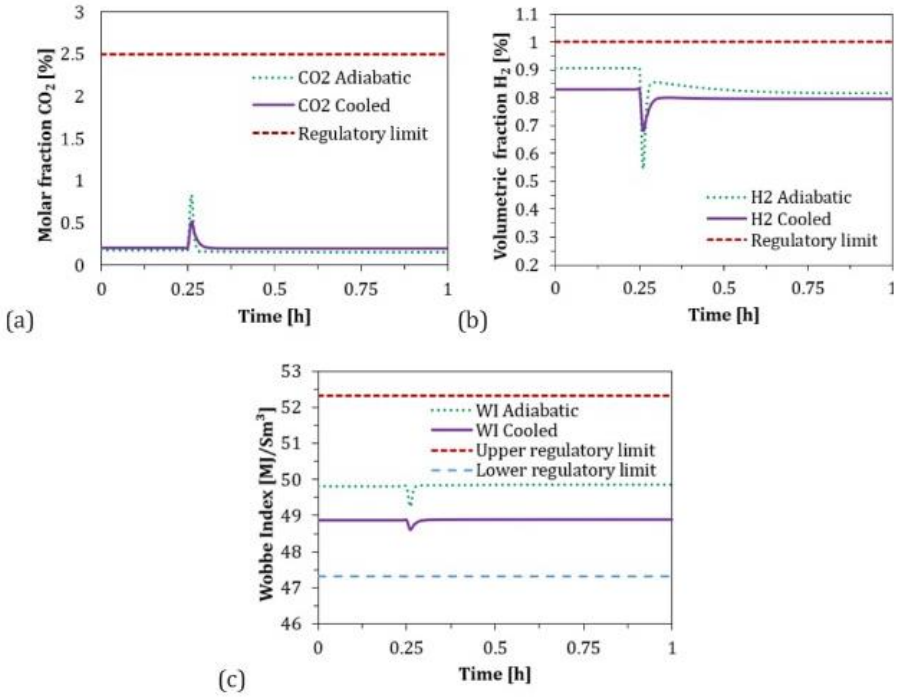

Figure 13. The differences in the results of configurations in H_2 load (–5%). [70]

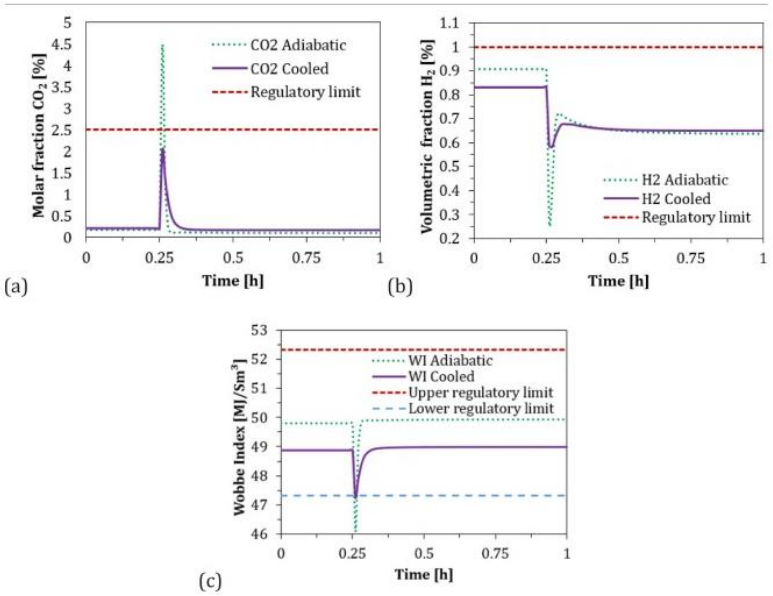

Figure 14. The differences in the results of configurations in H_2 load (–30%). [70]

In case of a quite significant decreasing in H_2 load (–30%), neither setup permitted the injection of CH_4 into the network during the transient. In the transient, the adiabatic setup surpasses both the value of the WI (Figure 14c) and the mole fraction of CO_2 (Figure 14a), but the cooled one only surpasses the WI. In the novel steady phase, the concentration of the reactants in the gas is basically equal; however, the WI is greater in adiabatic configuration.

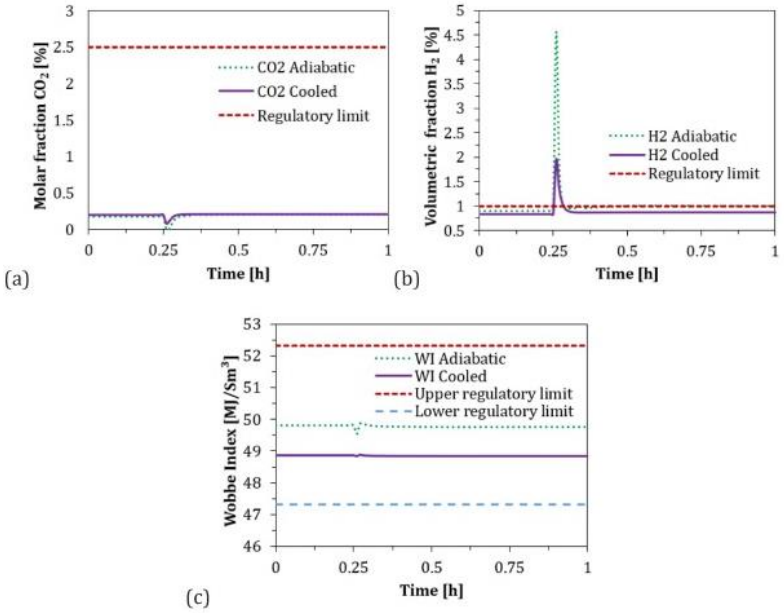

Figure 15. The differences in the results of configurations in H_2 load (+5%). [70]

In the last H_2 load changing variable (+5%), the adiabatic setup cannot introduce product both during the transient as well as the steady phase, even when the WI fell completely within the limits (Figure 15). In fact, the first high point of H_2, coordinating with the shock (Figure 15b), did not lead to equilibrium during the desired range, as demonstrated in the other two experiments. The volumetric fraction of H_2 stabilizes slightly above the upper threshold, indicating the system's limitation.

The start-up time is essential for transient methanation operations. It is necessary to investigate if the reactor might be affected by shutting down or restarting without any inert gases inside reactors. To guarantee catalyst preservation, flushing the reactors with H_2 or an inert gas was recommended [32,38,65]. To prevent the generation of nickel carbonyls, the reactor temperature should be above 200℃ [20]. Thermal ramps are important to take into account because rapid heating might produce thermal stress in the reactor. Frank et al. calculated the highest temperature increment in P2G plant modelling is 50℃/h or 10%/h [76]. Temperature management is particularly important in dynamic operations since load variations typically result in substantial temperature fluctuations. Since catalysts cannot withstand high temperatures for extended periods, the reactor must respond quickly to rising temperatures [20]. As mentioned above, Ni-based catalysts can be damaged by high temperatures in range 550 – 700℃ [51].

CO_2 staging is a pathway in which part of the CO_2 in inlet stream is delivered to the first reactor. The remaining part of the feed skips and passes to the next reactors. The approach helps improve thermal control since the reactants provided to the process are controlled [65]. Giglio et al. (2021) [65] used CO_2 staging method and evaluated the warm start-up for cooled FBR design. In this report, a series of three reactors was utilized with equal temperatures as coolants temperature (240℃). The process was completed when the CH_4 concentration in product stream reached 95 mol-%. Two scenarios were applied: hot standby and partial load. In the first scenario, in fact, when the methanation section was not operating, but to maintain the fast start-up, this scenario is applied. Three reactors were operated simultaneously, by this method, steady state was achieved after 60 seconds. In addition, another case was also applied, each of the three reactors was started sequentially, once the preceding reactor had reached steady-state conditions.; and the steady state of whole process reached after 130 seconds starting. To compare two cases of the first scenario, the temperature profiles in reactor 2 were used. As can be seen from Figure 16, in first case, the hot spot (650℃)

appeared after 20 seconds, and the equipment might be damaged. This spot occurred because the first reactor did not reach a steady phase and CO_2 partial pressure in reactor 2 would be over the limitation. Whereas, in case of one-by-one starting, the hot spot was prevented because reactor 1 reached a steady state and the CO_2 concentration at feed stream of reactor 2 was stable.

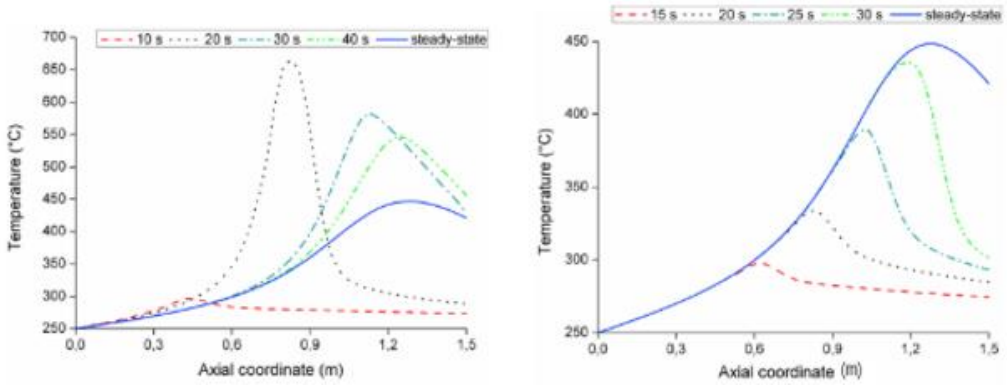

Figure 16. Temperature profiles of CO_2 methanation in cooled FBR (reactor 2) with two cases of hot standby scenario. [65]

In Giglio et al. [65] report, they also investigated dynamic behaviors of reactor in partial load. To improve the system's rangeability and prevent hot spot (more than 550℃) across the catalytic bed, CO_2 staging might be modified relative to the original steady state model: a portion of CO_2 might be injected to both the first reactors. Thus, the methanation reactors were safely operated at 45% to 100% of its normal load. At the lowest allowable partial load (45%), the proportion of CO_2 injected into third reactor is 22 mol-% of the stoichiometric feed flow.

In addition, another method, gas products recycling, was also applied to investigate dynamic methanation process. Matthischke et al. (2018) [77] examined the effects of recycling ratio (Rec) in a cooled FBR for CO_2 methanation. In the experiment, the Rec was set in range 0.05 to 5. Figure 17 and Figure 18 illustrates the experiment results.

From Figure 17, it can be clearly observed that Rec had negative effects on cooled FBR in terms of CH_4 concentration, however, these ratios helped to mitigate hot spots in cooled fixed bed reactors. Authors also gave a recommendation about recycle ratio in cooled FBR that uses a small Rec between 0.05 to 0.1 and suitable load velocity to reduce the catalyst bed temperature (Figure 18). Furthermore, an additional stream (dilution of 10% N_2, CH_4, or H_2O) was used to compare with Rec of 0.1, and the catalyst bed temperature decreased

by the dilutions based on its heat capacity (Figure 18). In the high CO_2 conversion scenario, the recycle stream consisted of 33% CH_4 and 67% H_2O (no water removal), which explained the lower catalyst bed temperature.

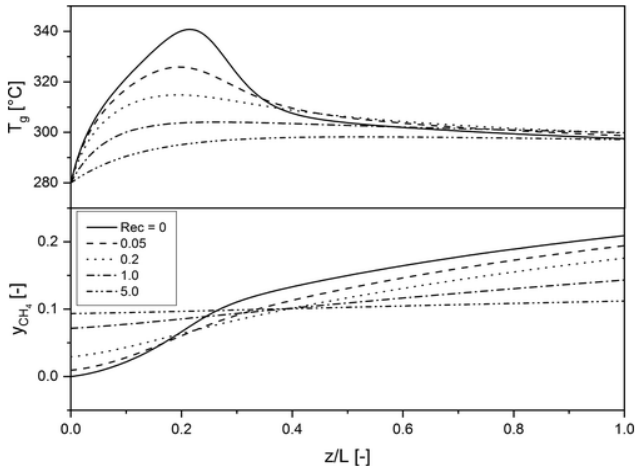

Figure 17. Profiles of gas temperatures and CH_4 concentration for various recycle ratio in cooled reactor. [77]

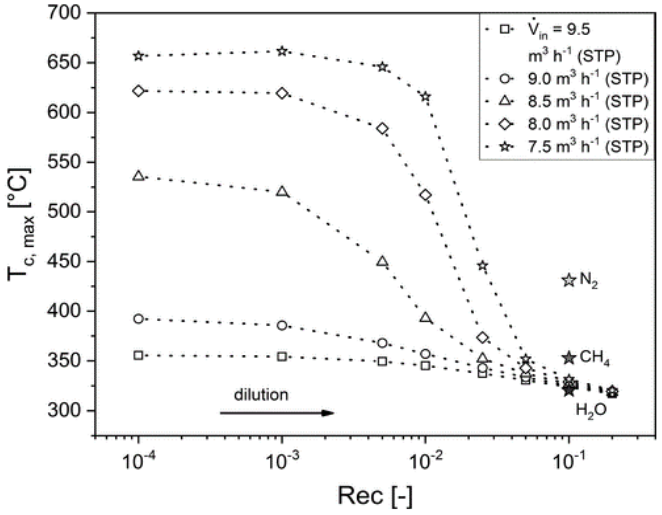

Figure 18. Catalyst bed temperature for various recycle ratios and feed stream flow rates (T = 300°C) in CO_2 methanation by cooled FBR, and effects of pure dilution (dilution of 10% N_2, CH_4, or H_2O in additional stream) on temperature (star marks on the right side). [77]

In this report, Matthischke et al. [77] also studied loading changes in methanation process. The authors used the H_2 load flow rate from 40% – 100% to evaluate the catalyst bed's temperature and quality of CH_4 in the process (Figure 19). In case of cooled reactor, a

constant temperature (T = 290°C) was applied while inlet velocity was 0.6 – 1.5 m s^{-1}. And the results showed that decreasing velocity increased CO_2 conversion up to 91.7% and hot spot was observed when using lower velocity of feed stream.

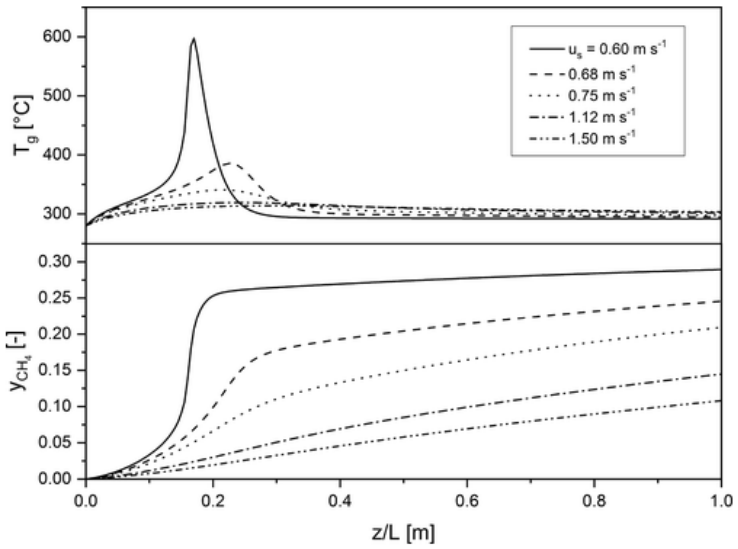

Figure 19. Temperature profile and CH_4 content in cooled FBR for different load flow with Rec = 0. [77]

In cooled FBR, coolant temperature can be adjusted to match fluctuating feed flow rates, allowing for greater thermal control. In case of reduction of the feed load, wrong-way behavior occurs, resulting in increased temperature. To minimize temperatures that lead to catalyst damage and significantly lower conversion, the cooling fluid temperature can be reduced [78]. Fischer & Freund (2020) [78] reported dynamic behaviors of wall-cooled tubular FBR. In an experiment, inlet load dropped feed rate from 100% to 50%. There were 6 cases, in total, used to evaluate the problem. As a result, the case, which used 10 seconds and 5 seconds as time constant and dead time respectively, was the optimize scenario. Figure 20 shows the results of applied case, coolant temperature decreases following the capacity drop and the temperature needs 50 seconds to reach a new steady state, the phenomenon is caused by dead time and slow temperature adjustment, approximately 60 seconds for changing loading rate from 100% to 50% to reach new steady state phase. On other hand, the temperature inside the reactor firstly increases after that the profile.

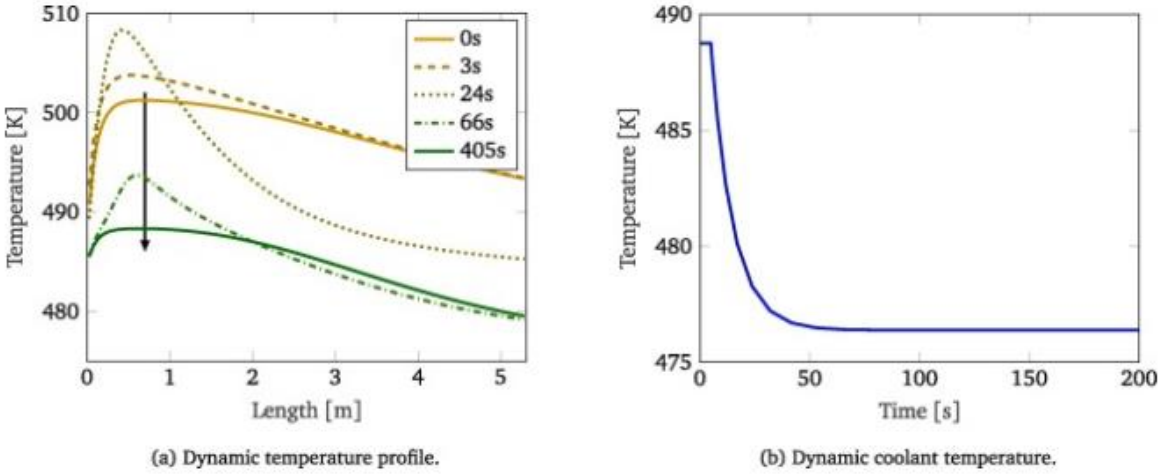

Figure 20. Temperature profile of cooled FBR and coolant in the Fischer and Freund research. [78]

Additionally, catalysts dilution or known as core-shell method is applied to control thermal problems in CO_2 methanation process [79,80]. Catalyst dilution is designed to replace certain catalyst particles with inert one to minimize the catalyst's local volumetric activity and hence the reaction rate and released temperature are reduced [79,80]. Zimmermann et al. (2021) [80] examined FBR's load-flexible by using fixed-bed dilution method. In the experiment, CO_2 load was changed in range from 30% to 100% with six different cases to evaluate the results (Figure 21). As can be observed in Figure 21, core-shell particles case (2a) reached the new steady state earlier than diluted fixed-bed case (1a). Aside from temporarily restricted conversion in increasing load changes, the temperature profile fluctuates slightly before settling into the new stable phase. The fluctuation is more obvious in the reactor with a uniformly diluted fixed bed (1a), particularly during decreasing variation in load. Significantly, more fluctuations in temperature properly over the permissible temperature limit occur during decrease load changes in reactors with two fixed-bed segments, the first of which is partially diluted with inert material (case 1b). The selection of core-shell particles in the first segment (case 2b) is preferred. For reactors with infinite fixed-bed segments (cases 1c and 2c), negative load fluctuations result in severe temperature overshoot. With diluted fixed bed (case 1c), the hot spots cross a substantially longer distance, with the temperature profile peaking in the second half of the single arc. On the other hand, with core-shell catalyst particles (case 2c), the hot spot temperatures promptly reduce, and the new steady phase is achieved considerably quicker than in case of employing a diluted catalyst bed.

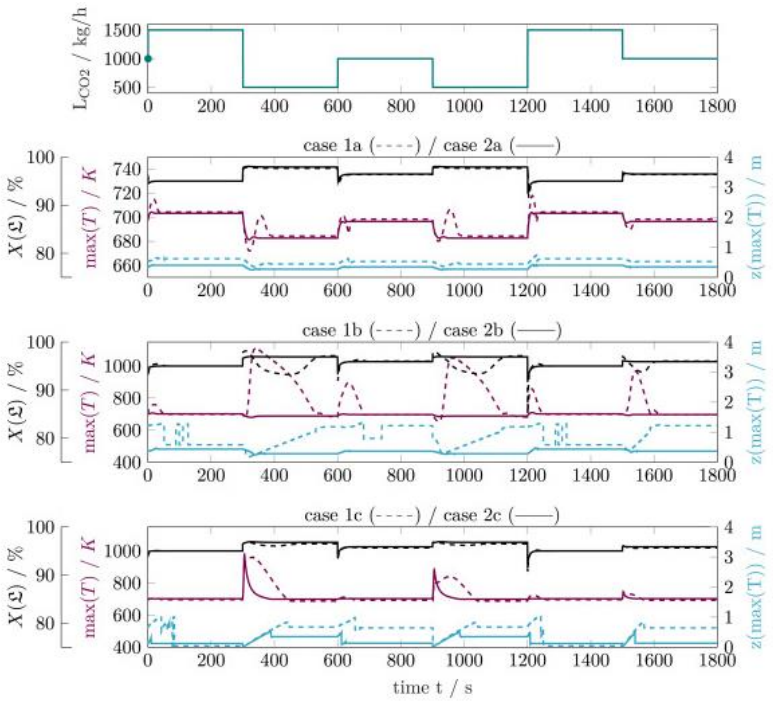

Figure 21. Dynamic performance of variation feed load, output conversion, peak temperature, and location for multi-period optimal scenarios. (fixed bed dilution is denoted as case 1; core-shell particles are denoted as case 2; sub-case **a** used uniform catalyst bed in whole reactor; sub-case **b** used 2 continuous beds with different compositions; in sub-case **c**, the dilution ratio and shell thickness varied along the length of reactor) [80]

The summary of discussed dynamic models in CO_2 methanation is given in Table 7.

Table 7. Summaries of dynamic modelling in CO_2 methanation process.

Author(s)	Method	Results
Colelli et al. [70]	Aspen Plus and Aspen Plus Dynamics were used to create adiabatic and cooled configurations of CO_2 methanation. The H_2 feed flows rates were changed by ± 5% and −30% after 15 minutes of operation time and the quality of CH_4 was evaluated.	When H_2 feed load decreased by 5%, the CH_4 quality was within the limit range of SNG in both configurations. The high CO_2 conversion was also achieved in the last reactor leading to high purity CH_4 in product stream. In case of increasing H_2 feed load by 5%, the H_2 volumetric fraction crossed over the limitation. However, in the cooled configuration, after transient period, the quality of CH_4 was still in limitation range. The last case applied 70 % of feed load, the configuration produced CH_4 with better WI value, but both configurations were over limitations of CH_4 quality.
Giglio et al. [65]	CO_2 staging method was applied to examine dynamic behaviors of cooled FBR and warm startup; partial load was also evaluated. The partial H_2 feed load changed in the range 45% to 100%. Reactors were controlled under 550℃ and CO_2 was fed to each reactor to maintain the target temperature.	The reactors were started one by one after the previous one reached a steady state. By this method, the catalyst stability was maintained and the new steady state for system was 130s and the products reached the SNG quality. When applying partial loads in range 45% to 100%, the quality of CH_4 always reached the target quality. However, when the load was 45% load, the temperature inside three reactors was close to peak temperatures (550℃).

Table 7. Summaries of dynamic modelling in CO_2 methanation process (continued).

Author(s)	Method	Result
Matthischke et al. [77]	Recycled product stream was applied to evaluate CO_2 methanation process. CH_4 quality and temperature profiles were studied when the feed load changed from 10% to 100% in cooled FBRs.	In cooled configuration, with lower load rate, the CO_2 conversion was higher and reached 91.7%, but hot spot appeared in process. And catalyst bed temperature decreased when a small Rec or suitable external stream was used.
Fischer & Freund [78]	Dynamic behaviors of wall-cooled tubular FBR were studied when the load flow was adjusted from 100% to 50% on nominal load.	A 10-second time constant and 5-second deadtime were applied to cooling process. As a result, the new steady state for coolant was 60 seconds after changing load flow without occurrences of hot spot inside reactor.
Zimmermann et al. [80]	The three methods of catalysts setup were applied for fixed bed reactor. Catalysts dilution method is applied to control thermal problems in the CO2 methanation process with the load fluctuating in the range 30% to 100% after 5 minutes of using previous load.	Diluted catalysts beds were investigated that high temperature hot spots occurred. In addition, the core-shell catalyst particles with infinite segments also had hot spots when the feed load changes. On the other hand, the filled core-shell catalyst particles reactors did not have any hot spot during fluctuation.

4.2.2 Plant Model

Werlte, Germany, has the largest P2G facility ever operated [81]. EtoGas GmbH collaborated with the Centre for Solar Energy and Hydrogen Research (ZSW) to develop the plant, which has a power input of 6.3 MW and has been operated by Audi AG. The site can create SNG that is utilized in automobiles or provided straight into the gas grid. The methanation process was implemented in a single reactor, minimizing the requirement for product purification, as shown in Figure 22. A basic cooled reactor using molten salts was utilized, allowing for reliable management of temperatures inside the reactor. At maximum load, the reactor received 325 (STP) m^3/h of CO_2, which had been removed from biomethane via amine scrubbing. The generated SNG was injected directly into the gas system. The generated heat was recycled in the CO_2 stripping stage. A 10-bar H_2 buffer tank was used between the electrolyzer and reactor to reduce discontinuous operations, particularly for hydrogen production. The SNG product was first added to the gas network in 2013.

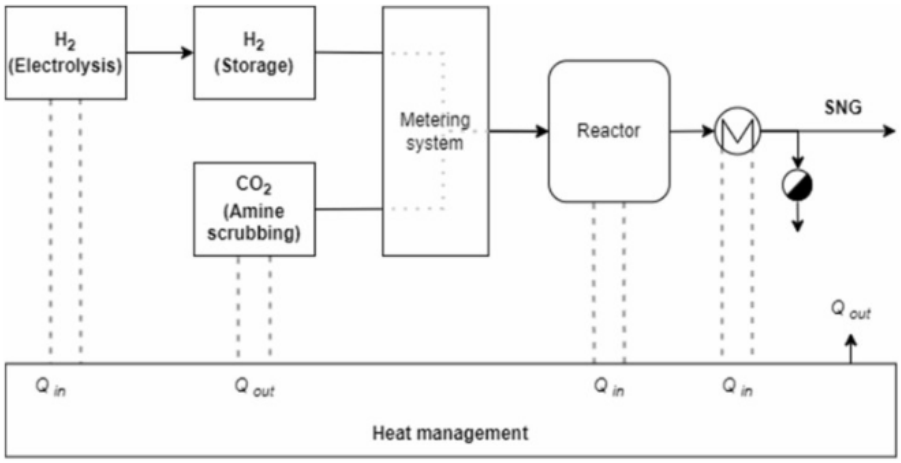

Figure 22. 6300kWel P2G plant, Audi AG/EtoGas GmbH/ZSW, Werlte, Germany. [81]

Another P2M demonstration plant using fluidized bed reactor was also reported by Hervy et al. [42]. The plant's capacity is 400kW SNG and the configuration of plant is shown in Figure 7. The research was performed using a fluidized bed reactor with a height of 5.4 m and a diameter of 30 cm. To minimize the start-up and shut down, pressurized CO_2 was used as cooling fluid in reactor system. Experiments were performed at 1 to 3 bar, 260 – 375℃, 1.5 to 4.8 H_2/CO_2 ratio, and 35 to 101 Nm^3/h feed flowrate. The fluidized bed reactor offered

the highest conversion above 280℃, demonstrating its flexibility and suitability for intermittent hydrogen generations by RES.

In Finland, Nordic Ren-Gas is developing a P2G plant in Tampere. The goal is to establish a P2G plant that produces sustainable synthetic CH_4, green H_2, and region heating from the surplus heat of process. The Tampere facility is part of a nationwide P2G fuel production and delivery network for heavy vehicle transportation. The plant's intended site is near the Tarastenjärvi power plant, allowing for effective CO_2 delivery and district heating integration. The Ren-Gas Tampere plant will be in operation from 2027 [82].

Additionally, Vantaa Energy Ltd proposes to develop a P2G plant that will generate carbon-neutral synthetic gas. The P2G plant uses water and CO_2 created during waste processing in a novel method to produce gas. The P2G plant generates carbon-neutral synthetic gas from captured CO_2, and the power required by the plant is already available from wind farms in which Vantaa Energy has a shareholding. Excess heat from the industrial process will be recycled, for instance, to use in the heating system of Vantaa municipality. The P2G plant is expected to be completed in 2025 [83].

APPLIED PART

5 Overview

In the applied part of thesis, a steady-state design of catalytic CO_2 methanation is simulated through Aspen Plus. The feed stream of H_2 is calculated based on available RES in Finland. After that, Aspen Plus Dynamics is applied to evaluate the quality of final product in intermittent conditions.

5.1 Production capacity

At the end of 2023, there were total 1601 installed wind turbines in Finland with total capacity was 6946 MW [6] and generated electricity was over 11.5 TWh [7]. Nieminen et al. (2019) [84] stated that 30 MW electrolyzer unit was suitable for wind electricity system in Finland. However, wind electricity infrastructure in Finland has improved in both the number of plants and the capacity; thus 35 MW electrolysis unit capacity can be proposed. Assuming the electrolysis unit has a capacity of 35 MW, the estimated production capacity could be calculated.

As mentioned above in section 3.1 , in catalytic CO_2 methanation, the stoichiometry ratio between H_2 and CO_2 should be over 4 to prevent coke formation in catalyst bed. So, the H_2: CO_2 ratio in the inlet stream is the stoichiometric ratio of 4.4 : 1.

The H_2 production from electrolysis unit can be calculated by using commercial electrolysers as reference. For example, GEL-1000 is a 5 MW PEM electrolyser system of FEST group, which can produce up to 90 kg/h (44.65 kmol/h) of H_2 [85]. Thyssenkrupp [86] also offers a scalum of 20 MW unit which can produce 4000 Nm^3/h (176 kmol/h) of H_2. With the production rate of 5 MW and 20 MW units, in theory, the production rate of H_2 is 8.8 kmol/h per 1 MW of electrolyser unit. Therefore, in the case of 35 MW unit, the assumed hydrogen production rate is 308 kmol/h.

5.2 Steady-State model

In this thesis, the cooled fixed-bed reactor is employed in CO_2 methanation process. Ni/Al_2O_3 is used as the catalyst, which has good catalytic performance and inexpensive price. According to Tomassi et al. [34], the optimum pressure for CO_2 methanation is 8 – 16 bar. So, the methanation reactor is operated continuously at 10.5 bar and a cooling fluid of 230℃ is applied.

The steady-state model was developed according to the initial supposed H_2 electrolysers design' capacity of 35 MW. In the steady-state model, the overall heat transfer coefficient U based on the tube's velocity was calculated by using (Eq. 36) [87] below.

$$U = 0.01545 + \frac{0.6885 \times 10^{-6}}{D_p} Re_0 \qquad \text{(Eq. 36)}$$

Where, D_p is particle diameter (m); Re_0, is particle Reynolds number, calculated by (Eq. 37).

$$Re_0 = \frac{\rho_v \times u \times D_p}{\mu} \qquad \text{(Eq. 37)}$$

In which, ρ_v is mass density of mixture (kg m^{-3}), u is fluid velocity (m s^{-1}), μ is fluid viscosity (Pa.s). These variables are provided by Aspen Plus.

The dynamic model is designed based on the steady-state ones; and the estimated capacity of the process is around 9000 tons CH_4 per year. The whole process is illustrated in Figure 23 and Appendix 3.

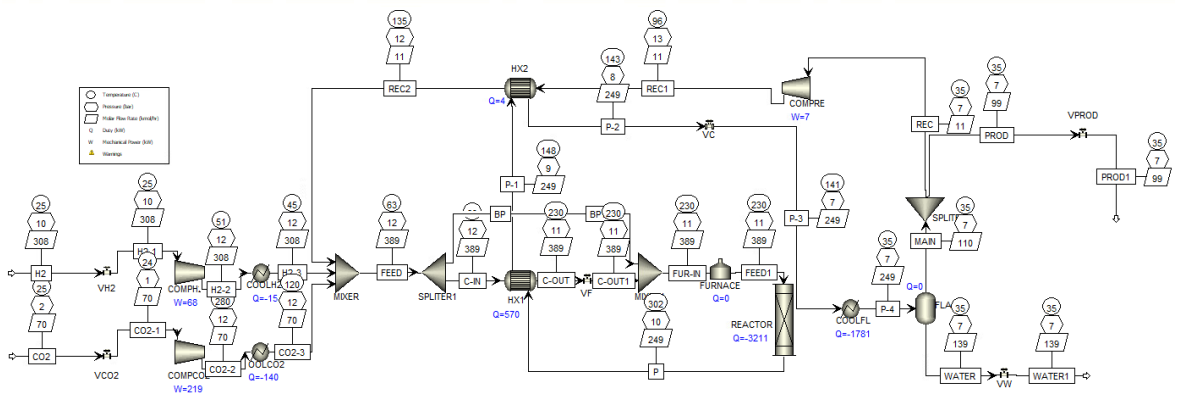

Figure 23. Steady-state flowsheet of catalytic CO_2 methanation.

In the steady-state flowsheet, green H_2 is compressed to 12 bar from 10 bar at inlet stream by using a single polytropic compressor (ASME method), whereas CO_2 is compressed from

1 bar to 12 bar by using the same type of compressor as H_2 stream. To maintain the temperature of compressors, COOLH2 and COOLCO2 coolers are used to keep the temperature at the recommended range. The COOLH2 cooler is specified as zero-duty in steady state model due to low temperature of compressor COMPH2; and the COOLCO2 cools the compressor's discharge temperature to 120℃. The compressed H_2 and CO_2 are mixed in MIXER with stoichiometric ratio of 4.4:1 and mixed with recycle stream (REC2) before being heated by shell-tube heat exchanger HX1. The bypass stream (BP and BP1) is used to control the temperature of reactor feed stream in dynamic conditions. The FURNACE is utilized to heat up the reactor's inlet stream (to 230℃) in case of needed. The heated mixture (230℃ & 10.5 bar) (FEED1) is delivered to a cooled multi-tubular fixed-bed reactor for CO_2 methanation process. A constant thermal fluid temperature at 230℃ is applied to cool the reactor during the reaction process. CO_2 methanation process is an extremely exothermic reaction, so the high temperature at the reactor outlet is utilized to heat the mixture of material in HX1 and HX2, respectively. Subsequently, the product stream (P-3) is cooled down to 35℃ by cooler COOLFL before being fed to the flash. In the flash, the large amount of H_2O in product is separated. Because of the excessive amount of H_2, the products of the reactor are CH_4, H_2O, and unreacted H_2. However, the recycle stream is still applied in this model, when the recycle stream is used, the highest temperature in reactor is lower (768℃ and 783℃ if no recycle stream is applied). The COMPRE compressor is used to compress the REC stream to 13 bar before delivering to MIXER to mix with material gases.

In the steady-state design, the VC valve is used to control the pressure of the system. Each valve is set 0.5 bar for specified pressure drop, only the valve VB for bypass stream is set 1.5 bar for pressure drop to balance pressure at stream FURIN. Furthermore, the pressure drops through heat exchangers HX1 and HX2 are set 1 bar for both hot and cold sides. Kinetic models, which are presented earlier in section 4.1 , are most frequently applied in CO_2 methanation. Among those models, the Koschany et al. model (Eq. 32) and (Eq. 33) was chosen because of the low operational temperature and suitable pressure range from 5 to 15 bar. In addition, in their experiment, the catalyst performed high activity at low temperature and CO formation via RWGS was negligible. In addition, following the European standards, the methane standard for automotive market is greater than 89 mol-% in CH_4 content, under 2 mol-% in H_2 and 1 – 8 mol-% of CO_2 [88]. Due to the over

stoichiometric ratio of 4.4:1, excess H_2 remains in the product need to be separated before injected into the grid; therefore, CO_2 concentration forms the acceptable impurity level in the product. The conditions and parameters of the design are given in Table 8.

Table 8. Operating condition and parameters of steady-state model.

	Parameters	Value
Operating conditions	H_2 flowrate (stream H_2), kmol/h	308
	CO_2 flowrate (stream CO_2), kmol/h	70
	Temperature of feed gases (H_2, CO_2), ℃	25
	Pressure of feed gases (H_2, CO_2), bar	10/1
	Flash temperature, ℃	35
	Flash pressure, bar	7
	Ratio of SPLITER (REC stream)	0.1
Reactor	Number of tubes	200
	Tube length, m	2.5
	Tube diameter, m	0.04
	Thermal fluid temperature, ℃	230
	Heat transfer coefficient (thermal fluid – process stream), kW m^{-2} K^{-1}	0.1835
	Catalytic bed voidage (ε)	0.4
	Catalytic density, kg m^{-3}	2355.2 [89]
	Particle diameter, m	0.004
	GHSV, h^{-1}	4113.5
Compressors	Type of compressor	Polytropic (ASME method)
	Polytropic efficiency	0.8
	Mechanical efficiency	0.95
Heat exchangers	Heat transfer coefficient, kW m^{-2} K^{-1}	0.142 [90]
	Pressure drop (each side), bar	1
Valves	Specified pressure drop, bar	0.5
	Specified pressure drop (valve VB), bar	1.5
Coolers	COOLH2	Zero duty
	COOLCO2 Outlet temperature, ℃	120
	COOLFL Outlet temperature, ℃	35

6 Dynamic Modelling of CO_2 methanation

Sizing equipment such as column diameters, catalysts heat capacity, plumbing configuration is an important step when converting from steady-state to dynamic model because this step directly impacts dynamic behaviors of that unit. Therefore, heat exchanger, reactor, and flash are required to be sized and adjusted before simulating the model in dynamic environment [98]. In addition, catalysts heat capacity also needs to be calculated in this section.

6.1 Sizing equipment

Following Luyben's recommendation [91], the size of equipment can be calculated by using approximate estimation. More details about the calculation are shown in Appendix 1.

6.1.1 Heat Exchanger

In dynamics simulation, the heat exchanger volume and its mass should be calculated if these values impact dynamics. In this thesis, all heat exchangers are supposed to be tube-in-shell heat exchangers.

HX1 and HX2 work based on reactor outlet temperature, and their heat transfer coefficients are mentioned in Table 8. Aspen Plus also provides the total heat transfer area of heat exchanger (A_{total}), so from this value, total volume of tubes (V_{tubes}) and mass of equipment (M_{tubes}) could be estimated. Tube's heat transfer area (A_{tube}) is calculated by using the (Eq. 38) [98], in which a typical tube diameter (D_t) is 0.0254 m and tube's length (L) is 2 m.

$$A_{tube} = \pi D_t L \quad (\text{m}^2) \qquad \text{(Eq. 38)}$$

The number of tubes (N_{tubes}) (Eq. 39) [98] is:

$$N_{tubes} = \frac{A_{total}}{A_{tube}} = \frac{A_{total}}{\pi D_t L} \qquad \text{(Eq. 39)}$$

The total volume of tubes (m^3) (Eq. 40) [98] is:

$$V_{tubes} = N_{tubes} \times V_{tube} = \frac{A_{total}}{\pi D_t L} \times \left(\frac{\pi D_t^2}{4}\right) \times L = \frac{D_t}{4} \times A_{total} \qquad \text{(Eq. 40)}$$

And, in this estimation, shell's volume is assumed to be equal the tubes volume (Eq. 41)[98].

$$V_{shell} \equiv V_{tubes} \qquad \text{(Eq. 41)}$$

To calculate the mass of equipment, the wall thickness of tube (Δw) is 0.002m and all equipment is made from Steel.316 density ρ_m = 8000 kg m^{-3} and heat capacity is 500 J kg^{-1} K^{-1} [92].

$$M_{tubes} = N_{tubes}\left(V_{tube} - \left(\frac{\pi(D_t - \Delta w)^2}{4}\right)L\right)\rho_m \qquad \text{(kg)} \qquad \text{(Eq. 42)}$$

The mass of tubes is the sum of cold-side and hot-side tubes weight, so the dimensions of HX1 and HX2 are shown in Figure 24.

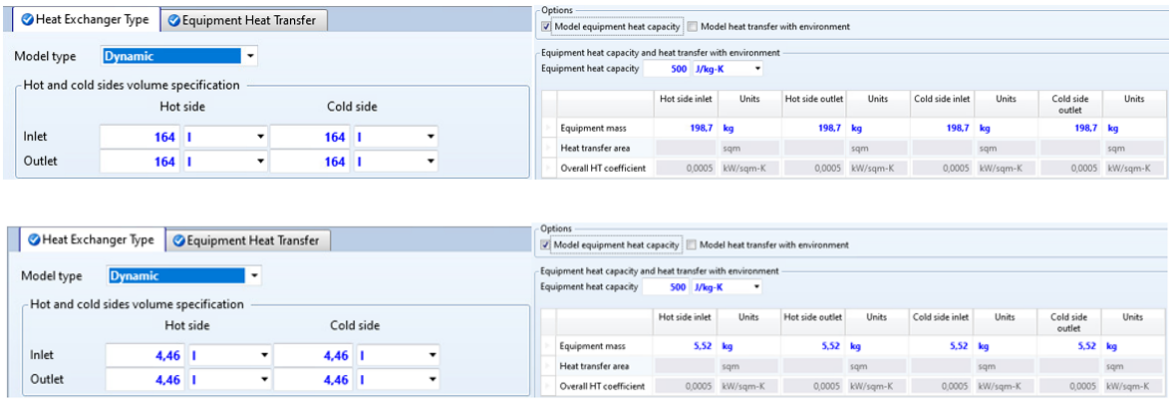

Figure 24. Dynamics specification in Aspen Plus for HX1(above) and HX2(below).

For Coolers (COOLH2, COOLCO2, COOLFL), the total volume is calculated by using (Eq. 43). And the mass of equipment is calculated the same as HX1 above.

$$V_{tubes} = \frac{Volume\ Flow}{gas\ residence\ time} \qquad (m^3) \qquad \text{(Eq. 43)}$$

In which, Volume Flow (m^3 s^{-1}) is given by Aspen Plus and the gas residence time = 1 second, which is recommended by Aspen Plus Support.

6.1.2 Flash tank

Flash's diameter (D_v) based on vapor velocity is calculated by the (Eq. 44) and (Eq. 45) [91].

$$V_{max} = \frac{F - Factor}{\sqrt{\rho_v}} = \frac{0.61}{\sqrt{\rho_v}} \quad (\text{m s}^{-1}) \quad \text{(Eq. 44)}$$

$$D_v = \sqrt{\frac{\frac{V_g}{V_{max}} \times 4}{\pi}} \quad (\text{m}) \quad \text{(Eq. 45)}$$

In which, V_{max} the maximum vapor velocity (m s^{-1})

ρ_v the vapor density (kg m^{-3})

V_g the vapor volumetric flow rate (m^3 s^{-1})

Flash's diameter (D_l) based on liquid velocity is calculated following the (Eq. 46) [91].

$$D_l = \sqrt[3]{\frac{2 \times 2 \times 5 \times V_l}{\pi}} \quad (\text{m}) \quad \text{(Eq. 46)}$$

In which, V_l the liquid volumetric flow rate (m^3 min^{-1})

The liquid hold up is considered in flash's diameter calculation. Normally, 5 minutes of hold up with half level of tank is used. The vessel diameter would be decided by D_v or D_l, in case of $D_v > D_l$, the vessel diameter is D_v and vice versa. In addition, in this thesis, the flash is assumed as vertical cylindrical vessel, and its height is double than its diameter.

6.1.3 Process heat transfer coefficient

The heat transfer coefficient between catalyst and process fluid (h_c) is one of parameters which need to be defined when transferring a steady-state simulation to dynamics simulation in Aspen environment. This value can be calculated following (Eq. 47) [93].

$$Nu = \frac{h_c \times D_p}{k_f} = 2 + 1.1 Pr^{1/3} Re^{0.6} \quad \text{(Eq. 47)}$$

In which, Nu is fluid-to-solid Nusselt number.

k_f is fluid thermal conductivity (W m^{-1} K^{-1}), given by Aspen Plus.

Pr is Prandlt number, calculated by (Eq. 48).

$$Pr = \frac{C_p \times \mu}{k} \quad \text{(Eq. 48)}$$

Where, C_p is the heat capacity of fluid (J kg^{-1} K^{-1}).

Furthermore, the heat transfer coefficient between wall reactor and process fluid (h_w) is also considered in dynamics estimation. The wall Nusselt number (Nu_w) is calculated by equations presented from (Eq. 49) to (Eq. 53) [94].

$$Nu_w = \frac{h_w \times D_p}{k_f} = Nu_{w0} \times \left(\frac{1}{\frac{1}{Nu_w^*} + \frac{1}{Nu_m}} \right) \quad \text{(Eq. 49)}$$

$$Nu_{w0} = \left(1.3 + \frac{5 \times D_p}{D_t}\right) \times \left(\frac{k_r^0}{k_f}\right) \quad \text{(Eq. 50)}$$

$$k_r^0 = k_f \left(\varepsilon + \frac{0.95(1-\varepsilon)}{0.2 + 0.667 \times \frac{k_f}{k_s}} \right) \quad \text{(Eq. 51)}$$

$$Nu_w^* = 0.3 \times Pr^{1/3} \times Re^{0.75} \quad \text{(Eq. 52)}$$

$$Nu_m = 0.54 \times Pr \times Re \quad \text{(Eq. 53)}$$

The overall heat transfer coefficient between process fluid and wall reactor (U_t) is calculated by (Eq. 54) to (Eq. 57) [94]. In which, thermal conductivity of steel (k_w) is 16.2 W m^{-1} K^{-1} [92].

$$\frac{1}{U_t} = \frac{1}{h_w} + \frac{D_t}{6 \times k_{er}} \times \frac{Bi + 3}{Bi + 4} + \frac{\Delta w}{k_w} \quad \text{(Eq. 54)}$$

$$Bi = \frac{h_w \times D_t}{k_{er}} \quad \text{(Eq. 55)}$$

$$\frac{k_{er}}{k_f} = \frac{k_r^0}{k_f} + \frac{Pr \times Re}{Pe_{h,r}} \quad \text{(Eq. 56)}$$

$$Pe_{h,r} = 8 \times \left(2 - \left(1 - \frac{2 \times D_p}{D_t}\right)^2\right) \quad \text{(Eq. 57)}$$

In addition, valve sizing is also an important step in transition step. Luyben [91] recommended the pressure drop value through valve is in range 2 to 4 bar. Nevertheless, according to Nguyen [95], in gas system, the cost to compress gas is higher if the pressure drops larger, so the pressure drop through valve is set at 0.5 bar at output (OP) 50% of valve. Equipment's dimension and catalyst heat transfer coefficient is illustrated in Table 9.

Table 9. Dimension and properties of equipment and catalyst using in dynamic simulation.

Equipment and catalyst heat transfer coefficient		Parameters	Value [ref]
RACTOR (catalyst)		Specific heat capacity, J Kg^{-1} K^{-1}	1107 [89]
		Specific surface area, m^2/m^3	1500
		Overall heat transfer coefficient between catalyst and process fluid, W m^{-2} K^{-1}	1583
		Catalyst thermal conductivity, W m^{-1} K^{-1}	3.6 [89]
		Overall heat transfer coefficient between reactor wall and process fluid, W m^{-2} K^{-1}	591
		Reactor's mass, kg	1030
Heat exchangers	COOLH2	Inlet & outlet volume, L	191.1
		Inlet & outlet mass, kg	250.8
	COOLCO2	Inlet & outlet volume, L	83.4
		Inlet & outlet mass, kg	109.48
	COOLFL	Inlet & outlet volume, L	312
		Inlet & outlet mass, kg	377.75
	FURNACE	Inlet & outlet volume, L	
		Inlet & outlet mass, kg	
	HX1	Hot side inlet & outlet volume, L	164
		Cold side inlet & outlet volume, L	164
		Hot side inlet & outlet mass, kg	198.7
		Cold side inlet & outlet mass, kg	198.7
	HX2	Hot side inlet & outlet volume, L	4.46
		Cold side inlet & outlet volume, L	4.46
		Hot side inlet & outlet mass, kg	5.52
		Cold side inlet & outlet mass, kg	5.52
FLASH		Vessel type	Vertical
		Head type	Elliptical
		Height, m	1.5
		Diameter, m	0.75

6.2 Control Structure

All equipment specifications needed for dynamic simulation was designed in Aspen Plus, after that, dynamics simulation file was exported to Aspen Plus Dynamics. When transforming to dynamics simulation, the H_2 feed stream pressure was changed from 10 bar to 9.85 bar in order to reach the initial value of 308 kmol/h. Following that, controllers and signal streams were applied to the model and the structure of them are illustrated in Figure 25 and Appendix 3.

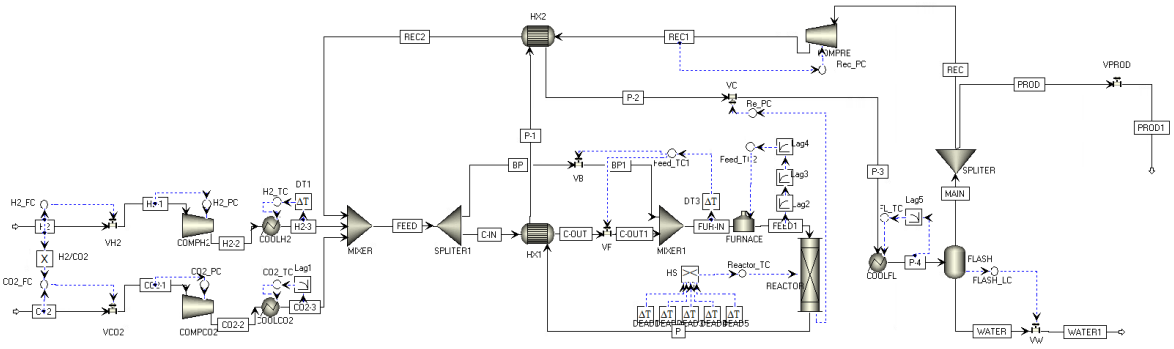

Figure 25. Design of all controllers in dynamic model of the P2M plant.

Figure 26 illustrates the control system of feed streams (H2 and CO2 stream of Figure 23). In this system, the H2_FC controller is set as an auto controller and CO2_FC is controlled by H2_FC process value (PV). The H2_FC controller and valve VH2 control the H_2 input value. In case the PV of feed stream is lower or greater than the setpoint (SP) of the H2_FC controller, the valve VH2 will receive the signal to decrease or increase the valve's position corresponding to the PV. To control the CO_2 flowrate, a similar system is applied to CO2_FC controller and valve VCO2. However, a multiply block is used to hold on the stoichiometric ratio between reactants, so the CO2_FC controller does not need a fixed SP. In this scenario, H2/CO2 block uses the PV of H2 stream to calculate the OP of CO2_FC controller by multiplying H2's PV by 1/4.4. As the result, the OP of multiply block will be the SP of CO2_FC controller. This controller set up is the only one which uses cascade control loop in this process, and other ones work as auto principle.

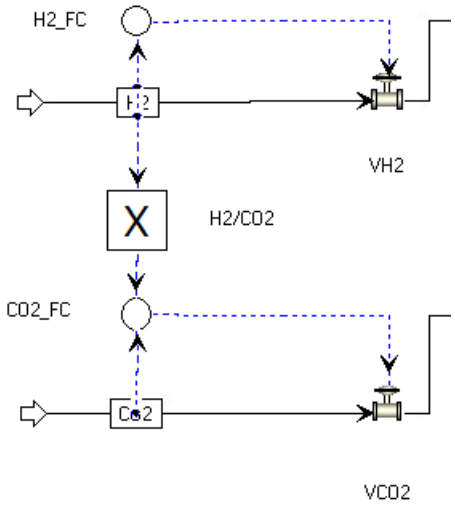

Figure 26. Control system of feed flows: H2_FC controller and valve VH2 for H_2 stream; CO2_FC controller and valve VCO2 for CO2 stream; and multiply block H2/CO2 for feed ratio control.

The inlet pressure and discharge temperature of compressors (COMPH2 and COMPCO2) is controlled by pressure controllers (H2_PC & CO2_PC) and temperature controllers (H2_TC & CO2_TC). Regarding compressor control, discharge pressure is usually manipulated rather than suction pressure. Nevertheless, in this setup, when this strategy is applied, the system cannot be stable, so the suction pressure control was alternatively selected. These two pressure controllers have the same action and properties. When the pressure of the inlet stream increases, the compressor works at a higher work rate to maintain the pressure of the system, and vice versa. Therefore, the pressure controllers (H2_PC & CO2_PC) receive pressure signals from H2-1 and CO2-1, respectively, and manipulate the brake power of the COMPH2 and COMPCO2 compressors. In this thesis, compressors are used as polytropic using ASME method, and in standard practice, discharge temperature of these compressors are kept under 150℃ [96]. For the compressors, coolers are used to control the discharge temperature of compressors, and these coolers are manipulated by H2_TC and CO2_TC controller. Deadtime blocks or lag blocks are applied for accurate thermal control in dynamic simulation. Therefore, the appearance of these blocks is necessary for dynamic simulation to achieve a safety aspect for future realistic improvement. According to Luyben [91], a deadtime block or a system of 3-lag blocks should be applied in temperature control. It should be same for two coolers, however, when applied deadtime block or system of 3-lag blocks for CO2-3 stream, the model got error then a lag block is used instead. In this case, when the temperature of discharge streams increases, the controller H2_TC and CO2_TC

will send the signal to increase the medium flowrate in coolers and the temperatures can be cooled down to SP of 120℃. The Figure 27 illustrates the compressor control system.

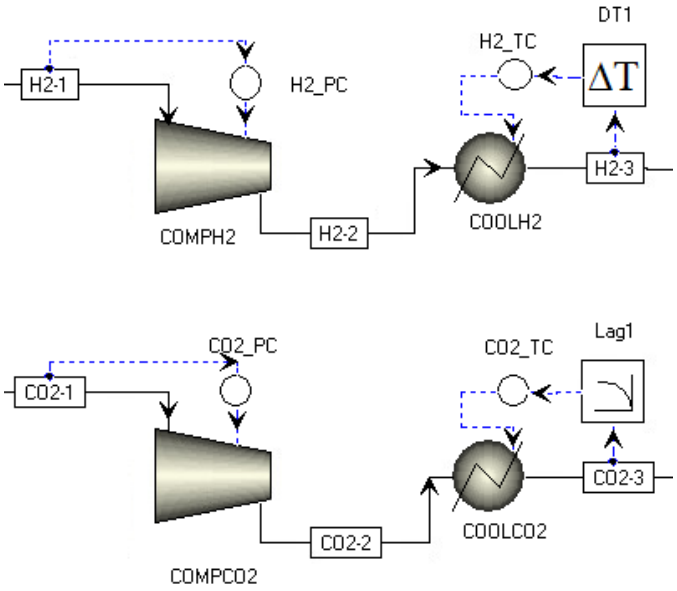

Figure 27. Control system of compressors: H2_PC and CO2_PC controller control COMPH2 and COMPCO2's suction pressure by using PV of inlet stream pressure and manipulating compressor's brake power, respectively; H2_TC and CO2_TC controller control COOLH2 and COOLCO2 by manipulating cooler's medium flowrate.

There is another compressor (Figure 28) which is used in this system, it is COMPRE, the compressor used in recycle stream. In typically, this compressor can be controlled by the same structure with H_2, or CO_2 stream, however, the SP is based on the discharge stream of compressor instead of suction pressure. In addition, in this compressor, the temperature controller was not used because it was forgotten during the build of the model, however, the equipment temperature was always below 130℃ during the tests.

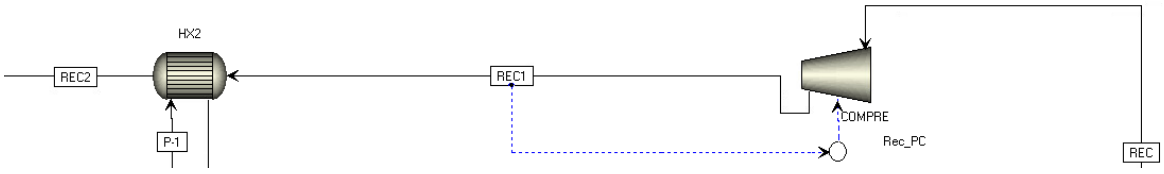

Figure 28. Control system of compressor COMPRE, Rec_PC controller controls COMPRE's discharge pressure by manipulating compressor's brake power.

In this thesis, only the BYPASS stream is applied to manage the temperature of the feed stream of reactor (Figure 29). In this system, temperature of feed stream (FUR-IN) is used

as PV to control the position of valves VB and VF to control the temperature. The VB and VF valves are set as direct and reverse action, respectively, and controlled by Feed_TC1 controller. When the temperature of FUR-IN stream increases greater than SP value, the Feed_TC1 controller will receive the signal and transfer it to increase the opening position of VB and at the same time the opening position of valve VF will decrease; and vice versa. Notably, in steady-state model, the outlet temperature of HX1 cold side is set as 230℃, so the feed stream temperature is also 230℃. In this case, the VB valve is totally closed, and the VF valve is opened at its 50% opening position. In addition, FURNACE is used to heat the reactor inlet stream if necessary. The FURNACE medium flow rate is controlled by Feed_TC2 controller, if the REACTOR inlet temperature is lower than 230℃, FURNACE medium flow rate (reverse action) is gained by signal of Feed_TC2 controller and vice versa.

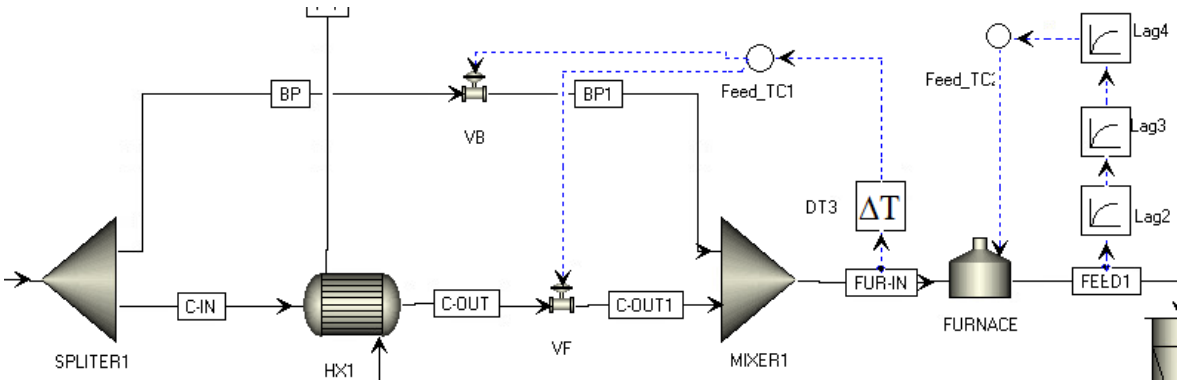

Figure 29. Control system of feed stream of reactor: Feed_TC1 controller controls the opening position of valve VB and VF, in which VB valve works in direct action and VF is set as reverse action; Feed_TC2 controller controls the REACTOR inlet temperature by manipulating FURNACE medium flow rate.

Figure 30 shows the temperature and pressure control of REACTOR. For temperature control, a high selector block (HS) is employed to collect the highest temperature of reactor during operation. Firstly, DEAD blocks will collect temperature along the reactor length (temperature sensors placed at position of 3.33%, 6.66%, 13.33%, 20%, 26.66% of reactor length), and HS selects the highest temperature of these places. After that, the HS sends the signal to Reactor_TC controller, and based on the peak temperature, the suitable temperature of coolant will be selected and changed in reactor. The controller action is set at reverse action, which means if the peak temperature is greater than the setpoint, the coolant temperature will be decreased to cool down the reactor and vice versa. Regarding pressure controlling, the VC valve is used to control the outlet pressure of reactor and also maintain

the whole system pressure. The outlet pressure of reactor is used as PV of Re_PC controller, and the opening position of valve VC is controlled with direct action by Re_PC controller. When the reactor outlet pressure (PV) decreases or increases, the valve VC will also decrease and increase the opening position corresponding to the PV value.

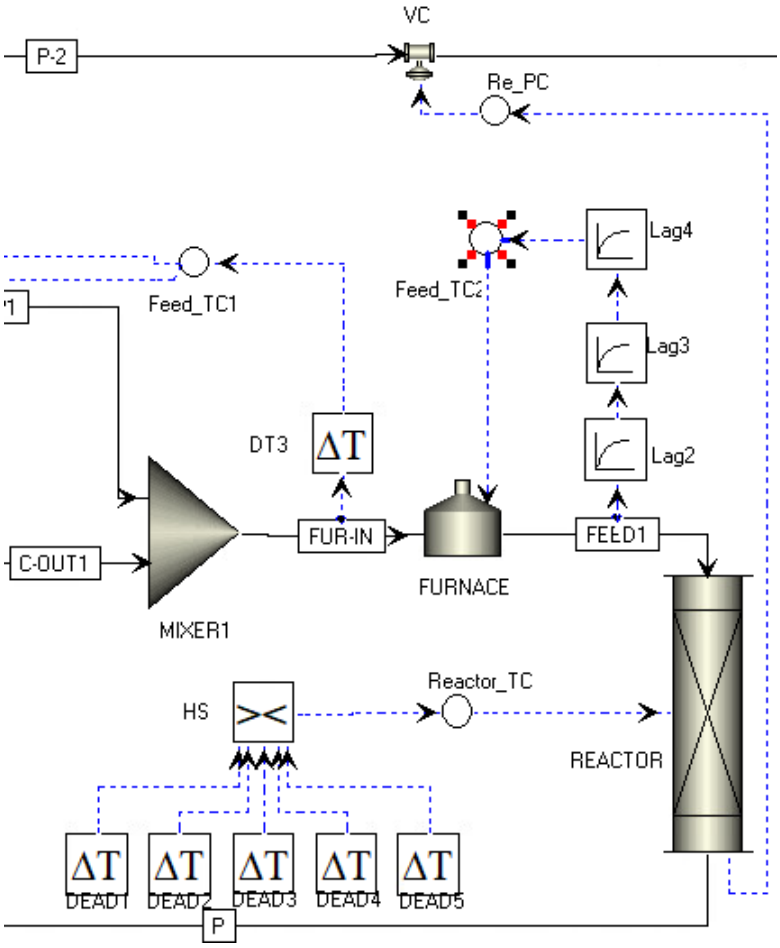

Figure 30. Temperature and Pressure control loop of reactor: HS block chooses the highest temperature which collect from reactor and Reactor_TC controls the coolant in reactor, and Re_PC controller controls the system pressure by manipulating valve VC opening position.

Flash separator is the last piece of equipment that needs to be controlled in this process. The liquid level inside the flash and inlet temperature are controlled by level controller (FLASH_LC) temperature controller (FL_TC) as shown in Figure 31. An auto controller and a valve are manipulated by FLASH_LC controller. When the liquid level inside FLASH (PV) is higher than the SP of controller, the VC valve will receive the signal from FLASH_LC controller and simultaneously increases its the opening position to hold the flash's liquid level at SP value. Besides the flash's liquid level, the inlet stream temperature of the flash (P-4) is also controlled. The temperature of P-4 is recorded and sent to FL_TC

controller via Lag5 block (time constant = 1 minute). The FL_TC controller has direct action, it means when the temperature of P-4 increases or decreases, the controller will send the signal to increase or decrease the cooler (COOLFL) medium flowrate to maintain the P-4 temperature at SP of 35℃ before feeding to flash separator.

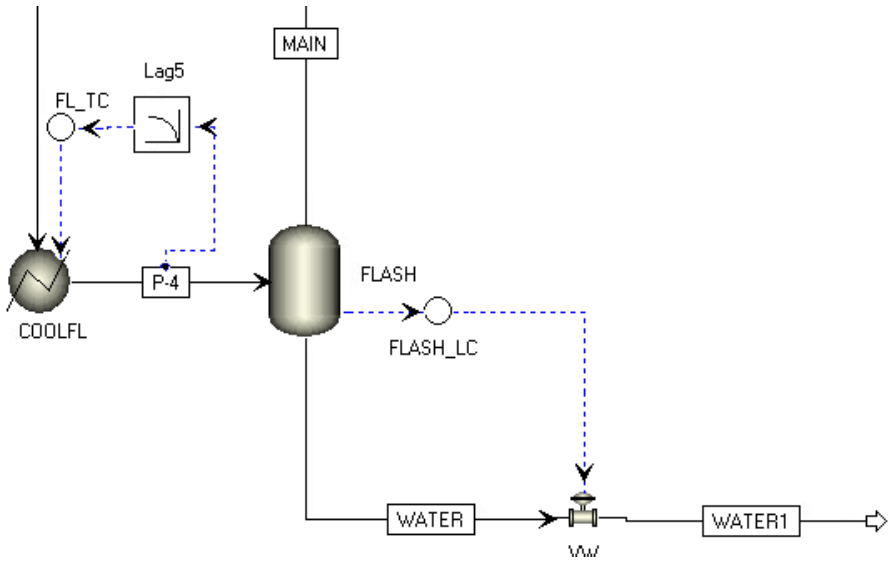

Figure 31. The control system of flash separator: the FL_TC controller controls the temperature of the feeding stream to flash by using the signal from P-4 stream and manipulating the cooler's medium flowrate, FLASH_LC controller control the liquid level inside the flash by manipulating the VW valve opening position.

In this model, proportional – integral (PI) controller type is applied to all controllers. The controller tuning was carried out by Aspen Plus Dynamics using Tyreus – Luyben rule. The closed loop autotune variation (ATV) is applied and 5% of the relay amplitude of output range was chosen in testing setup. The controller tuning parameters were calculated and updated to controllers automatically by Aspen Plus Dynamics. However, Reactor_TC and FLASH_LC tune testing result are extremely high in gain parameter (P%/%) and when applying these values to controllers, the controller responses are aggressive and lead the model to fluctuate running during intermittent loading. To overcome this problem, the lower value of gain parameter was chosen to have a stable running process. The detail controller settings are presented in Table 10.

Table 10. The details of controllers apply in the dynamic simulation.

Controller	Controlled stream/equipment	Set point	Manipulated factor	Range of output	P %/%	Integral time (min)	Control action	**Type of control**
H2_FC	H2's flowrate	308 kmol/h	Valve VH2	0 – 100%	5.19	0.264	Reverse	Auto
CO2_FC	CO2's flowrate	70 kmol/h	Valve VCO2	0 – 100%	2.03	0.264	Reverse	Cascade
H2_PC	Inlet pressure of COMPH2	9.4 bar	Brake power	0 – 500 kW	8.09	0.264	Direct	Auto
CO2_PC	Inlet pressure of COMPCO2	1 bar	Brake power	0 – 1000 kW	0.8	0.264	Direct	Auto
H2_TC	Discharge temperature of COMPH2	120℃	COOLH2's medium flowrate	0 – 5000 kg/h	5	2.64	Direct	Auto
CO2_TC	Discharge temperature of COMPCO2	120℃	COOLCO2's medium flowrate	0 – 5000 kg/h	1	2.64	Direct	Auto
Feed_TC1	Inlet temperature of reactor	230℃	Valve VB and VF	0 – 100%	26.84	5.28	Direct/reverse	Auto
Feed_TC2	Inlet temperature of reactor	230℃	FURNACE	0 – 1000 kg/h	30.6	11.88	Reverse	Auto
Reactor_TC	Reactor's peak temperature	700℃	Temperature of coolant	180 – 300℃	10	5.28	Reverse	Auto
Re_PC	Reactor outlet pressure/system pressure	9.6 bar	Valve VC	0 – 100%	49.6	0.264	Direct	Auto
FL_TC	Temperature of flash's inlet stream	35℃	COOLFL's medium flowrate	0-27500 kg/h	1.52	3.96	Direct	Auto
FLASH_LC	Liquid level of flash	0.95 m	Valve VW	0 – 100%	20	2.64	Direct	Auto
Rec_TC	Discharge pressure of COMPRE	12.9 bar	Brake power	0 – 50kW	0.1	0.264	Direct	Auto

7 Results and Discussion

In this section, the results of steady-state and dynamics simulation are given and discussed. Firstly, the results of steady-state design in Aspen Plus are examined. After that, the result of dynamics model is shown and discussed, based on the product quality and reactor's temperature. In the case dynamics simulation, the intermittent H_2 flow rates (+10%, − 10%, and – 30% of load) are tested, and the results are discussed concerning the dynamics aspects.

7.1 Steady-state model

In this thesis, the steady-state process was designed in Aspen Plus and after that the dynamic model was done in Aspen Plus Dynamics. Through the steady-state model, the temperature and composition profile in reactor were determined.

As can be observed from Figure 32, the reactor's temperature profile is determined. At the starting zone of the reactor, the fluid process is fed at 230℃ and the temperature rapidly jumps to the peak temperature of 768℃. A coolant is used to absorb the released heat by reactions, consequently, the temperature slightly decreases to 302℃ at the outlet of reactor. Furthermore, the service coolant's temperature can be adjusted during dynamics simulation to keep the peak temperature in an acceptable range, this point will be discussed further in the next section. The stream results and conditions of steady-state mode are listed in Appendix 2.

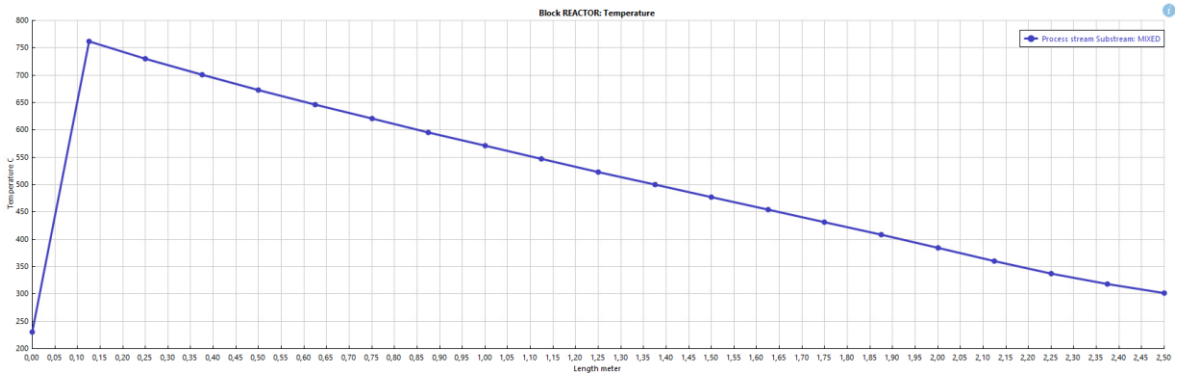

Figure 32. The temperature profile along reactor's length in steady-state model. The peak temperature is 768℃ at the inlet zone of reactor and decreases gradually by service coolant.

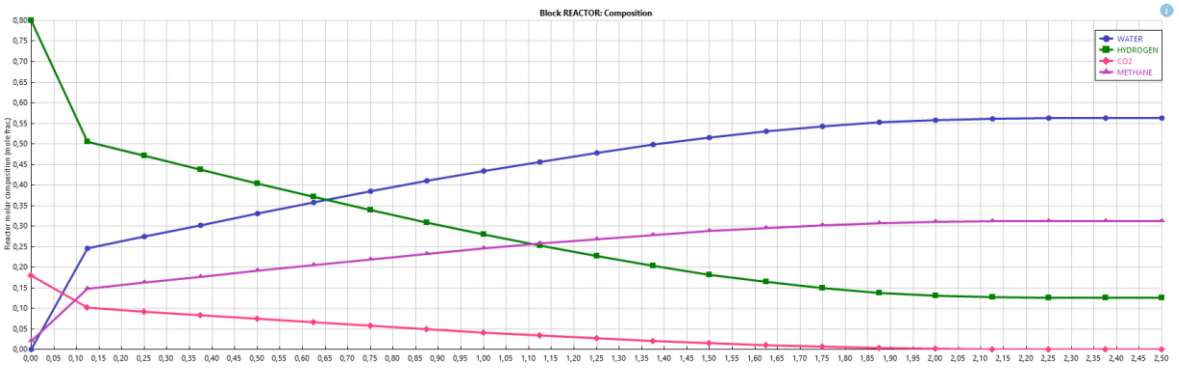

Figure 33. The composition of reactants (CO_2 & H_2) and products (CH_4 & H_2O) along reactor's length in steady-state model. The reaction rate is highest at the first part of reactor and the reaction almost reaches equilibrium state at the end of reactor.

The peak temperature is extremely high because of the high reaction rate at this location. As can be observed from Figure 33, the composition of reactants (H_2 and CO_2) quickly decreases from 80% to 50% and 18% to 10%, respectively; and the reactants continue to react till the end of the reactor, and almost reaches to equilibrium phase. The formation of CH_4 mainly occurs in the first 2 m of the reactor and slowly apart. Due to excessive H_2 amount (stoichiometric ratio between H_2 and CO_2 is 4.4:1), the remaining CO_2 at the outlet of reactor is only 0.00142 mol-%, it means the CO_2 conversion is 99.99% in the reactor. Using the high stoichiometric ratio causes an extremely high peak temperature, which also may cause catalyst deactivation and reduce the catalyst's lifetime. As the result of model, the composition of product stream (PROD stream Figure 23) is used to evaluate the quality of model's products. After water removal in flash, the product contains 70.8% of CH_4, 28.33% of H_2, and H_2O. To inject the product gas into the SNG grid, the H_2 content must be removed and recycled by separation technologies such as membrane [97] or pressure swing adsorption [98]. As mentioned above, CO_2 mole fraction is supposed to be the impurity limit of model's product. For example, in the product stream, the mole flow of CH_4 is 69.98 kmol/h, so the maximum acceptable CO_2 is 6.15 kmol/h.

In addition, there is a recycle stream in process (Figure 23). Theoretically, the recycling stream is used to enhance the efficiency of the process by recycling the unreacted materials to reactor. In this process, although the CO_2 conversion is high, and reactants leave the reactor with a very small amount; the recycle stream was still applied. As mentioned above, Matthischke et al. [77] investigated with appearance of recycling stream, the peak temperature is lower than without recycle stream. The recommended value of Rec is from 0.05 to 0.1, so the Rec = 0.05 was chosen. From the Figure 34, it can be seen that the peak

temperature reaches to 782℃ without using a recycling stream. As a thermal aspect, the recycle stream may be helpful in thermal control, but as an economic aspect, it is needed further investigation.

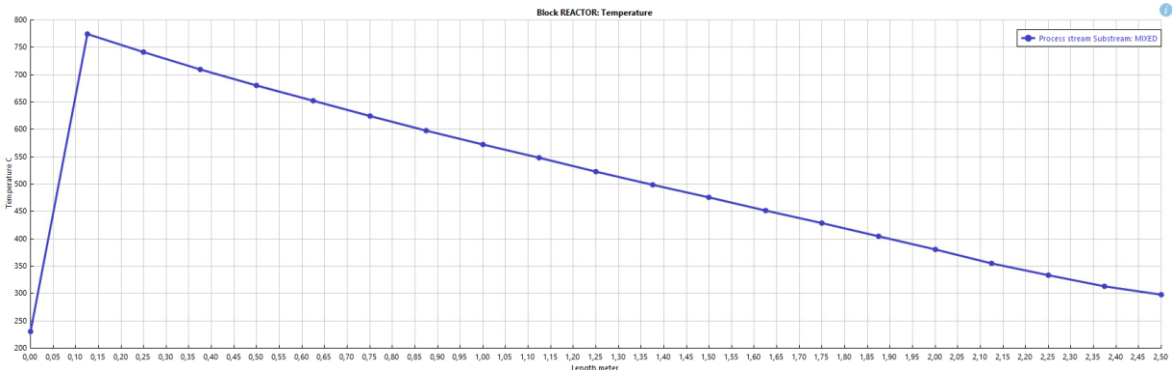

Figure 34. The temperature profile along reactor's length in steady-state model without recycle stream. The peak temperature is 782℃ at the inlet zone.

7.2 Dynamic model

The dynamic simulation is performed to investigate the quality of the product and how well it fits to the required limits before feeding into the network, as control system responds to variations in the H_2 load to the reactors (+10%, −10%, and –30% of normal flowrate in steady-state simulation). This allows for a thorough analysis of the potential impact that fluctuating power from RES may have on this technology and the viability of using the generated gas. In addition, operational limitations (minimum loading and maximum achievable ramping rate) will also be discussed. In all cases, the peak temperature is kept at 700℃ to manage the hot spot that may appear and harm the catalyst bed; after one hour at full load, the feed load changes following the value mentioned above.

7.2.1 Increasing of H_2 flow rate (+10%)

After one hour of simulation time, the feed flowrate was increased by 10% and the H_2 flow rate changes up to 338.8 kmol/h (Figure 36). Due to the no ramping rate, the feed flowrate is changed directly from SP of H2_FC controller. Although the REACTOR's peak temperature is set at 700℃ by Reactor_TC controller and the coolant temperature decreases to 180℃, the peak temperature in REACTOR goes higher values around 752℃ (in full load

design, the peak temperature is 745℃) and after 30 minutes from changing feed load, the new steady state is established (Figure 35). In addition, because of lower coolant temperature, the temperature of REACTOR's outlet stream decreases to 264℃ leading to the HX1 cold outlet temperature also decreases to 204℃ instead of 230℃ in steady-state phase. However, the FURNACE medium flow rate increases to maintain the REACTOR inlet temperature at 230℃. Notably, differences peak temperatures between dynamics and steady-state simulation are caused by choosing numbers of profile intervals in Aspen Plus.

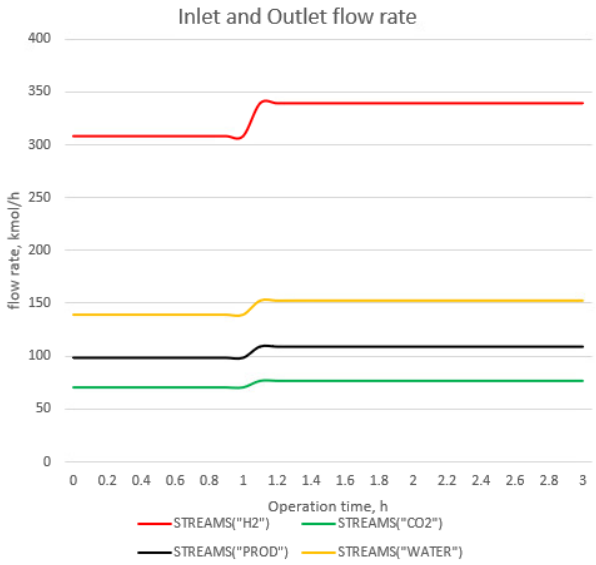

Figure 36.Inlet and Outlet flowrate (kmol/h) in case of increasing H_2 feed load (+10%). Inlet: H_2 stream and CO_2 stream; Outlet: PROD stream and WATER stream.

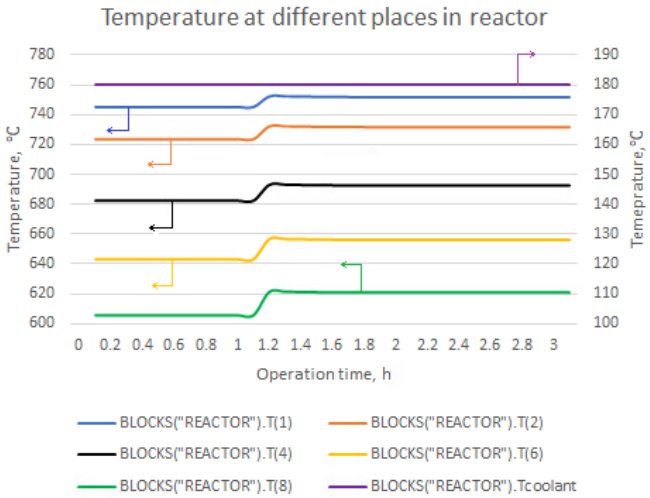

Figure 35.Temperature at different length in REACTOR in case of increasing H_2 feed load (+10%): T(1), T(2), T(4), T(6), and T(8) placed at position of 3.33%, 6.66%, 13.33%, 20%, 26.66% of reactor length and T_coolant is coolant fluid temperature.

The composition of PROD stream (in Figure 23) is also tested during the loading change. As presented in Figure 37, when the feed load increases, there are some fluctuations in composition of stream. H_2 and CH_4 mole fractions have no significant changes and almost keep stable values at 28% and 71%, respectively. Otherwise, H_2O mol-% increases rapidly in seconds of changing load and decreases gradually to the new steady values after 30 minutes of changing. Through these values, it can be recognized that when the feed load increases, the product stream's composition is still stable and contains mostly CH_4 and H_2. However, when the H_2 load changes, the hot spot appears in the inlet zone of REACTOR that may affect catalyst bed lifetime (over 700℃). Besides that, all controllers have good responses with flow rate changing, and the process runs smoothly.

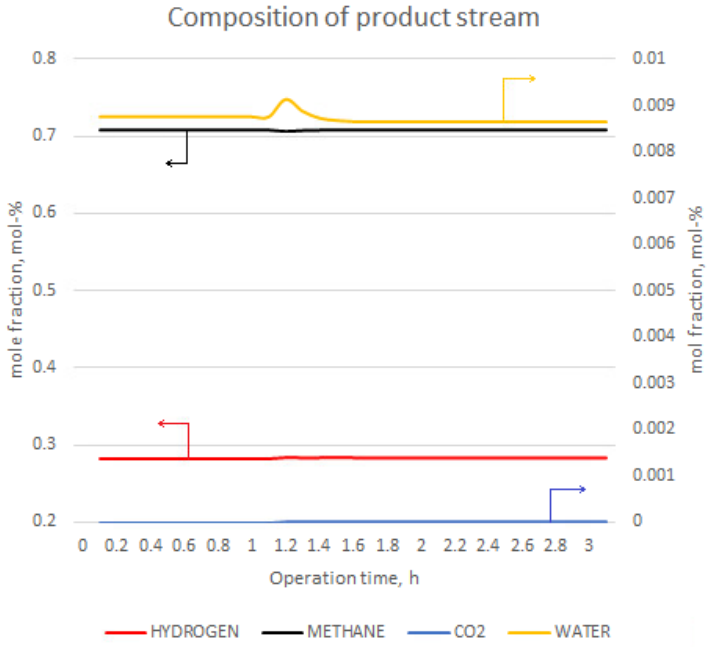

Figure 37. The composition of PROD stream during feed load change +10%, the product contains almost H_2 and CH_4.

7.2.2 Diminishment of H_2 flow rate (−10%)

After one hour of simulation time, the feed flowrate decreased by 10% and the H_2 flow rate changes to 277.2 kmol/h (Figure 38). As can be seen from Figure 39, OP of controller Reactor_TC remains the coolant temperature at 180℃, then the peak temperature in REACTOR is 738℃, and lower than in full load design. With this SP of Reactor_TC

controller, the fluid temperature at outlet of REACTOR is 220.5℃ leading to the reduction of HX1's cold side outlet temperature to 189℃ instead of 230℃. However, FURNACE's medium flow rate increases to maintain the REACTOR inlet temperature at 230℃. In reduction of H_2 feeding load (−10%), the system just has slight fluctuations and backs to new steady-state in shorter time (around 20 minutes) than the increasing case.

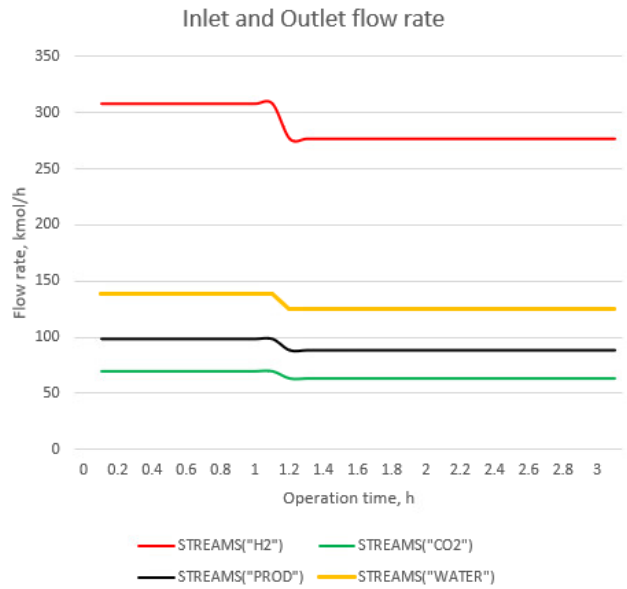

Figure 38. Inlet and Outlet flowrate (kmol/h) in case of decreasing H_2 feed load (–10%). Inlet: H_2 stream and CO_2 stream; Outlet: PROD stream and WATER stream.

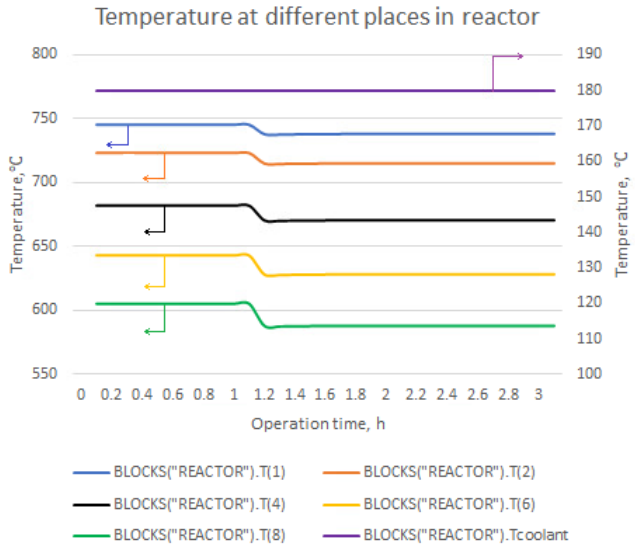

Figure 39. Temperature at different length in REACTOR in case of decreasing H_2 feed load (–10%): T(1), T(2), T(4), T(6), and T(8) placed at position of 3.33%, 6.66%, 13.33%, 20%, 26.66% of reactor length respectively, and T_coolant is coolant fluid temperature.

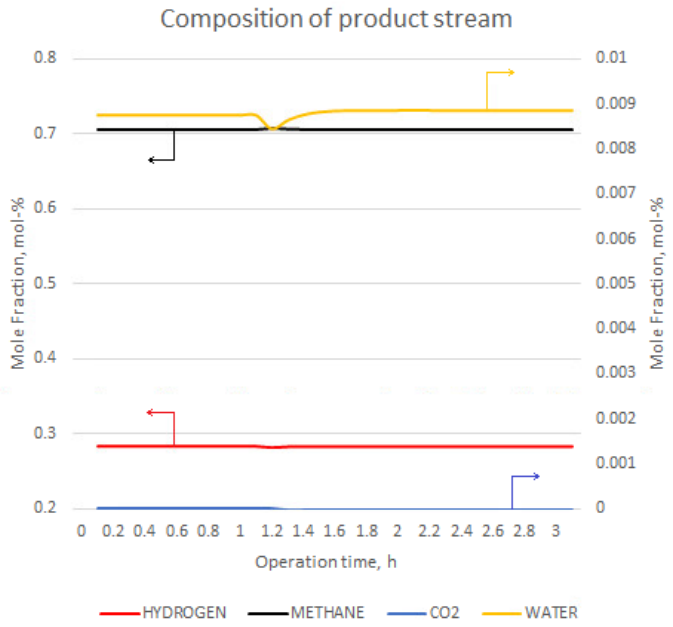

Figure 40. The composition of PROD stream during feed load change –10%.

The composition of PROD stream is shown in Figure 40. As results show, there is a similar trend in mole fraction of CO_2 of this case and the increasing case, the product contains mainly H_2 and CH_4. Meanwhile, H_2 and CH_4 mole fraction remain around 71% and 28%, respectively. Lastly, the proportion of water in product stream slightly gains to 0.9% after feed load diminishing. With a low CO_2 content of 5.55 mmol/h, the product stream meets the requirements of the model in terms of CO_2 impurities. Notably, in this case, the peak temperature goes down to 738℃, however, it is still higher than the Ni-based catalyst's maximum heat tolerance of 700℃. In addition, the catalyst bed temperature is always higher than 240℃ during operation time. As mentioned above, the catalyst temperature should be in range 230℃−700℃ to avoid catalyst sintering.

7.2.3 Diminishment of H_2 flow rate (−30%)

At 1h of simulation time, the reduction of 30% (to 215.6 kmol/h) H_2 feed flow rate is applied which prompts the control action needed to keep the over-stoichiometric ratio in place. As can be observed from Figure 41, the response of feed flow controllers quickly brings the stoichiometric ratio between reactants back to the desirable value. As can be observed from Figure 42, the temperature in REACTOR is also oscillated by the changing feed flow rate.

During the test, coolant temperature remains at OP of Reactor_TC controller of 180℃, while the peak temperature is 722℃ in the new steady state, lower than two cases above.

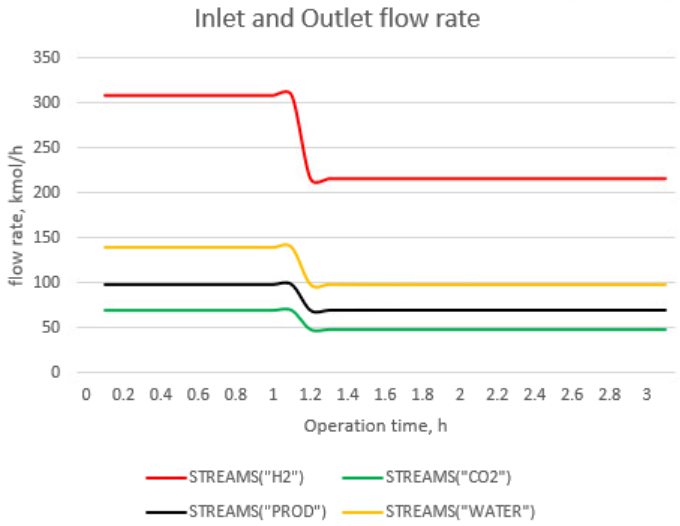

Figure 41. Inlet and Outlet flowrate (kmol/h) in case of decreasing H_2 feed load (–30%). Inlet: H_2 stream and CO_2 stream; Outlet: PROD stream and WATER stream.

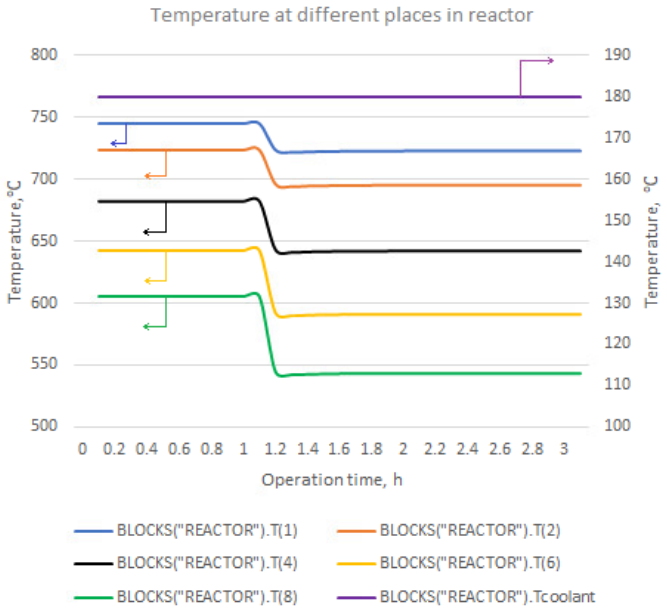

Figure 42. Temperature at different length in REACTOR in case of decreasing H_2 feed load (–30%): T(1), T(2), T(4), T(6), and T(8) placed at position of 3.33%, 6.66%, 13.33%, 20%, 26.66% of reactor length respectively, and T_coolant is coolant fluid temperature.

The changes in product stream (PROD in Figure 23) during simulation time are shown in Figure 43. About H_2 and CH_4 mole fractions, fluctuations occur in short time of simulation, and the new steady value is almost same before changing feed load. As same as diminishment of 10% case, the water content also gains to higher value ~ 0.91%. In general, because of the high stoichiometric ratio between reactants, CO_2 mostly reacts and transforms to CH_4, so the product stream mainly contents CH_4 and H_2. As mentioned above, the products could be separated by a separator system; therefore, the H_2 content will be removed from the mixture and pure CH_4 can be supplied to the market. In addition, as other tests, when diminishing H_2 feed flow rate to 70% of full load, the hot spot still appears at the inlet zone of REACTOR. Through these tests, the peak temperature decreases when the H_2 feed load decreases, and quality of product stream keeps stable trends; it is possible to separate CH_4 and H_2 by further steps.

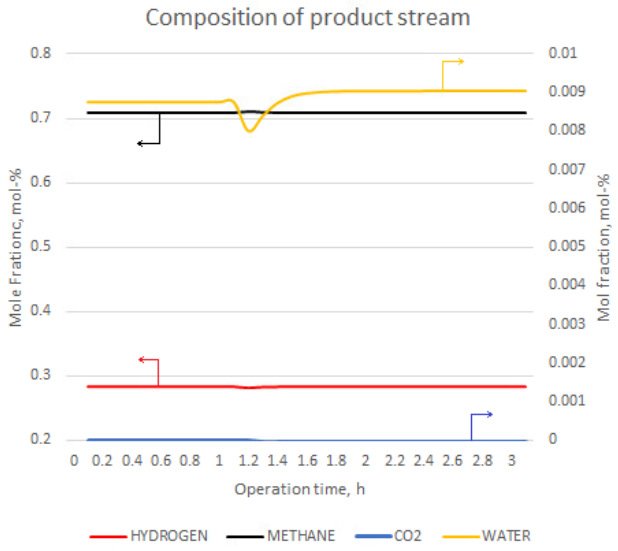

Figure 43. The composition of PROD stream during feed load change –30%. The CO_2 mole fraction in the test is almost 0%.

7.3 Model's limitation

In the last section, the H_2 feed flow rate was changed directly from the SP of H2_FC controller which are instantaneous step changes. The results show the fluctuations in the system during tests, so in this section, the ramping rate is applied to have a smoother and

more realistic model. In addition, the lowest H_2 feed loading limitations will also be determined.

7.3.1 Ramping rate

There are four cases of ramping rate tested: ±50% in 1 hour, ±50% in 0.5 hours, ±50% in 0.25 hours, and ±50% in 0.083 hours (5 minutes). In each case, the H_2 feed flow rate drops 50% of full capacity (308 kmol/h) during the time (t = 1 to 2h, 1.5h, 1.25h, and 1.083 respectively) and gains with same ramping rate back to normal at t = 4, 3.5h, 3.25h, and 3.083h. As same as diminishing cases above, the SP of Reactor_TC is set at 700℃ for these tests. The purpose of these tests is to determine the highest ramping rate in which model can be handled. The responses of Reactor_TC controller and H_2 mole fraction in product stream are evaluated.

The results of tests are illustrated in Figure 44 to Figure 47. The highest ramping rate in test is 50% change in 5 minutes (0.083 hours), and the simulation still can handle smoothly, with the SP of 700℃ of Reactor_TC controller, the temperature inside reactor can be managed leading to a successful model. In all cases, HX1's cold side outlet temperatures are in range from 176 to 195℃; and as mentioned above, the REACTOR's inlet temperatures are always kept at 230℃ by FURNACE heat flow rate. Therefore, the REACTOR's outlet temperature is 204℃ at full load and drops to 183℃ at 50% of load (154 kmol/h). Notably, the coolant temperature has significant changes when the feed load decreases to 50% of load and with higher ramping time, the higher coolant temperature is achieved; however, when the peak temperature comes back to SP value of 700℃, the coolant temperature decreases to 180℃ within 1 to 2 hours of operation time.

Furthermore, the H_2O molar fractions also fluctuate during load tests but this value quickly back to steady state. In all cases, the product stream contains mainly CH_4, H_2, and H_2O which means mostly CO_2 is converted in reactor during simulation. The results also show that with a higher ramping rate, the process has more intense oscillations. During ramping time tests, the impurities' bound of CO_2 are still in favorable range, and the product can be purified and injected into national grid.

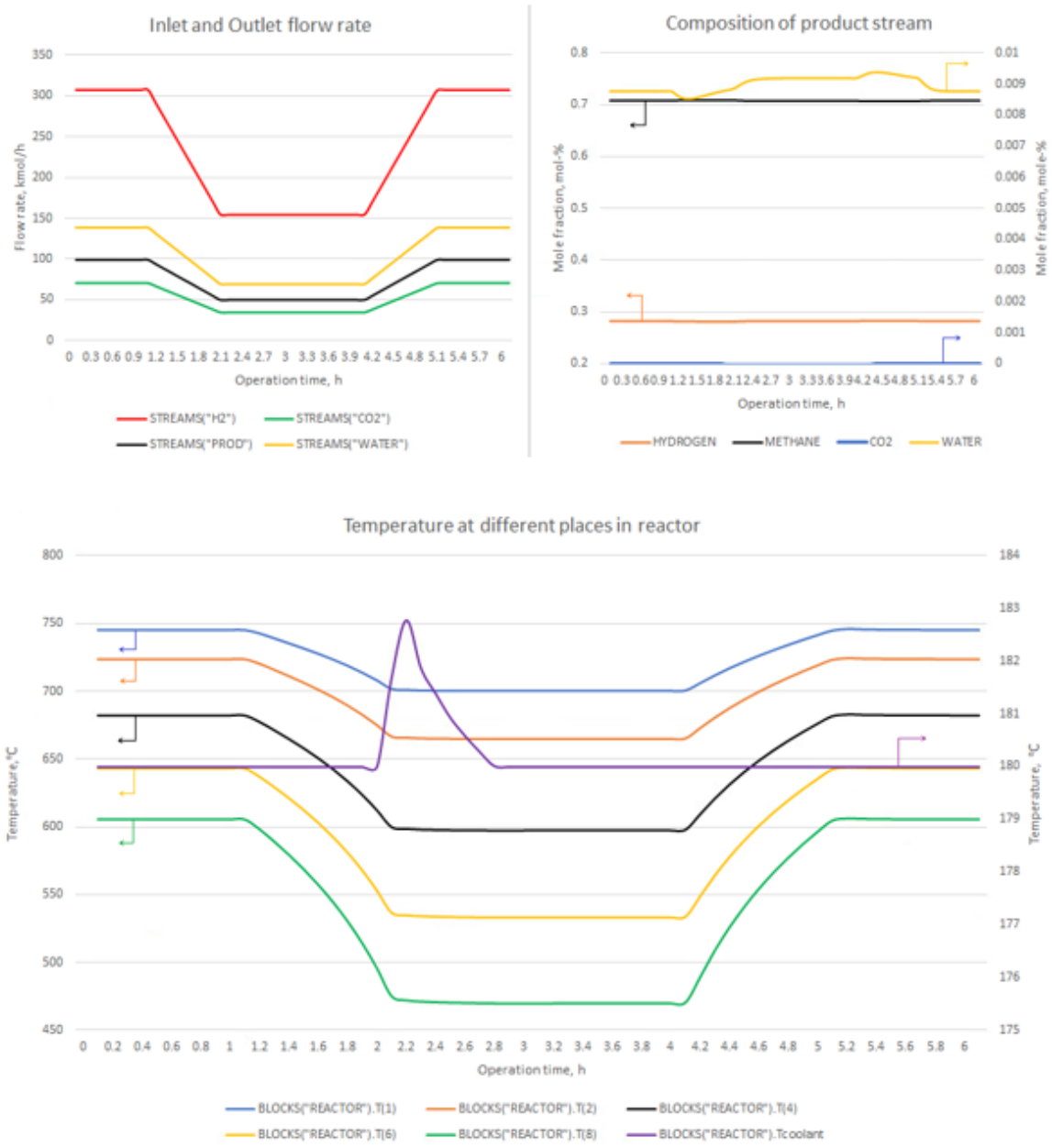

Figure 44. Flowrate (kmol/h) of inlet and outlet streams (top-left), composition of product stream (top-right), and reactor temperatures (bottom) in case of H_2 feeding ramping rate of ± 50% in 1 hour.

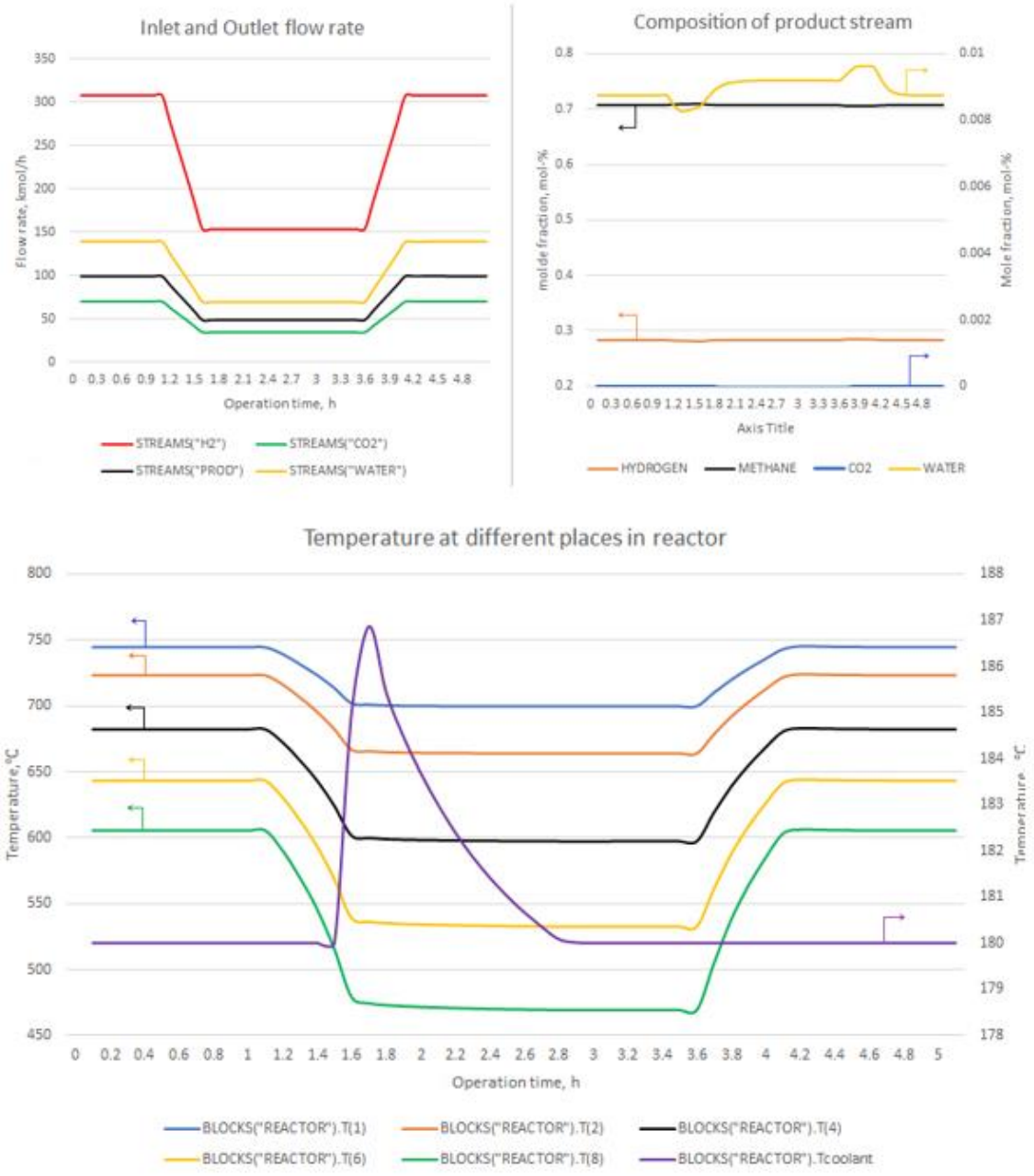

Figure 45. Flowrate (kmol/h) of inlet and outlet streams (top-left), composition of product stream (top-right), and reactor temperatures (bottom) in case of H_2 feeding ramping rate of ± 50% in 0.5 hours.

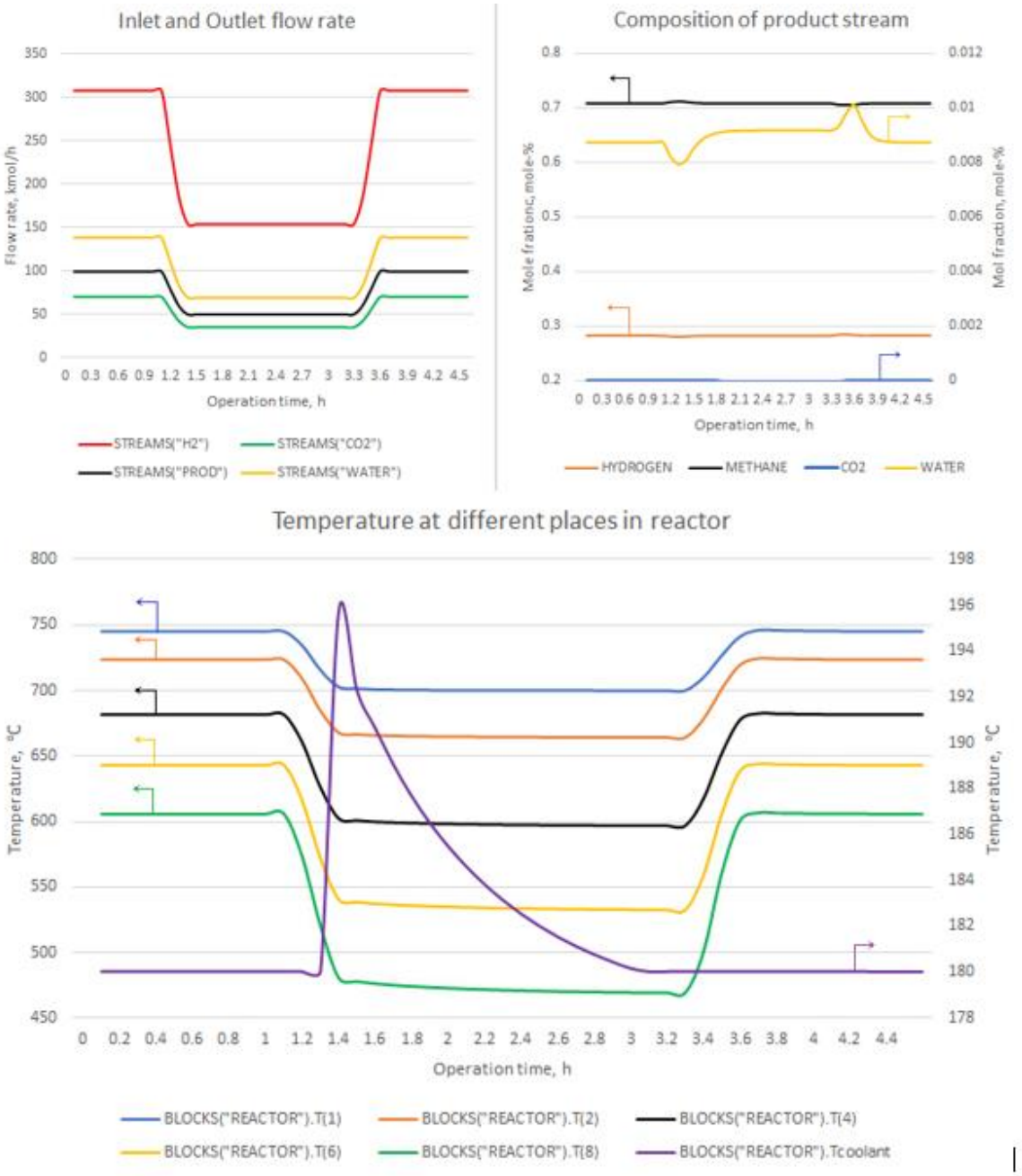

Figure 46. Flowrate (kmol/h) of inlet and outlet streams (top-left), composition of product stream (top-right), and reactor temperatures (bottom) in case of H_2 feeding ramping rate of ± 50% in 0.25 hours.

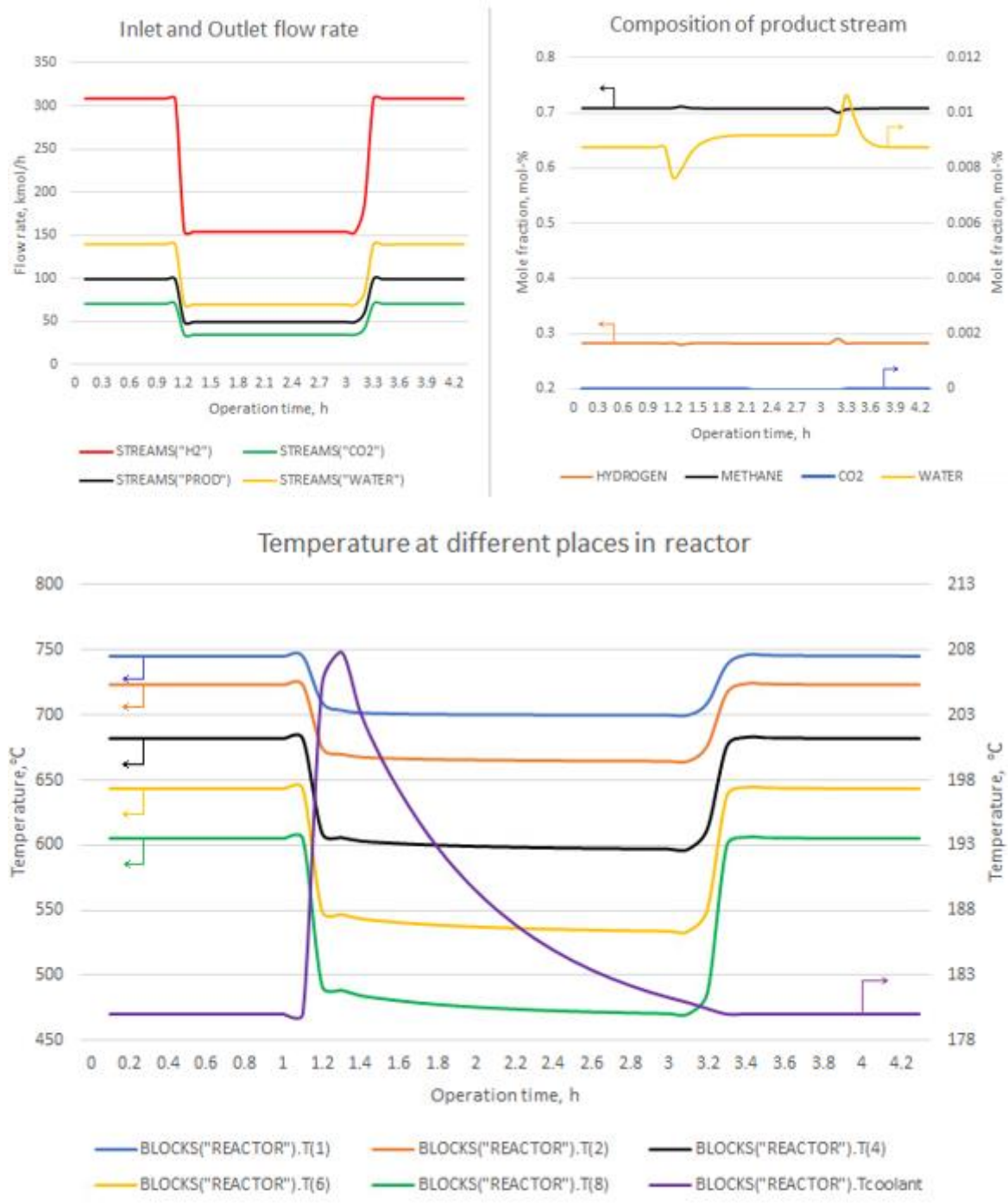

Figure 47. Flowrate (kmol/h) of inlet and outlet streams (top-left), composition of product stream (top-right), and reactor temperatures (bottom) in case of H_2 feeding ramping rate of ± 50% in 0.0833 hours.

7.3.2 Minimum H_2 feed load

To determine the minimum H_2 feed load in which the model can be handled, the decreasing by 8 kmol of H_2 feed flow rate per 30 minutes is applied. As can be observed from Figure 48, the minimum value of H_2 feed flow is 138 kmol/h ~ 44.8% of normal load. The following step of 137 kmol/h was tested, and Aspen Plus Dynamics met an error in solving the nonlinear equation after 0.25 hours of simulation time. Therefore, the model could be faulted by either the Aspen Plus Dynamics computation limitations or the model's design.

In addition, the Reactor_TC controller's SP of 700℃ is applied during the test, and the coolant temperature increases to 250℃ causing the REACTOR's outlet temperature to be around 250℃ at t = 11h and the cold outlet stream of HX1 to be 238℃. Due to low H_2 feed flow rate, the residence time of fluid inside HX1 is increased leading to higher temperature in cold side outlet stream. Therefore, when the new feed load of 137 kmol/h applied to model at t = 12h; and the valve VF is totally closed by Feed_TC1 controller because of overheating in stream FUR-IN and FURNACE is the one heats the fluid process before feeding to REACTOR. From the temperature results of REACTOR and heat exchanger HX1, the minimum H_2 inlet flowrate is dependent on design of heat exchanger as well as the coolant temperature in reactor. Besides that, the hot spot appeared at the inlet of reactor until the H_2 feed load decreased to 148 kmol/h, the peak temperature was 697℃ that is considered a safe temperature for catalyst bed.

Moreover, the water content in the PROD stream gradually gains in lower H_2 loads and could be removed by water vapor condenser in next steps. As same as cases above, in this test, the CO_2 content in product stream is very low. Besides that, H_2 and CH_4 molar fraction have intense fluctuations at lower flow rates, but generally, these values are still in favorable ranges. As a result, during the test, the quality of the product stream maintains a favorable range of CO_2 content.

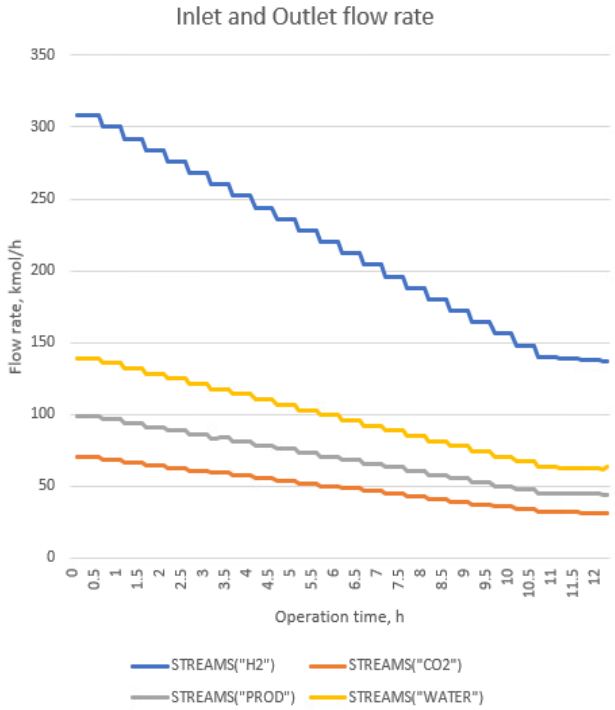

Figure 48. Inlet and Outlet flowrate (kmol/h) in case of determining minimum feed load. Inlet: H_2 stream, CO_2 stream; Outlet: PROD stream, WATER stream.

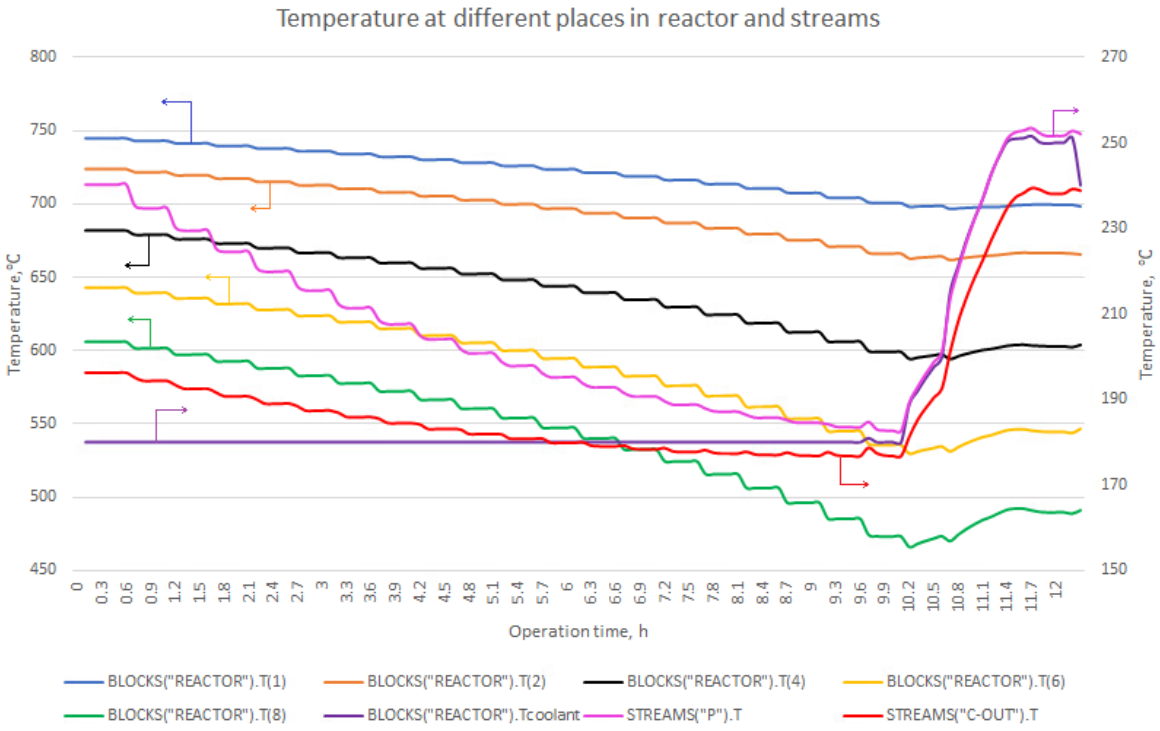

Figure 49. Temperature at different places in REACTOR and streams (outlet stream of reactor and outlet stream of HX1's cold side) in model during the minimum load tests.

8 Conclusion

Power-to-gas is an intriguing technology that can contribute to the European Union's objectives for decarbonization. In this concept, generated CH_4 from electrolytic H_2 and captured CO_2 can be an effective solution. But maintaining a steady flow rate of H_2 is a major challenge, because of the instability of renewable energy sources. Therefore, the dynamic investigation of the CO_2 methanation process's behavior is a significant step in optimizing reaction conditions, enhancing the overall efficiency and sustainability of CH_4 production, especially in the frame of renewable energy integration and captured carbon utilization. In this study, steady-state and dynamics models of CO_2 methanation were developed according to the capacity of 35 MW electrolysis unit in Aspen Plus and Aspen Plus dynamics to evaluate the model's dynamic performance, operational limitations (minimum loading and maximum achievable ramping rate), and the feasibility of accepting the generated gas into the network during the transition phase.

Firstly, the steady-state model was built in Aspen Plus based on initial information about H_2 feed flow rate (308 kmol/h) and Koschany et al.'s kinetic model. With a stoichiometric ratio of 4.4:1 between H_2 and CO_2, CO_2 mostly was reacted and converted to CH_4 in a multi-tubular reactor leading to a very high CO_2 conversion in reactor ~ 99.99 mol-%. However, the hot spot (768℃) appeared and might harm the catalyst bed. Recycling of reactant stream was used to reduce the peak temperature from 782℃ to 768℃.

Following the steady-state phase study, the model was exported to Aspen Plus Dynamics to investigate the dynamic behavior of methanation process. A control system was applied to the model by using feedback controllers and valves. In dynamic study, the H_2 feed flow rates were changed discontinuously with three values (+10%, −10%, and –30% of steady designed flow rate). The results showed the fast and good responses of the controllers; especially, the reactor's peak temperatures were selected by selector block, then the cooling fluid temperature was adjusted corresponding to the selected value. In all tests, the hot spots appeared in the inlet zone of REACTOR and were higher than the maximum catalyst tolerance. However, when compared to the peak temperature of 768℃ in steady state model, the peak temperature at the full load was mitigated to 745℃ by the control structure. With

the applied control scheme, the product stream contains mainly CH_4 and H_2 which adopted favorable ranges.

In addition, the highest ramping rate and the minimum H_2 feed load were determined. The ramping rate was test in four cases ±50% in 1 hour, ±50% in 0.5 hours, ±50% in 0.25 hours, and ±50% in 0.083 hours (5 minutes) with the peak temperature controller's SP of 700℃; and the highest achieved ramping rate is 50% change in 5 minutes ~ 10%/min. As the result of the dynamic simulation, 44.8% of steady-designed H_2 feed load was determined as the minimum capacity of the model. The lower feed rate was tested, but the Aspen Plus Dynamics met the integrator error, which means the model could be faulted by either the Aspen Plus Dynamics computation limitations or the model's design. The model's limitations are dependent on the reactor's coolant temperature, heat exchanger and control valve design, so the minimum feed load might be lower if these factors could be developed.

The present study was designed and applied to improve and investigate the CO_2 methanation process in dynamic conditions. With the control system and recycling stream, the hot spot temperature was mitigated from 782℃ to 745℃ at full-load. However, the appearance of hot spot in the inlet zone of the reactor in steady-state design and during the transition period may damage the catalyst bed. Hence, in further research, the control system, equipment, or feeding strategies should be studied to minimize the high peak temperature in the reactor as well as achieve the highest efficiency process. Besides that, the higher recycle ratio (Rec) could be investigated to minimize the peak temperature in reactors. In addition, the H_2 in the final stream should be separated by a separator system, e.g., membrane to achieve desired specifications before injecting CH_4 product into the national SNG grid.

References

[1] Tan, C. H., Nomanbhay, S., Shamsuddin, A. H., Park, Y., Hernández-Cocoletzi, H. & Show, P. L. 2022. Current Developments in Catalytic Methanation of Carbon Dioxide—A Review. Front. Energy Res., 2022-1, Vol.9.

[2] International Energy Agency, IEA. World energy outlook 2023. 2023. Available https: //www.iea.org/reports/world-energy-outlook-2023. Accessed 18.04.2024.

[3] Park, S., Choi, K., Lee, C., Kim, S., Yoo, Y. & Chang, D. 2021. Techno-economic analysis of adiabatic four-stage CO2 methanation process for optimization and evaluation of power-to-gas technology. International journal of hydrogen energy, 2021-06, Vol.46 (41), p.21303-21317

[4] Balsalobre-Lorente, D., Shahbaz, M., Roubaud, D. & Farhani, S. 2018. How economic growth, renewable electricity and natural resources contribute to CO_2 emissions? Energy Policy, 113, 356–367.

[5] International Trade Administration. 2023. Finland - Country Commercial Guide. Available https://www.trade.gov/country-commercial-guides/finland-energy. Accessed 19.04.2024.

[6] Finnish Wind Power Association. 2024. About Wind Power in Finland. Available https://tuulivoimayhdistys.fi/en/wind-power-in-finland-2/about-wind-power-in-finland. Accessed 19.04.2024.

[7] State Treasury Republic of Finland. 2022. Debt Management Annual Review 2022.

[8] Burger, T. 2021. CO_x Methanation over Ni-Al-Based Catalysts: Development of CO_2 Methanation Catalysts and Kinetic Modelling. Available https://mediatum.ub.tum.de/doc/1574621/1574621.pdf#page36. Accessed: 19.04.2024.

[9] Bremer, J., Sundmacher, K. 2019. Operation range extension via hot-spot control for catalytic CO2 methanation reactors. React. Chem. Eng. Vol.4(6), p.1019–1037.

[10] Blanco, H., Nijs, W., Ruf, J. & Faaij, A. 2018. Potential of Power-to-Methane in the EU energy transition to a low carbon system using cost optimization. Applied energy, 2018-12, Vol.232, p.323-340.

[11] McKenna, R. C., Bchini, Q., Weinand, J. M., Michaelis, J., König, S., Köppel, W. & Fichtner, W. 2017. The future role of Power-to-Gas in the energy transition: Regional and local techno-economic analyses in Baden-Württemberg. Applied Energy, 2018-2, Vol.212, p.386-400.

[12] König, S., Bchini, Q., McKenna, R., Köppel, W., Bachseitz, M. & Michaelis, J. 2017. Spatially-resolved analysis of the challenges and opportunities of Power-to-Gas (PtG) in Baden-Württemberg until 2040. Energy Procedia, 2017-10, Vol.135, p.434-444.

[13] Burre, J., Bongartz, D., Brée, L., Roh, K. & Mitsos, A. 2019. Power-to-X: Between Electricity Storage, e-Production, and Demand Side Management. Chemie ingenieur technik, 2020-01, Vol.92 (1-2), p.74-84.

[14] de Vasconcelos, B. R. & Lavoie, J. 2019. Recent advances in Power-to-X technology for the production of fuels and chemicals. Frontiers in chemistry, Vol.7, 2019.

[15] Inkeri, E. 2021. Modelling of component dynamics and system integration in power-to-gas process. Available https://lutpub.lut.fi/bitstream/handle/10024/163488/Eero%20Inkeri_A4.pdf?sequence=1&isAllowed=y. Accessed: 19.04.2024.

[16] Buffo, G., Marocco, P., Ferrero, D., Lanzini, A. & Santarelli, M. 2019. Power-to-X and power-to-power routes. Solar Hydrogen Production - Processes, Systems and Technologies, 2019, Chapter 15, p.530-557.

[17] Tichler, R. & Bauer, S. 2016. Power-to-Gas. Storing Energy - With Special Reference to Renewable Energy Sources, 2016, part E, chapter 18, p.373-387

[18] Boudellal, M. 2018. Power-to-gas: Renewable hydrogen economy for the energy transition.

[19] Sasaki, K., Li, H., Hayashi, A., Yamabe, J., Ogura, T. & Lyth, S. M. 2016. Hydrogen Energy Engineering A Japanese Perspective. Green Energy and Technology. Springer Japan, 2016.

[20] Götz, M., Lefebvre, J., Mörs, F., Koch, A. M., Graf, F., Bajohr, S., Reimert, R. & Kolb, T. 2015. Renewable Power-to-Gas: A technological and economic review. Renewable Energy, 2016-1, Vol.85, p.1371-1390.

[21] Gahleitner, G. 2012. Hydrogen from renewable electricity: An international review of power-to-gas pilot plants for stationary applications. International Journal of Hydrogen Energy, 2013-2, Vol.38(5), p.2039-2061.

[22] Buttler, A. & Spliethoff, S. 2017. Current status of water electrolysis for energy storage, grid balancing and sector coupling via power-to-gas and power-to-liquids: A review. Renewable and Sustainable Energy Reviews, 2018-2, Vol.82, p.2440-2454.

[23] Specht, M., Brellochs, J., Frick, V., Stürmer, B., Zuberbühler, U., Sterner, M. & Waldstein, G. 2010. Storage of renewable energy in the natural gas grid. Erdöl Erdgas Kohle, 2010, Vol.126, p.342-346.

[24] Hoekman, S. K., Broch, A., Robbins, C. & Purcell, R. 2010. CO2 recycling by reaction with renewably-generated hydrogen. International Journal of Greenhouse Gas Control, 2010-1, Vol.4(1), p.44-50.

[25] Lehner, M., Tichler, R, Steinmüller, H. & Koppe, M. 2014. Power-to-Gas: Technology and business model.

[26] Wulf, C., Zapp, P. & Schreiber, A. 2020. Review of Power-to-X Demonstration Projects in Europe. Frontiers in Energy Research, 2020, Vol.8.

[27] Najjar, Y. S. H. 2013. Hydrogen safety: The road toward green technology. International Journal of Hydrogen Energy, 2013-8, Vol.38(25), p.10716-10728.

[28] European Commission. 2023. Renewable energy targets. Available: https://energy.ec.europa.eu/topics/renewable-energy/renewable-energy-directive-targets-and-rules/renewable-energy-targets_en. Accessed: 16.05.2024.

[29] McDonagh, S., O'Shea, R., Wall, D. M., Deane, J. P. & Murphy, J. D. 2018. Modelling of a power-to-gas system to predict the levelised cost of energy of an advanced renewable gaseous transport fuel. Applied Energy, 2018-4, Vol.25, p.444-456.

[30] Fambri, G., Diaz-Londono, C., Mazza, A., Badami, M., Sihvonen, T. & Weiss, R. 2022. Techno-economic analysis of Power-to-Gas plants in a gas and electricity distribution network system with high renewable energy penetration. Applied Energy, 2022-4, Vol.312.

[31] Gasum. 2024. Biogas and natural gas prices at filling stations. Available: https://www.gasum.com/fi/kaasu-liikenteelle/yksityisille-kaasuautoilijoille/tankkaushinnat/. Accessed: 16.05.2024.

[32] Rönsch, S., Schneider, J., Matthischke, S., Schlüter, M., Götz, M., Lefebvre, J., Prabhakaran, P. & Bajohr, S. 2015. Review on methanation–From fundamentals to current projects. Fuel, 2016-2, Vol.166, p.276–296.

[33] Schildhauer, T. J. & Biollaz, S. M. A. 2016. Synthetic natural gas from coal, dry biomass, and power-to-gas applications. Chapter 4, p.77-151.

[34] Tomassi, M., Degerli, S. N., Ramis, G. & Rosetti, I. 2023. Advancements in CO2 methanation: A comprehensive review of catalysis, reactor design and process optimization. Chemical engineering research and design, 2024-1, Vol.201, p.457-482.

[35] Alam, M. I., Cheula, R., Moroni, G., Nardi, L.& Maestri, M. 2021. Mechanistic and multiscale aspects of thermo-catalytic CO2 conversion to C1 products. Catalysis Science and Technology, 2021, Vol.11(20), p.6601-6629.

[36] Lee, W. J., Li, C., Prajitno, H., Yoo, J., Patel, J., Yang, Y. & Lim, S. 2020. Recent trend in thermal catalytic low temperature CO2 methanation: A critical review. Catalysis today, 2021-5, Vol.368, p.2-19.

[37] Sahebdelfar, S. & Ravanchi, M. T. 2015. Carbon dioxide utilization for methane production: A thermodynamic analysis. Journal of Petroleum Science and Engineering, 2015, Vol.134, p.14-22.

[38] Gao, J., Wang, Y., Ping, Y., Hu, D., Xu, G., Gu, F. & Su, F. 2011. A thermodynamic analysis of methanation reactions of carbon oxides for the production of synthetic natural gas. Royal Society of Chemistry, 2012, Vol.2, p.2358-2368.

[39] Jürgensen, L., Ehimen, E. A., Born, J. & Holm-Nielsen, J. B. 2014. Dynamic biogas upgrading based on the Sabatier process: Thermodynamic and dynamic process simulation. Bioresource Technology, 2015-2, Vol.178, p.323-329.

[40] Kopyscinski, J., Schildhauer, T. J., Biollaz, S. M. A. 2010. Production of synthetic natural gas (SNG) from coal and dry biomass – A technology review from 1950 to 2009. Fuel (Guildford), 2010-08, Vol.89(8), p.1763-1783.

[41] Dannesboe, C., Hansen, J. B., Johannsen, I. 2020. Catalytic methanation of CO2 in biogas: experimental results from a reactor at full scale. Reaction Chemistry and Engineering, 2020, Vol.5(1), p.183-189.

[42] Hervy, M., Maistrello, J., Brito, L., Rizand, M., Basset, E., Kara, Y. & Maheut, M. 2021. Power-to-gas: CO2 methanation in a catalytic fluidized bed reactor at demonstration scale, experimental results and simulation. Journal of CO2 Utilization, 2021-8, Vol.50.

[43] Lefebvre, J., Götz, M., Bajohr, S., Reimert, R. & Kolb, T. 2014. Improvement of three-phase methanation reactor performance for steady-state and transient operation. Fuel processing Technology, 2015-4, Vol. 132, p.83-90.

[44] Meng, F., Li, Z., Liu, J., Cui, X. & Zheng, H. 2015. Effect of promoter Ce on the structure and catalytic performance of Ni/Al2O3 catalyst for CO methanation in slurry-bed reactor. Journal of Natural Gas Science and Engineering, Vol.23, 2015-3, p.250-258.

[45] Zhang, J., Bai, Y., Zhang, Q., Wang, X., Zhang, T., Tan, Y. & Han, Y. 2014. Low-temperature methanation of syngas in slurry phase over Zr-doped Ni/γ-Al2O3 catalysts prepared using different methods. Fuel, 2014-9, Vol.132, p.211-218.

[46] Ghaib, K. & Ben-Fares, F. 2018. Power-to-Methane: A state-of-the-art review. Renewable and Sustainable Energy Reviews, 2018-1, Vol.81, p.433-446.

[47] Mills, G. A. & Steffgen, F. W. 1974. Catalytic Methanation. Catalysis Reviews, 1974, Vol.8(1), p.159-210.

[48] Lee, G. D., Moon, M. J., Park, J. H., Park, S. S. & Hong, S. S. 2005. Raney Ni catalysts derived from different alloy precursors Part II. CO and CO2 methanation activity. Korean journal of chemical engineering, 2005, Vol.22, p.541-546.

[49] Garbarino, G., Belloti, D., Riani, P., Magistri, L. & Busca, G. 2015. Methanation of carbon dioxide on Ru/Al2O3 and Ni/Al2O3 catalysts at atmospheric pressure: Catalysts activation, behavior and stability. International Journal of Hydrogen Energy, 2015-8, Vol.40(30), p.9171-9182.

[50] Quindimil, A., De-La-Torre, U., Pereda-Ayo, B., Davó-Quiñonero, A., Bailón-García, E., Lozano-Castelló, D., González-Marcos, J., Bueno-López, A. & González-Velasco, J. R. 2019. Effect of metal loading on the CO2 methanation: A comparison between alumina supported Ni and Ru catalysts. Catalysis Today, 2020-10, Vol.356, p.419-432.

[51] Younas, M., Kong, L. L., Bashir, M. J. K., Nadeem, H., Shehzad, A. & Sethupathi, S. 2016. Recent Advancements, Fundamental Challenges, and Opportunities in Catalytic Methanation of CO2. Energy Fuels, 2016, Vol.30(11), p.8815-8831.

[52] Italiano, C., Llorca, J., Pino, L., Ferraro, M., Antonucci, V. & Vita, A. 2019. CO and CO2 methanation over Ni catalysts supported on CeO2, Al2O3 and Y2O3 oxides. Applied Catalysis B: Environmental, 2020-5, Vol.264.

[53] American Biogas Council. 2023. World's Largest Full Scale Biological Methanation Plant Uses Biogasclean's Methanation System. Available: https://americanbiogascouncil.org/worlds-largest-full-scale-biological-methanation-plant-uses-biogascleans-methanation-system/. Accessed 30.05.2024.

[54] van Leeuwen, C. 2018. Innovative large-scale energy storage technologies and Power-to-Gas concepts after optimisation. Available: https://ec.europa.eu/research/participants/documents/downloadPublic?documentIds=080166e5ba3ba6a8&appId=PPGMS. Accessed 30.04.2024.

[55] Lecker, B., Illi, L., Lemmer, A. & Oechsner, H. 2017. Biological hydrogen methanation – A review. Bioresource Technology, 2017-12, Vol.245, p.1220-1228.

[56] Seifert, A. H., Rittmann, S., Bernacchi, S. & Herwig, S. 2013. Method for assessing the impact of emission gasses on physiology and productivity in biological methanogenesis. Bioresource Technology, 2013-5, Vol.136, p.747-751.

[57] Rittmann, S. K. M. R. 2015. A Critical Assessment of Microbiological Biogas to Biomethane Upgrading Systems. Biogas Science and Technology, 2015, p.117-133.

[58] Angelidaki, I., Treu, L., Tsapeukos, P., Luo, G.,Campanaro, S., Wenzel, H. & Kougias, P. G. 2018. Biogas upgrading and utilization: Current status and perspectives. Biotechnologies Advances, 2018-3, Vol.36(2), p.452-466.

[59] Kopyscinski, J. 2010. Production of synthetic natural gas in a fluidized bed reactor.

[60] Thema, M., Bauer, F. & Sterner, M. 2019. Power-to-Gas: Electrolysis and methanation status review. Renewable and Sustainable Energy Reviews, Vol.112, 2019-9, p.775-787.

[61] Xu, J & Froment, G. F. 1989. Methane Steam Reforming, Methanation and Water-Gas Shift: 1. Intrinsic Kinetics. AIche Journal, 1989, Vol.35(1), p.88-96.

[62] Koschany, F., Schlereth, D. & Hinrichsen, O. 2015. On the kinetics of the methanation of carbon dioxide on coprecipitated NiAl(O)x. Applied Catalysis B: Environmental, 2016-2, Vol.181, p.504-516.

[63] Falbo, L., Martinelli, M., Visconti, C. G., Lietti, L., Bassano, C. & Deiana, P. 2017. Kinetics of CO2 methanation on a Ru-based catalyst at process conditions relevant for Power-to-Gas applications. Applied Catalysis B: Environmental, 2018-6, Vol.255, p.354-363.

[64] Lunde, P. J. & Kester, F. L. 1973. Rates of methane formation from carbon dioxide and hydrogen over a ruthenium catalyst. Journals of catalysis, 1973-9, Vol.30(3), p.423-429.

[65] Giglio, E., Pirone, R. & Bensaid, S. 2020. Dynamic modelling of methanation reactors during start-up and regulation in intermittent power-to-gas applications. Renewable Energy, 2021-6, Vol.170, p.1040-1051.

[66] Konttila, E. 2022. Cost Optimization of Power-to-Methane Process with Dynamic Modelling. Master's thesis, Aalto University.

[67] Ducamp, J., Bengaouer, A. & Baurens, P. 2017. Modelling and experimental validation of a CO2 methanation annular cooled fixed-bed reactor exchanger. Canadian journal of chemical engineering, 2017-02, Vol.95 (2), p.241-252.

[68] Salomone, F., Marocco, P., Ferrario, D., Lanzini, A., Fino, D., Bensaid, S. & Santarelli, M. Process simulation and energy analysis of synthetic natural gas production from water electrolysis and CO2 capture in a waste incinerator. Applied energy, 2023-08, Vol.343, p.121200.

[69] Tripodi, A., Conte, F. & Rosetti, I. 2020. Carbon Dioxide Methanation: design of a fully integrated plant.

[70] Colelli, L., Bassano, C., Verdone, N., Segneri, V. & Vilardi, G. 2024. Power-to-Gas: Process analysis and control strategies for dynamic catalytic methanation system. Energy Conversion and Management, 2024, Vol.305.

[71] Process Ecology. 2015. Dynamic process simulation: When do we really need it? Available: https://processecology.com/articles/dynamic-process-simulation-when-do-we-really-need-it. Accessed 09.05.2024.

[72] Gray, M. A. 2010. Introduction to the Simulation of Dynamics Using Simulink.

[73] Partopour, B. & Dixon, A. G. 2019. Integrated multiscale modeling of fixed bed reactors: Studying the reactor under dynamic reaction conditions. Chemical engineering journal, 2019-12, Vol.377, p.119738, Article 119738.

[74] Bristol. 2007. The Wobbe Index and Natural Gas Interchangeability. Available: https://metersolution.com/wp-content/uploads/2013/02/wobbe-index.pdf. Accessed 31.05.2024.

[75] CEN, 2021. The Wobbe Index in the H-gas standard and renewable gases in gas quality standardization. Available: https://commission.europa.eu/document/download/aed356e7-ac99-4697-aded-d0df798831ed_en?filename=07.02_mf35-presentation-cen-wires_on_gas_quality_standard-schulken.pdf. Accessed: 31.05.2024

[76] Frank, E., Gorre, J., Ruoss, F. & Frield, M. J. 2018. Calculation and analysis of efficiencies and annual performances of Power-to-Gas systems. Applied Energy, 2018-05, Vol.218, p.217-231.

[77] Matthischke, S., Roensch, S. & Güttel, G. 2018. Start-up Time and Load Range for the Methanation of Carbon Dioxide in a Fixed-Bed Recycle Reactor. Industrial & engineering chemistry research, 2018-05, Vol.57(18), p.6391-6400.

[78] Fischer, K. L. & Freund, H. 2020. On the optimal design of load flexible fixed bed reactors: Integration of dynamics into the design problem. Chemical Engineering Journal, 2020-8, Vol. 393.

[79] Gruber, M., Weinbrecht, P., Biffar, L., Harth, S., Trimis, D., Brabandt, J., Posdziech, O. & Blumentritt, R. 2018. Power-to-Gas through thermal integration of high-temperature steam electrolysis and carbon dioxide methanation-experimental results. Fuel Processing Technology, 2018, Vol.181, p.61-74.

[80] Zimmermann, R. T., Bremer, J. & Sundmacher, K. 2021. Load-flexible fixed-bed reactors by multi-period design optimization. Chemical Engineering Journal, 2022-02, Vol.428.

[81] Specht, M., Brellochs, J., Frick, V., Stürmer, B., Zuberbühler, U. 2023. Synthetic natural gas from coal, dry biomass, and Power-to-gas applications, chapter 7.

[82] Ren-Gas. 2022. Clean Power-to-Gas fuel production and CO2-free district heating plant planned in Tampere Tarastenjärvi. Available: https://ren-gas.com/en/projekti/tampere-2/. Accessed 14.05.2024.

[83] Vantaa Energia, 2022. Vantaa Energy's Power-to-Gas Plant utilises new technology to process carbon dioxide into raw materia. Available: https://www.vantaanenergia.fi/en/vantaa-energys-power-to-gas-plant-utilises-new-technology-to-process-carbon-dioxide-into-raw-material/. Accessed 14.05.2024.

[84] Nieminen, H., Laari, A. & Koiranen, T. 2019. CO2 Hydrogenation to Methanol by a Liquid-Phase Process with Alcoholic Solvents: A Techno-Economic Analysis. Processes, 2019, Vol. 7 (7), p.405.

[85] FEST. Green electrolyzer: The state-of-the-art integrated electrolysis system for on-site production of hydrogen. Available: https://www.fest-group.de/en/hydrogen-technology/electrolysis-systems/. Accessed 30.06.2024.

[86] Thyssenkrupp. Industrial-Scale Water Electrolysis for Green Hydrogen Production. Available: https://thyssenkrupp-nucera.com/wp-content/uploads/2023/11/thyssenkrupp-nucera_green-hydrogen_brochure_web.pdf. Accessed 30.06.2024.

[87] Luyben, W. L. 2007. Steady-State Design of Tubular Reactor System. Chemical Reactor Design and Control. Hoboken, New Jersey: John Wiley & Sons; 2007, p. 251-286.

[88] IEA-AMF. Methane (natural gas, biomethane). Available: https://www.iea-amf.org/content/fuel_information/methane#legislation. Accessed 30.06.2024.

[89] Bremer, J. & Sundmacher, K. 2019. Operation range extension via hot-spot control for catalytic CO2 methanation reactor. Reaction Chemistry and Engineering, 2019.

[90] Luyben, W. L. 2007. Heat Exchanger/Reactor System. Chemical Reactor Design and Control. Hoboken, New Jersey: John Wiley & Sons; 2007, p. 369-406.

[91] Luyben, W. L. 2002. Plantwide Dynamic Simulators in Chemical Processing and Control, p. 1-24.

[92] EzLOK. 316 Stainless Steel Mechanical Properties. Available: https://www.ezlok.com/316-stainless-steel-properties. Accessed 31.08.2024.

[93] Wakao, N., Kaguei, S. & Funazkri, T. 1979. Effect of fluid dispersion coefficients on particle-to-fluid heat transfer coefficients in packed beds: correlation of Nusselt numbers, Chemical engineering science 34, 1979, p. 325–336.

[94] Dixon, A. G. 2011. Fixed bed catalytic reactor modelling—the radial heat transfer problem. The Canadian Journal of Chemical Engineering, 2012, Vol. 90, p. 507–527.

[95] Nguyen, V. H. 2022. Dynamic modeling of methanol synthesis from electrolytic hydrogen and captured carbon dioxide. LUT Master's Thesis.

[96] Cowan, A. Enalysis Tip 1.10 - Reciprocating Compressor Limitations. Available: https://www.detechtion.com/learningcenter/enalysis-tip-1.10-reciprocating-compressor-limitations. Accessed 18.09.2024.

[97] Sharifian, S., Asasian-kolur, N. & Harasek, M. 2019. Process Simulation of Syngas Purification by Gas Permeation Application. Chemical Engineering, 2019, Vol.76, p.829-834.

[98] Lider, A., Kudiiarov, V., Kurdyumov, N., Lyu. J., Koptsev, M., Travitzky, N. & Hotza, D. 2022. Materials and techniques for hydrogen separation from methane-containing gas mixtures. International Journal of Hydrogen Energy, 2023, Vol. 48(73), p.28390-28411.

Appendices

Appendix 1: Equipment sizing and heat transfer coefficient calculations

Table A-I. Equipment sizing of flash separator.

Parameters	Symbol	Equation	Value
Mass density of vapor mixture, kg m^{-3}	ρ_v		3.345
Maximum vapor velocity, m s^{-1}	V_{max}	$V_{max} = \frac{F - Factor}{\sqrt{\rho_v}} = \frac{0.61}{\sqrt{\rho_v}}$	0.334
Vapor volumetric flow rate, m^3 s^{-1}	V_v		0.11
Diameter based on vapor phase, m	D_v	$D_v = \sqrt{\frac{\frac{V_g}{V_{max}} \times 4}{\pi}}$	0.65
Height, m	H_v	$H_v = 2 \times D_v$	1.3
Mass density of liquid mixture, kg m^{-3}	ρ_l		747.7
Maximum liquid velocity, m s^{-1}	V_{max}	$V_{max} = \frac{F - Factor}{\sqrt{\rho_l}} = \frac{0.61}{\sqrt{\rho_l}}$	0.0223
Liquid volumetric flow rate, m^3 s^{-1}	V_l		0.0559
Diameter based on liquid phase, m	D_l	$D_l = \sqrt[3]{\frac{2 \times 2 \times 5 \times V_l}{\pi}}$	0.71
Height, m	H_v	$H_v = 2 \times D_l$	1.42

Table A-II. Heat transfer coefficient parameters, equations, and results (1/2).

Parameters	Symbol	Equation	Value
Number of tubes	$No.$		200
Tube diameter, m	D_t		0.04
Tube length, m	L		2.5
Mass density of vapor mixture, kg m^{-3}	ρ_v		2.47259
Cross section area of tube, m^2	A	$A = \pi (\frac{D_t}{2})^2$	0.0012566
Volumetric flowrate, $m^3 s^{-1}$	V		0.430761
Fluid's velocity, m s^{-1}	u	$u = V \div A \div No.$	1.714
Fluid viscosity, Pa s	μ		$1.73603e^{-5}$
Fluid thermal conductivity, W $m^{-1}K^{-1}$	k_f		0.111494
Fluid's heat capacity, J kg^{-1} K^{-1}	C_p		3299.54
Catalyst diameter, m	D_p		0.004
Bed voidage	ε		0.4
Wall thickness, m	Δw		0.002
Wall thermal conductivity, W $m^{-1}K^{-1}$	k_w		16.2
Reynold number	Re_0	$Re_0 = \frac{\rho_v \times u \times D_p}{\mu}$	976.44
Overall heat transfer coefficient, W $m^{-2}K^{-1}$	U	$U = 0.01545 + \frac{0.6885 \times 10^{-6}}{D_p} Re_0$	0.18352
Prandlt number	Pr	$Pr = \frac{C_p \times \mu}{k}$	0.51377
Nusselt number (fluid-to-solid)	Nu	$Nu = \frac{h_c \times D_p}{k_f} = 2 + 1.1 Pr^{1/3} Re^{0.6}$	56.798
Heat strafer coefficient of material fluid and catalyst, W $m^{-2}K^{-1}$	h_c	$h_c = \frac{Nu \times k_f}{D_p}$	1583
Catalyst thermal conductivity, W $m^{-1}K^{-1}$	k_s		3.6
Effective catalyst thermal conductivity, W $m^{-1}K^{-1}$	k_r^0	$k_r^0 = k_f \left(\varepsilon + \frac{0.95(1-\varepsilon)}{0.2 + 0.667 \times \frac{k_f}{k_s}} \right)$	0.33261
Nusselt number of fluid mechanical	Nu_m	$Nu_m = 0.54 \times Pr \times Re$	27.09

Table A-III. Heat transfer coefficient parameters, equations, and results (2/2).

Parameters	Symbol	Equation	Value
Wall film Nusselt number	Nu_w^*	$Nu_w^* = 0.3 \times Pr^{1/3} \times Re^{0.75}$	41.97
Wall Nusselt number at zero flowrate	Nu_{w0}	$Nu_{w0} = \left(1.3 + \frac{5 \times D_p}{D_t}\right) \times \left(\frac{k_r^0}{k_f}\right)$	5.3697
Wall Nusselt number	Nu_w	$Nu_w = \frac{h_w \times D_p}{k_f} = Nu_{w0} \times \left(\frac{1}{\frac{1}{Nu_w^*} + \frac{1}{Nu_m}}\right)$	88.404
Heat transfer coefficient between process fluid and wall reactor, W $m^{-2}K^{-1}$	h_w	$h_w = \frac{Nu_w \times k_f}{D_p}$	2664.14
Radial fluid phase Peclet number	$Pe_{h,r}$	$Pe_{h,r} = 8 \times \left(2 - \left(1 - \frac{2 \times D_p}{D_t}\right)^2\right)$	10.88
Effective radial thermal conductivity, W $m^{-1}K^{-1}$	k_{er}	$\frac{k_{er}}{k_f} = \frac{k_r^0}{k_f} + \frac{Pr \times Re}{Pe_{h,r}}$	5.4734
Tube Biot number	Bi	$Bi = \frac{h_w \times D_t}{k_{er}}$	18.008
Overall heat transfer coefficient between process fluid and wall reactor, W $m^{-2}K^{-1}$	U_t	$\frac{1}{U_t} = \frac{1}{h_w} + \frac{D_t}{6 \times k_{er}} \times \frac{Bi + 3}{Bi + 4} + \frac{\Delta w}{k_w}$	591

Appendix 2: stream results

Table A-IV. Stream results of the model at full load.

Streams	Temperatures, ℃	Pressure, bar	Mole flow, kmol/h	CO_2 mole fraction, %	H_2 mole fraction, %	CH_4 mole fraction	H_2O mole fraction, %	Mass flow, kg/h
H2	25	10	308	0	1	0	0	620.891
H2-1	25	9.5	308	0	1	0	0	620.891
H2-3	51	12	308	0	1	0	0	620.891
CO2	25	1.5	70	1	0	0	0	3080.69
CO2-1	24.45	1	70	1	0	0	0	3080.69
CO2-2	280	12	70	1	0	0	0	3080.69
CO2-3	120	12	70	1	0	0	0	3080.69
FEED	67.91	12	388.984	0.17996	0.7998	0.01999	2.5×10^{-3}	3834.34
C-OUT	230	11	388.984	0.17996	0.7998	0.01999	2.5×10^{-3}	3834.34
C-OUT1	229.98	10.5	388.984	0.17996	0.7998	0.01999	2.5×10^{-3}	3834.34
FEED1	230	10.5	388.984	0.17996	0.7998	0.01999	2.5×10^{-3}	3834.34
P	302	9.567	248.99	2×10^{-5}	0.125	0.31235	0.56263	3834.34
P-1	148	8.567	248.99	2×10^{-5}	0.125	0.31235	0.56263	3834.34
P-2	143.55	7.567	248.99	2×10^{-5}	0.125	0.31235	0.56263	3834.34
P-3	143.55	7.067	248.99	2×10^{-5}	0.125	0.31235	0.56263	3834.34
P-4	35	7.067	248.99	2×10^{-5}	0.125	0.31235	0.56263	3834.34
WATER	35	7.067	139.146	2.6×10^{-5}	9.4×10^{-8}	9.9×10^{-5}	0.99988	2506.67
MAIN	35	7.067	109.844	3.2×10^{-5}	0.2833	0.70789	0.0088	1327.67
PROD	35	7.067	98.8594	3.2×10^{-5}	0.2833	0.70789	0.0088	1194.9
REC	35	7.067	10.9844	3.2×10^{-5}	0.2833	0.70789	0.0088	132.766
REC1	96.42	13	10.9844	3.2×10^{-5}	0.2833	0.70789	0.0088	132.766
REC2	135	12	10.9844	3.2×10^{-5}	0.2833	0.70789	0.0088	132.766

Appendix 3: steady state and dynamic flowsheet of catalytic CO_2 methanation.

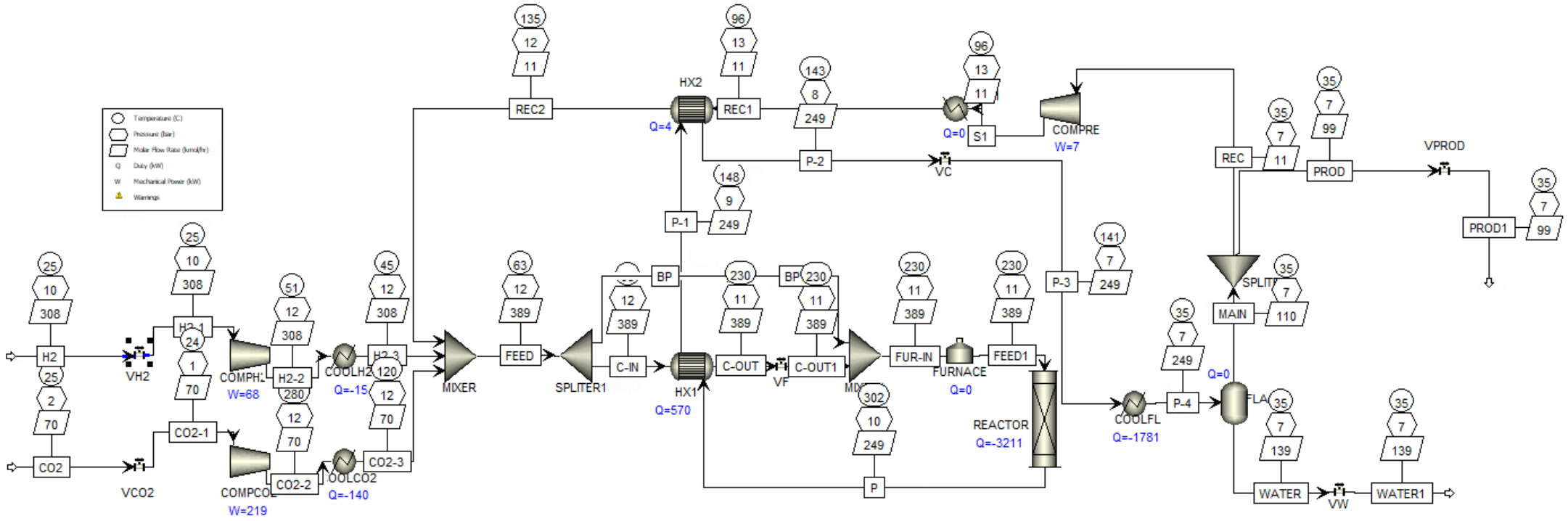

Figure A-I. Steady-state flowsheet of catalytic CO_2 methanation.

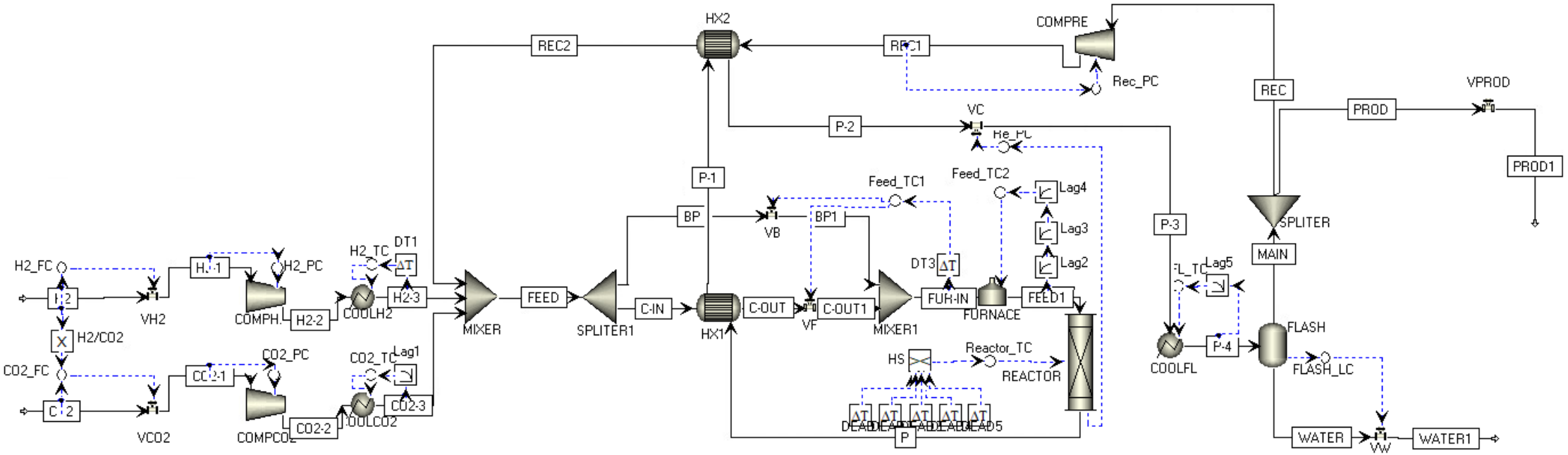

Figure A-II. Design of all controllers in dynamic model of the P2M plant.